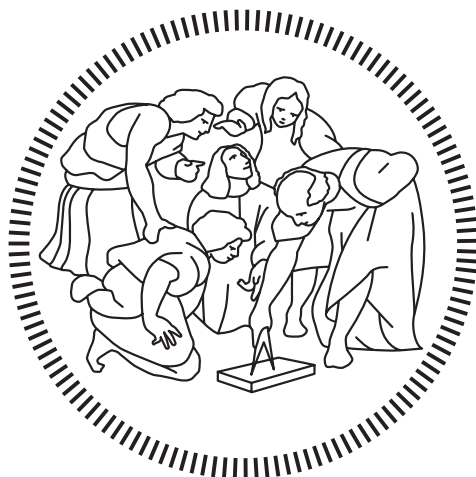


Politecnico di Milano

SCHOOL OF INDUSTRIAL AND INFORMATION ENGINEERING

Master of Science – Nuclear Engineering



**A computational method for assessing the
dose due to chronic release of radioactive air:
a hadron therapy facility case study**

Supervisor

Prof. Stefano AGOSTEO

Co-Supervisor

Ing. Michele FERRARINI

Candidate

Tommaso LORENZON – 919453

Academic Year 2019 – 2020

Alla mia famiglia

Abstract

In the last decades, the use of particle accelerators for the treatment of tumours has undergone a relevant development. These complex machines, originally built for Physics research, are used for irradiating tumour masses with energetic protons and ions. The practice is known as hadron therapy.

Operating medical accelerators represents a complex task, characterised by a strong interconnection of professionals and expertise. In this context, a careful design phase and continuous monitoring of every segment of the treatment line must ensure rigid and effective safety measures. Among these, the control of radioactivity is extremely important. In fact, particle beams inevitably collide with accelerator and treatment hall structures, producing radiation fields that represent a potential hazard for exposed workers and patients.

In this framework, the present M.Sc. thesis is focused on one aspect of radiation protection at hadron therapy facilities: air activation and management. As said, when particle accelerators are run and treatments are performed in the dedicated rooms, several nuclear reactions are responsible for the production of radioactive isotopes, which must be removed to maintain indoor air safe from a radiologic viewpoint. After filtration, radioactive air is ultimately discharged into the atmosphere. The process, known as chronic release, may be a source of dose to the population and must be carefully assessed.

For this purpose, in this work, a generic computational method for assessing the dose due to chronic release of radioactive air in the surrounding area of a hadron therapy facility is proposed. The transport of contaminants in the atmosphere is addressed using the Gaussian Plume Model, a physical model which has been extensively discussed and applied in the literature. In particular, this model is used inside two toolbox codes (HotSpot and GENII V2.10) certified by the Department Of Energy of the United States of America, whose algorithm for dose computation is here analysed, highlighting major assumptions and limits, mainly related to radiation transport. The Monte Carlo transport code FLUKA is introduced as a possible solution for exhaustively addressing this physical phenomenon. Hence, the Gaussian Plume Model is implemented in a user-written source routine and tested in several ways, including a comparison of its performance with HotSpot and GENII V2.10 in a generic scenario.

In the successive development of the work, dose calculations are produced for Centro Nazionale di Adroterapia Oncologica (CNAO) – the hadron therapy facility considered as a case study. Estimates of the annual airborne activity generated and then released into the atmosphere are given under a conservative approach. Local meteorological data is gathered from two weather stations to obtain information about

the annual wind rose and the state of stability of the atmosphere, two factors that affect the dispersion of radioactive contaminants.

The inhalation dose is calculated using GENII V2.10. Realistic activation data and the user-written source routine implementing the Gaussian Plume Model are used to produce submersion dose estimates in a two-step computational method. Firstly, a FLUKA simulation of the stochastic radiation transport due to the radioactive plume is completed; secondly, a MATLAB code allows weighting the dose in each compass direction on the base of the corresponding wind frequency, thus taking into account the variability that wind itself introduces in the dispersion of contaminants. In all the steps, the code is designed to be flexible and easily reusable.

Results of the case study depict a reassuring situation, in which the submersion dose rarely exceeds some hundreds of nanosievert per year with the only exception of the first metres around the emission point. There, several factors contribute to a higher degree of uncertainty of the evaluations. In this regard, a critical discussion about the approximations made is given, together with some hints about future developments of the overall work.

Sommario

Negli ultimi decenni, l'uso degli acceleratori di particelle per il trattamento dei tumori ha subito un grande sviluppo. Queste complesse macchine, originariamente nate per scopi di ricerca nell'ambito della Fisica, sono sfruttate per irraggiare le masse tumorali con protoni e ioni estremamente energetici. Questa pratica è nota con il nome di adroterapia.

La gestione degli acceleratori medicali è sicuramente complessa e caratterizzata da una forte interconnessione di figure professionali e conoscenze diverse. In questo contesto, un'attenta fase di progettazione e il costante monitoraggio di ogni segmento della linea di cura devono garantire rigide ed efficaci misure di sicurezza. Tra queste, il controllo della radioattività è estremamente importante. Infatti, i fasci di particelle accelerate collidono inevitabilmente con alcune strutture degli acceleratori e delle sale di trattamento, producendo dei campi di radiazione che rappresentano un potenziale fattore di rischio per lavoratori e pazienti esposti.

In questo quadro teorico, la presente tesi magistrale è focalizzata su un aspetto della radioprotezione nei centri di adroterapia: l'attivazione dell'aria e la sua gestione. Come anticipato, quando gli acceleratori di particelle sono in funzione o si svolgono i trattamenti adroterapici nelle sale dedicate, alcune reazioni nucleari sono responsabili della produzione di isotopi radioattivi, i quali devono essere rimossi per mantenere l'aria all'interno dei locali sicura da un punto di vista radiologico. Dopo essere stata filtrata, l'aria radioattiva è espulsa nell'atmosfera. Questo processo, noto come rilascio cronico, può impartire dosi alla popolazione e deve essere attentamente valutato.

Per questo motivo, in questo lavoro si propone un metodo computazionale per calcolare la dose dovuta ai rilasci cronici di aria attivata nei dintorni di un centro adroterapico. Il trasporto dei contaminanti nell'atmosfera è descritto dal pennacchio gaussiano (*Gaussian Plume Model*), un modello fisico ampiamente illustrato e applicato in letteratura. In particolare, questo modello è usato in due software (HotSpot e GENII V2.10) certificati dal Dipartimento di Energia degli Stati Uniti d'America e il cui algoritmo per il calcolo della dose è qui analizzato, evidenziandone le ipotesi essenziali e i limiti connessi, principalmente riguardanti il trasporto della radiazione. Il codice Monte Carlo FLUKA è introdotto come possibile soluzione per trattare in modo completo questo fenomeno fisico. Di conseguenza, il pennacchio gaussiano è implementato anche in una sorgente FLUKA e il suo funzionamento è verificato in più modi, incluso un confronto con HotSpot e GENII V2.10 in uno scenario generico.

Nel proseguimento del lavoro sono formulate delle stime di dose per un caso di studio riguardante il Centro Nazionale di Adroterapia Oncologica (CNAO), il centro presso il quale questa tesi è stata svolta. Le valutazioni sulle quantità di radioattività generata in aria e successivamente scaricata in atmosfera sono svolte seguendo un

approccio conservativo. I dati meteorologici locali sono raccolti da due centraline, al fine di ottenere informazioni riguardo alla distribuzione dei venti e lo stato di stabilità dell'atmosfera, due fattori che influiscono sensibilmente sulla dispersione aerea dei contaminanti.

La dose da inalazione è calcolata con GENII V2.10. I dati realistici di attività e la sorgente FLUKA che implementa il pennacchio gaussiano sono usati per fornire delle valutazioni della dose da somministrazione seguendo un metodo sviluppato in due fasi. In un primo momento vengono completate le simulazioni FLUKA che descrivono il trasporto stocastico della radiazione; successivamente, un codice MATLAB consente di pesare la dose in ogni direzione sulla base della corrispondente frequenza annuale con cui spira il vento, permettendo, perciò, di tenere conto della variabilità che il vento stesso introduce nella dispersione dei contaminanti. In tutti i passaggi, il codice è progettato per essere flessibile e facilmente riutilizzabile.

I risultati del caso di studio ritraggono una situazione complessivamente rassicurante, in cui la dose da somministrazione supera in rari casi le centinaia di nanosievert annuali, con l'unica eccezione dei primi metri attorno al punto di emissione. In quella zona, alcuni fattori contribuiscono a rendere più incerta la valutazione della dose. A questo proposito, è presentata una discussione critica delle approssimazioni compiute, insieme con alcuni cenni riguardo ai possibili futuri sviluppi del lavoro nella sua interezza.

Estratto

Negli ultimi decenni, l'uso degli acceleratori di particelle per il trattamento dei tumori ha subito un grande sviluppo [1]. Queste complesse macchine, originariamente nate per scopi di ricerca nell'ambito della Fisica, sono sfruttate per irraggiare le masse tumorali con protoni e ioni estremamente energetici. Questa pratica, nota con il nome di adroterapia, presenta alcuni vantaggi rispetto alla radioterapia convenzionale con fotoni [2] [3] [4]. In primo luogo, la dose assorbita (l'energia per unità di massa depositata dalle radiazioni ionizzanti), anziché mostrare un profilo di deposizione esponenzialmente decrescente all'interno dei tessuti, presenta un picco – detto di Bragg – ad una profondità variabile sulla base di energia e carica della particella incidente e della densità del target (Figura 1). Questo fatto, unito alla traiettoria estremamente rettilinea che le particelle incidenti mantengono all'interno del corpo, consente di ottenere risultati analoghi alla radioterapia convenzionale riducendo i danni collaterali nei tessuti sani (oppure, a parità di effetti collaterali, si può ottenere un irraggiamento del tumore più massiccio) [3] [4]. I trattamenti con particelle cariche di massa maggiore dei protoni, poi, offrono una serie di vantaggi biologici [4]. L'adroterapia, al netto degli attuali limiti, soprattutto in termini di un'esatta quantificazione della dose depositata all'interno del corpo e di altre difficoltà tecniche, presenta degli indubbi vantaggi fisici che rendono possibile il trattamento di tumori solidi ricorrenti, radioresistenti, pediatrici, spesso con promettenti prospettive di guarigione (come nel caso del melanoma oculare) [4] [5].

Un altro tipo di adroterapia, concepita già negli anni trenta del secolo scorso, è la terapia a cattura neutronica (*Boron Neutron Capture Therapy, BNCT*), la cui idea

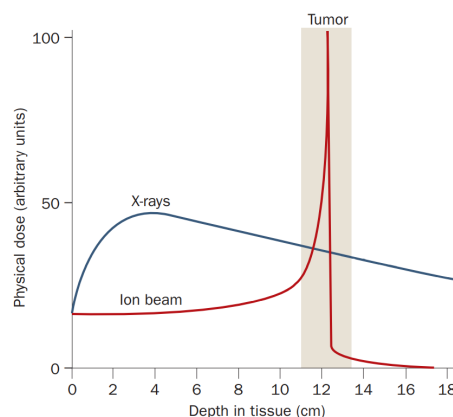


Figura 1. Rappresentazione schematica del profilo di deposizione di dose all'aumentare della profondità nel tessuto per fotoni e un generico fascio di ioni. Nel secondo caso si può osservare il peculiare picco di Bragg.



Figura 2. Vista della sala del sincrotrone del CNAO di Pavia. Questo acceleratore ha forma circolare, con diametro di 25 m e circonferenza di circa 80 m.

fondamentale è irradiare i tumori, precedentemente caricati di boro attraverso l'uso di farmaci specifici, con neutroni; la reazione nucleare tra neutroni e boro, durante il trattamento, riesce ad inattivare le cellule tumorali grazie alla conseguente deposizione di energia in una zona estremamente limitata, proprio nell'ordine delle dimensioni cellulari [3] [6] [7]. A patto di caricare selettivamente di boro solo le cellule maligne, quindi, anche questa terapia garantisce di risparmiare i tessuti sani da dose indebita.

Il Centro Nazionale di Adroterapia Oncologica (CNAO) di Pavia è l'unica struttura italiana, e una delle sei nel mondo, predisposta per fornire trattamenti adroterapici con protoni e ioni carbonio. Nella sua storia ventennale, il centro ha attraversato varie fasi di progettazione e costruzione fino al 2011, anno in cui sono iniziati i trattamenti di protonterapia. Presso questo centro, un sincrotrone (Figura 2) permette di accelerare protoni e ioni verso tre sale di trattamento e una sperimentale, dove sistemi tecnologici d'avanguardia assicurano una distribuzione precisa degli adroni terapeutici [8]. Il CNAO, collocato in un'area parzialmente urbanizzata della periferia della città pavese, verrà prossimamente ampliato con la costruzione di un'ulteriore protonterapia e di una BNCT [5].

La gestione degli acceleratori medicali è sicuramente complessa e caratterizzata da una forte interconnessione di figure professionali e conoscenze diverse. In questo contesto, un'attenta fase di progettazione e il costante monitoraggio di ogni segmento della linea di cura devono garantire rigide ed efficaci misure di sicurezza. Tra queste, il controllo della radioattività è estremamente importante e regolato dalla legge [9]. Infatti, i fasci di particelle accelerate collidono inevitabilmente con alcune strutture degli acceleratori e delle sale di trattamento, producendo dei campi di radiazione che rappresentano un potenziale fattore di rischio per lavoratori e pazienti esposti [10].

In questo quadro teorico, la presente tesi magistrale, svolta presso l'ufficio di radioprotezione del CNAO, è focalizzata sull'attivazione dell'aria e la sua gestione nei centri di adroterapia. Come anticipato, quando gli acceleratori di particelle sono in funzione o si svolgono i trattamenti nelle sale dedicate, alcune reazioni nucleari (principalmente di spallazione, ma anche di cattura radiativa, come nel caso di ^{40}Ar) sono responsabili della produzione di isotopi radioattivi, i quali devono essere rimossi per mantenere l'aria all'interno dei locali sicura da un punto di vista radiologico. Per questo motivo, dei sistemi di ventilazione sono attivi in tutti i centri di terapia.

Dopo essere stata filtrata, l'aria radioattiva è espulsa nell'atmosfera. Questo

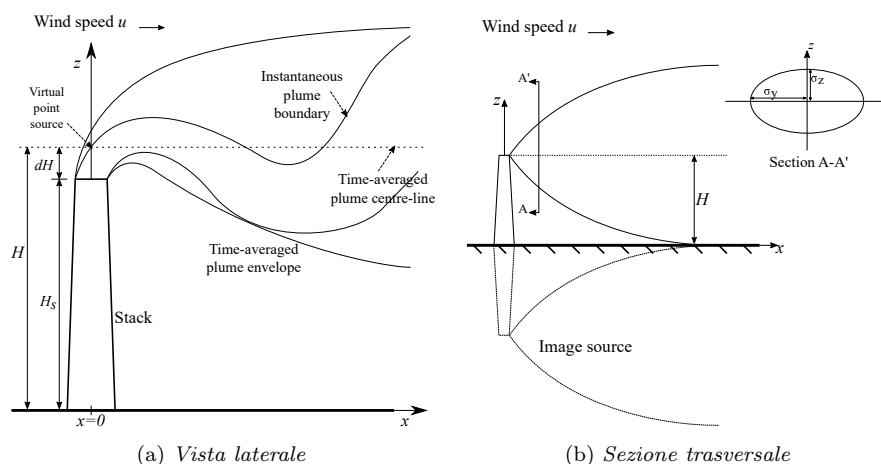


Figura 3. Rappresentazione schematica del modello a pennacchio gaussiano (GPM) per il trasporto dei contaminanti in aria e sue principali grandezze caratteristiche.

processo, noto come rilascio cronico, può impartire dosi alla popolazione e deve essere attentamente valutato. Per questo motivo, in questo lavoro si propone un metodo computazionale per calcolare la dose dovuta ai rilasci cronici di aria attivata nei dintorni di un centro adroterapico.

Il trasporto dei contaminanti nell'atmosfera è stato descritto con il pennacchio gaussiano (*Gaussian Plume Model, GPM*), un modello fisico ampiamente illustrato e applicato in letteratura, che considera la diffusione molecolare e il trasporto monodirezionale del vento come principali mezzi di dispersione degli inquinanti. Il modello permette di calcolare la loro concentrazione χ nello spazio sottovento rispetto al punto di emissione [11] [12]. La sua formulazione matematica per radioisotopi è [11]:

$$\chi(x, y, z) = \frac{Q}{2\pi\sigma_y(x)\sigma_z(x)u} \exp\left(-\frac{y^2}{2\sigma_y^2(x)}\right) \exp\left(-\frac{\lambda x}{u}\right) \left[\exp\left(-\frac{(z-H)^2}{2\sigma_z^2(x)}\right) + \exp\left(-\frac{(z+H)^2}{2\sigma_z^2(x)}\right) \right]$$

in cui Q è il termine di sorgente in $[\text{Bq s}^{-1}]$, H l'altezza di rilascio effettiva in $[\text{m}]$, u la velocità media del vento all'altezza di rilascio $[\text{m s}^{-1}]$, $\sigma_y(x)$ e $\sigma_z(x)$ i coefficienti di dispersione laterale e verticale in $[\text{m}]$, λ la costante di decadimento in $[\text{s}^{-1}]$ (Figura 3). Le grandezze H , u , $\sigma_y(x)$ e $\sigma_z(x)$ sono funzione di altri parametri. In primo luogo, la configurazione del comignolo e la modalità di espulsione in aria (velocità di emissione, temperatura del gas e dell'aria ambientale), insieme con l'influenza che gli edifici circostanti esercitano sull'aerodinamica del trasporto, modificano l'altezza di rilascio effettivo [13]. Inoltre, le condizioni meteorologiche influiscono in modo rilevante sulla concentrazione in aria dei contaminanti: un'elevata turbolenza, data da moti convettivi delle masse d'aria o da venti intensi, ne favorisce la dispersione. La stabilità atmosferica è descritta in modo approssimato da un indice, detto classe di stabilità, calcolato seguendo le indicazioni presenti in letteratura [14] [11]. I coefficienti di dispersione, funzione della distanza sottovento e della classe di stabilità, sono calcolati sulla base dei risultati delle pubblicazioni di Briggs [15] [16].

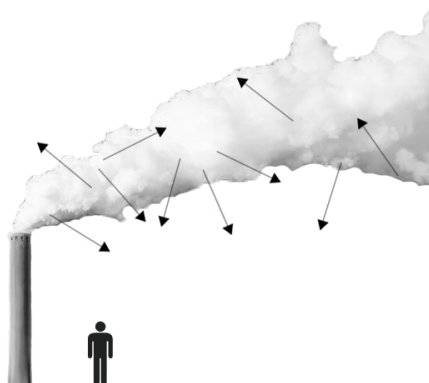


Figura 4. Immagine semplificata di una nube radioattiva che si estende sopra ad un recettore, il quale non risulta perciò immerso al suo interno. In questa specifica, ma non rara, situazione, i codici HotSpot e GENII V2.10 prevedono una dose nulla a terra. In realtà, particelle con un libero cammino medio elevato possono raggiungere il livello del suolo e dare dose agli individui.

Il modello a pennacchio gaussiano è stato usato in due software (HotSpot e GENII V2.10 [17] [18] [19]) certificati dal Dipartimento di Energia degli Stati Uniti d’America [20] e il cui algoritmo per il calcolo della dose è stato qui analizzato, evidenziandone le principali ipotesi e i limiti connessi. Come detto, la concentrazione dei contaminanti è calcolata con il GPM in $[Bq\ m^{-3}]$; successivamente, le dosi da inalazione e sommersione sono stimate moltiplicando questo valore per dei coefficienti di conversione concentrazione-dose (*Dose Conversion Factor, DCF*). I DCF sono calcolati con dei codici Monte Carlo sotto l’ipotesi di nube semi-infinita [21] [22] [23]. Le principali problematiche rilevate sono:

1. La validità dell’approssimazione di nube semi-infinita è verificata solo ad una certa distanza dalla sorgente, cioè dove il contaminante è sufficientemente disperso. Questa distanza dipende dalla velocità del vento, dalla classe di stabilità atmosferica, dal tipo di radionuclide e dai suoi prodotti di decadimento. A brevi distanze dentro la nuvola, l’approssimazione di nube semi-infinita porta ad una significativa sovrastima della dose.
2. Il prodotto di un DCF per la concentrazione di attività porta ad una previsione di dose nulla laddove il contaminante sia assente o poco concentrato, cioè, ad esempio, alla periferia della nuvola o in aree in cui la stessa si trova molto al di sopra dei recettori (Figura 4). Questo risultato è scorretto nel caso in cui le particelle emesse durante il decadimento abbiano un percorso in aria significativo, come ad esempio i fotoni, tale da coprire distanze rilevanti e giungere a terra [23] [24].
3. Il calcolo della dose da inalazione non presenta, invece, particolari criticità nell’uso dei DCF [25] [11].

Il codice Monte Carlo FLUKA [26] [27] è stato introdotto come possibile soluzione per trattare in modo completo il fenomeno del trasporto della radiazione in scenari caratterizzati da atmosfera stabile, rilasci a pochi metri da terra, presenza di aree accessibili al pubblico anche in prossimità dei camini di scarico (dove, a causa delle

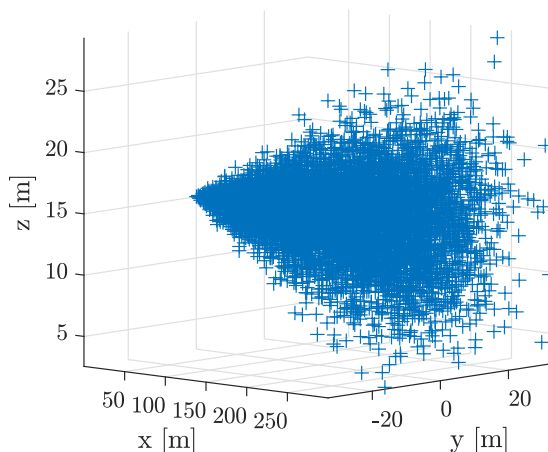


Figura 5. Rappresentazione tridimensionale di un pennacchio gaussiano in classe F implementato in FLUKA. La nuvola è composta da 1×10^4 punti sorgente ed è emessa a 15 m di altezza.

dimensioni limitate del pennacchio, l'approssimazione di nube semi-infinita non vale). In tutti questi casi, è estremamente probabile che un utente si trovi al di fuori della nube radioattiva, ma non per questo non sia soggetto ad un bagno di fotoni o altre particelle energetiche. Di conseguenza, il pennacchio gaussiano è stato implementato anche in una sorgente FLUKA e il suo funzionamento è stato verificato in più modi, incluso un confronto con i valori di dose da sommersione dati da HotSpot e GENII V2.10 in uno scenario generico con rilascio di 10 GBq di ^{41}Ar .

La sorgente FLUKA campiona, attraverso le funzioni disponibili nel codice, la posizione iniziale e la direzione delle particelle primarie emesse dai radionuclidi (dispersi in aria) nel momento in cui decadono. In altre parole, il codice preparato colloca nello spazio i punti di decadimento dei radionuclidi secondo il GPM, cioè con distribuzione gaussiana nella direzione verticale e trasversale, ed esponenziale decrescente nella direzione sottovento (Figura 5). La dose è stata valutata sull'asse del pennacchio, all'altezza del terreno e a quella di rilascio. Nel secondo caso, un semplice modello analitico a nube sferica è stato aggiunto per avere un riferimento numerico semplice con cui confrontare le simulazioni Monte Carlo.

Il confronto tra i tre software è stato svolto per due differenti classi di stabilità, la minima (A, elevata dispersione degli inquinanti, qui non riportata) e la massima (F). I risultati (Figura 6) hanno permesso di evidenziare la sovrastima che l'uso dell'approssimazione di nube semi-infinita comporta quando le nubi radioattive sono piccole e, solo in FLUKA, la componente di dose da sommersione che si registra a terra nel caso in cui la nube sovrasti il recettore (Figura 4).

Nel proseguimento del lavoro sono state formulate delle stime dei rilasci del CNAO, sia per il sincrotrone già in funzionamento sia per il progetto di espansione prima menzionato. Le valutazioni sulle quantità di radioattività generata in aria sono state preparate a partire dai risultati di una precedente tesi magistrale [28]. Le stime dell'attività scaricata in atmosfera sono state svolte seguendo l'approccio indicato in letteratura e i dati riguardo al sistema di ventilazione del centro [29] [10]. A titolo di esempio, ipotizzando conservativamente l'uso del sincrotrone per 7355 h y^{-1} con corrente di protoni massima e energia del fascio massima, è stato calcolato un rilascio in aria annuale di $5.39 \times 10^{10} \text{ Bq y}^{-1}$, suddiviso tra ^{11}C , ^{13}N , ^{15}O e ^{41}Ar (Tabella 1).

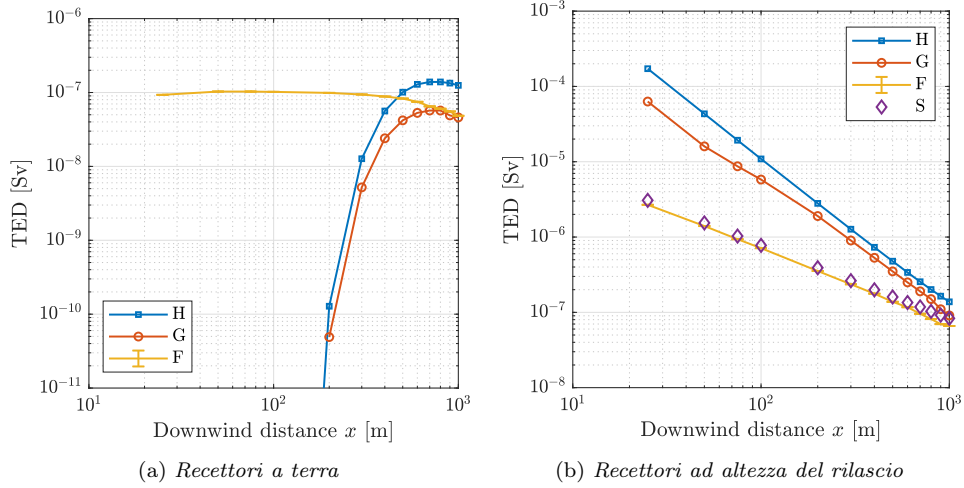


Figura 6. Risultati del confronto tra software in termini di dose efficace (*Total Effective Dose, TED*). A sinistra, nel primo centinaio di metri, i codici HotSpot e GENII V2.10 calcolano una dose da sommersione nulla se i recettori sono a terra, non immersi nella nuvola radioattiva. A destra, per recettori posti all'interno della stessa (all'altezza di rilascio), i codici HotSpot e GENII V2.10 producono una sovrastima rilevante della dose a causa dell'approssimazione di nube semi-infinita. H: HotSpot; G: GENII V2.10; F: FLUKA; S: modello sferico semplificato.

Tabella 1. Stime dell'attività rilasciata annualmente dal CNAO in condizioni di funzionamento nominale, espresse in $[\text{Bq y}^{-1}]$.

Radionuclide	Rilascio $[\text{Bq y}^{-1}]$
^{11}C	5.10×10^9
^{13}N	2.14×10^{10}
^{15}O	2.67×10^{10}
^{41}Ar	7.16×10^8
Total	5.39×10^{10}

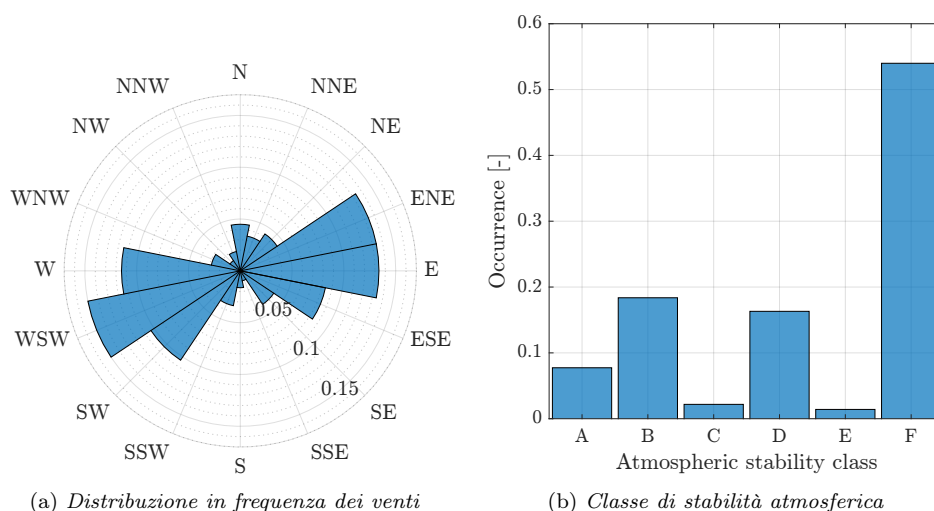


Figura 7. Frequenza di distribuzione dei venti (rilevata dalle centraline meteorologiche) e della classe di stabilità atmosferica (calcolata) per il biennio 2018-2019.

Sono stati raccolti da due centraline i dati meteorologici locali [30] [31], al fine di ottenere informazioni riguardo alla distribuzione dei venti e allo stato di stabilità dell'atmosfera, due fattori che influiscono sensibilmente sulla dispersione aerea dei contaminanti. I risultati più rilevanti (Figura 7) dell'analisi, completata in MATLAB, hanno mostrato una prevalenza di venti sull'asse WSW-ENE e di un'atmosfera stabile durante la maggior parte del periodo considerato (biennio 2018-2019).

La dose da inalazione è stata calcolata con GENII V2.10 ed è risultata non rilevante a circa 100 m dal punto di emissione. I dati realistici di attività e la sorgente FLUKA che implementa il pennacchio gaussiano sono stati usati per fornire delle valutazioni della dose da somministrazione seguendo un metodo sviluppato in due fasi. In un primo momento sono state completate le simulazioni FLUKA che descrivono il trasporto stocastico della radiazione per tutti i radionuclidi di interesse (Tabella 1), considerando il rilascio annuale e un vento in una singola direzione (verso est, Figura 8); l'equivalente di dose ambientale è stato valutato in un'area circolare con raggio di 300 m attorno al punto di emissione. Successivamente, la stesura di un codice MATLAB ha permesso di pesare la dose in ogni direzione del vento (sedici settori angolari) sulla base della corrispondente frequenza annuale con cui il vento spira, permettendo, perciò, di mettere a punto un modello più dinamico e realistico della dispersione dei contaminanti. L'importazione dei dati di dose è stata completata mettendo a punto un sistema rapido ed efficace per leggere automaticamente i file contenenti i risultati prodotti da FLUKA. Nel codice, le mappe di dose circolari di FLUKA sono state trattate come matrici; pertanto, la rotazione fisica della nuvola di contaminanti (e della corrispondente mappa di dose circolare) dovuta ad una differente direzione del vento è stata fatta coincidere con delle permutazioni circolari delle matrici stesse (Figura 9). In tutti i passaggi, il codice è stato progettato per essere flessibile e facilmente riutilizzabile.

L'equivalente di dose ambientale annuale (calcolato considerando i contributi di tutti i radionuclidi rilasciati) per il sincrotrone attualmente in funzione e per le previste protonterapia e BNCT è stato graficato in mappe di dose, di cui è stato riportato un esempio (Figura 10). I risultati ritraggono una situazione complessivamente

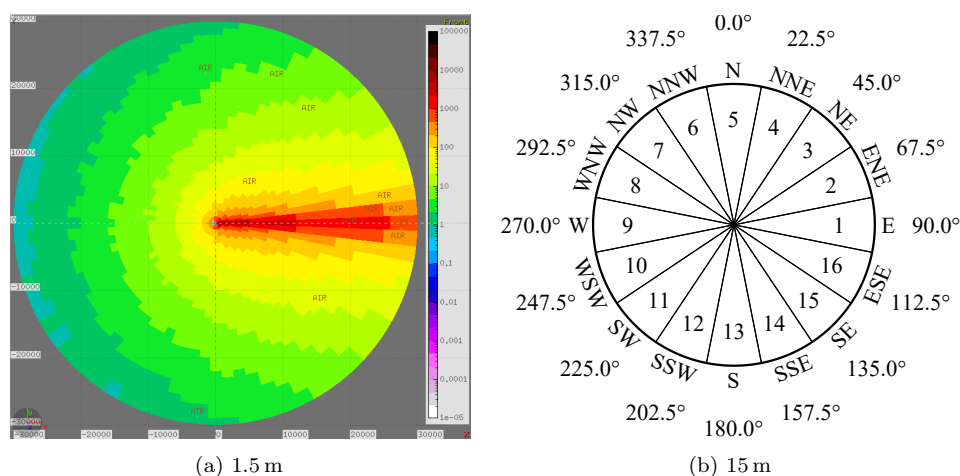


Figura 8. Visualizzazione di un risultato delle simulazioni FLUKA per una direzione di vento e il rilascio annuale di 3.7×10^{10} Bq di ^{41}Ar , in equivalente di dose ambientale [nSv y^{-1}] all'altezza di rilascio (a sinistra). Rosa dei venti e rappresentazione dei sedici settori angolari tipicamente usati in letteratura (a destra).

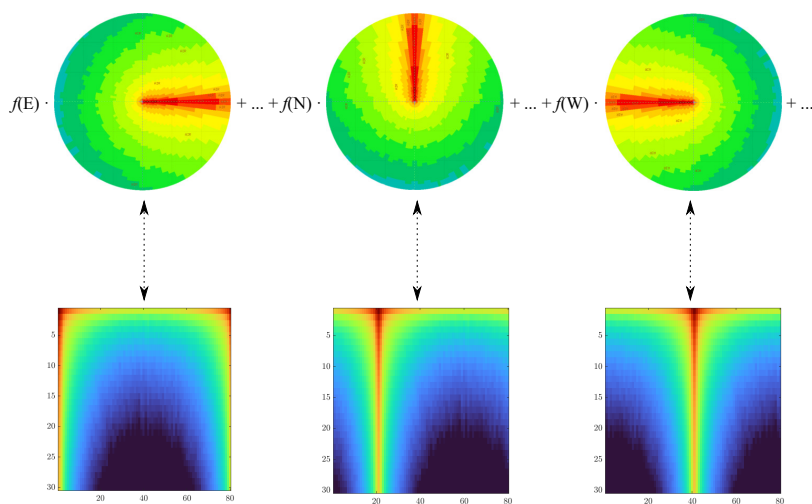


Figura 9. Visualizzazione dell'algoritmo ideato per collegare i dati delle simulazioni (statiche) di FLUKA con la distribuzione in frequenza dei venti. Nella parte superiore, le mappe di FLUKA sono fatte ruotare graficamente e vengono pesate per la frequenza del vento corrispondente. Nella parte inferiore, la corrispondente matrice MATLAB di dose è fatta permutare circolarmente per riprodurre la stessa rotazione.

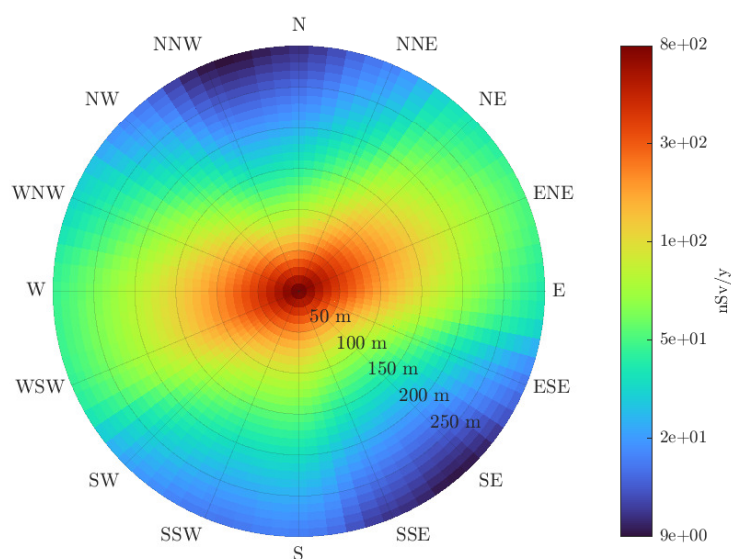


Figura 10. Mappa di dose da sommersione in termini di equivalente di dose ambientale [nSv y^{-1}] calcolata a livello del terreno, per le emissioni annuali di sincrotrone e sale trattamento e i dati meteorologici del biennio 2018-2019.

rassicurante, in cui la dose da sommersione supera in rari casi le centinaia di nanosievert annuali, con l'unica eccezione dei primi metri attorno al punto di emissione. In quella zona, alcune limitazioni – principalmente nel modello della sorgente e dei coefficienti di dispersione – contribuiscono a rendere più incerta la valutazione della dose.

In conclusione, i fenomeni fisici di attivazione dell'aria e del trasporto di contaminanti sono stati studiati attraverso riferimenti di letteratura e i software FLUKA, HotSpot e GENII V2.10. Il pennacchio gaussiano è stato inserito in un codice FLUKA per modellizzare in modo completo il trasporto stocastico della radiazione, operazione necessaria alla luce dei limiti degli altri software di calcolo in particolari condizioni meteorologiche e di rilascio. Dopo aver prodotto delle stime riguardanti le emissioni annuali del CNAO e aver raccolto i dati meteo, sono state proposte delle mappe di dose dell'area circostante il centro. I principali risultati sono stati raggiunti in termini di approccio generale al problema del calcolo della dose da sommersione. In più, riguardo al caso di studio esaminato, l'applicazione del metodo proposto ha mostrato come l'attività di gestione ed espulsione dell'aria non costituisca un problema radiologico per la popolazione.

Contents

Abstract	v
Sommario	vii
Estratto	ix
Contents	xix
List of Figures	xxi
List of Tables	xxiii
1 Introduction	1
1.1 Particle therapy in cancer treatment	1
1.1.1 Hadron therapy	2
1.1.2 Boron Neutron Capture Therapy	4
1.2 CNAO	6
1.2.1 Particle accelerator and therapy	7
1.2.2 Topography	9
1.2.3 Expansion project	9
1.3 Concluding remarks and aim of this work	9
2 Theoretical background	13
2.1 Air activation at accelerator facilities	13
2.1.1 Radionuclides produced in air	14
2.1.2 Ventilation system	15
2.2 Atmospheric dispersion models for the transport of contaminants . .	15
2.2.1 Gaussian Plume Model	17
2.3 Introductory meteorological concepts	19
2.3.1 Wind	19
2.3.2 Solar radiation	20
2.3.3 Atmospheric stability classes	20
2.3.4 Briggs' coefficients for dispersion modeling	21
2.4 Fundamentals of radiation protection	23
2.4.1 Dose contributions	24
2.4.2 Radiation protection and dosimetric quantities	24
3 Software	27
3.1 HotSpot	27

3.2	GENII V2.10	29
3.2.1	Basics of the software	29
3.2.2	GENII Chronic Plume Model	30
3.3	Limits of the software	31
3.3.1	Gamma-ray dose from an overhead plume	31
3.3.2	Semi-infinite cloud approximation	33
3.3.3	Monte Carlo techniques as a possible approach	35
3.4	FLUKA	35
4	Software comparison	37
4.1	Scenario description and rationale of the comparison	37
4.2	Methods	38
4.2.1	HotSpot	38
4.2.2	GENII V2.10	39
4.2.3	FLUKA	41
4.2.4	Simplified model for dose evaluations	48
4.3	Results and discussion	49
5	The CNAO case: radioactive releases and meteorological data	55
5.1	Quantitative formulation of air management	55
5.2	Releases at CNAO	56
5.2.1	Synchrotron, experimental and treatment rooms	56
5.2.2	Expansion project	59
5.3	Meteorological data analysis	61
6	The CNAO case: dose evaluations	67
6.1	Inhalation dose	67
6.1.1	GENII V2.10 simulation	67
6.1.2	Results and discussion	68
6.2	Submersion dose	68
6.2.1	FLUKA: radiation transport simulation	69
6.2.2	MATLAB: merge dose and meteorological data	72
6.2.3	Results and discussion	77
6.3	Concluding remarks and future studies	83
	Conclusions	85
	Bibliography	90
	A FLUKA SOURCE user routine	91
	B Meteorological data analysis	95
	C Importing USRBIN data to MATLAB	99
	D Guide to MATLAB scripts	101
	Acronyms	103

List of Figures

Figura 1.1	Dose-tissue depth profile for photons, protons and charged ions.	2
Figura 1.2	Schematic view of the ab-BNCT system.	6
Figura 1.3	View of the CNAO synchrotron bunker.	7
Figura 1.4	Schematic representation of the <i>active dose distribution system</i> .	8
Figura 1.5	Aerial map of CNAO.	11
Figura 2.1	Schematic representation of the GPM.	18
Figura 2.2	Wind directions and corresponding angles and sector numbers.	20
Figura 3.1	Screen shot of <i>Source Term</i> panel in HotSpot.	28
Figura 3.2	Screen shot of <i>User Defined Module</i> in GENII V2.10.	30
Figura 3.3	Image of an overhead plume of radioactive contaminants.	32
Figura 3.4	1 MeV photons fluence rate at the centre of a sphere.	34
Figura 3.5	Screen shot of Flair GUI for FLUKA.	36
Figura 4.1	GENII V2.10 conceptual site model.	40
Figura 4.2	Cross-sectional area of a GPM and totally reflective ground.	44
Figura 4.3	3D spatial representation of a GPM.	45
Figura 4.4	Downwind distribution of a GPM's source points.	46
Figura 4.5	Lateral and vertical distributions of a GPM's source points.	46
Figura 4.6	⁴¹ Ar decay scheme.	47
Figura 4.7	Software comparison: TED results for receptors at ground level.	50
Figura 4.8	Software comparison: TED results for receptors at release height.	51
Figura 5.1	Wind rose of 2018 and 2019 wind directions.	62
Figura 5.2	Histogram of 2018 and 2019 wind speed data.	62
Figura 5.3	Histogram of 2018 and 2019 solar irradiation data.	65
Figura 5.4	Histogram of 2018 and 2019 atmospheric stability classes data.	65
Figura 6.1	Scheme of wind sectors and USBINs used in simulations.	70
Figura 6.2	Downwind distribution of an F class GPM of ¹⁵ O source points.	71
Figura 6.3	Results of FLUKA simulations for the annual release of ⁴¹ Ar.	72
Figura 6.4	Schematic of prepData function main steps.	74
Figura 6.5	Schematic of elabData function algorithm.	77
Figura 6.6	$H^*(10)$ dose map at release height for synchrotron emissions.	80
Figura 6.7	$H^*(10)$ dose map at ground level for synchrotron emissions.	80
Figura 6.8	$H^*(10)$ dose map at release height for PT emissions.	81
Figura 6.9	$H^*(10)$ dose map at ground level for PT emissions.	81
Figura 6.10	$H^*(10)$ dose map at release height for ab-BNCT emissions.	82
Figura 6.11	$H^*(10)$ dose map at ground level for ab-BNCT emissions.	82

List of Figures

Figura B.1	Weather stations comparison: 2019 wind speed data.	96
Figura B.2	Weather stations comparison: 2019 solar irradiation data.	96
Figura B.3	Weather stations comparison: 2019 stability classes data.	97
Figura B.4	Weather stations comparison: 2019 wind directions data.	97

List of Tables

Table 1.1	Description of the buildings surrounding CNAO.	11
Table 2.1	Qualitative description of atmospheric stability classes.	21
Table 2.2	SRDT method for estimating P-G stability categories.	22
Table 2.3	Briggs' coefficients for open country and urban conditions.	23
Table 4.1	Elemental composition of soil and air in mass fraction.	47
Table 4.2	Software comparison: results for receptors at ground level.	53
Table 4.3	Software comparison: results for receptors at release height.	53
Table 5.1	Particles per year in each beam line at CNAO.	58
Table 5.2	Example of calculation of the activity discharged in one year.	59
Table 5.3	Relevant radionuclides released in the air by CNAO.	60
Table 5.4	Estimated annual activity released by CNAO.	60
Table 6.1	Estimated annual activity released by CNAO.	75

Chapter 1

Introduction

In this Chapter, the major concepts concerning hadron therapy for treating cancer are addressed. Successively, one hadron therapy facility – Centro Nazionale di Adroterapia Oncologica (CNAO), *Italian national center for Oncological Hadron therapy* – is briefly introduced and described. The main activities and site itself are analysed with reference to literature and its geographical location in the city of Pavia (Italy). These aspects constitute the framework in which the present thesis work is inserted, as discussed in the last part of the Chapter.

1.1 Particle therapy in cancer treatment

Cancer is a generic term for a large group of diseases that can affect any part of the body. One defining feature of this pathology is the uncontrollable growth of abnormal cells, which go beyond their usual boundaries and can then spread to other tissues and organs (the latter process is known as metastasis), owing to dynamic changes in the genome [32].

Cancer is a leading cause of death worldwide. In 2020, nearly 10 million cancer deaths were observed, of which the most common cause was lung, colon and rectum, liver, stomach, breast tumour [33]. Correct prevention, screening programmes and early diagnosis are essential to guarantee an effective treatment of the disease; in some cases, early detection and best practices in treatment can lead to significantly high cure rates. Treatment usually includes radiotherapy, chemotherapy and/or surgery.

Over the years, fundamental discoveries in Modern Physics have provided some key concepts and tools to treat cancer in more effective and sophisticated ways. Radiation medicine – in both its major divisions, diagnosis and therapy – originated from Röntgen’s discovery of X-rays more than a century ago and developed through the years together with treatment refinements and technology, which has become able to manufacture higher-energy accelerators [2].

Nowadays, 50 % of all the patients with localized malignant tumours are treated with radiation, usually high-energy X-rays. Typical treatments for solid cancer consists in 60 Gy to 70 Gy delivered in 30 to 35 daily fractions of 2 Gy over 6 to 7 weeks¹.

¹The gray ($1\text{ Gy}=1\text{ J kg}^{-1}$) is the SI unit for the absorbed energy, i.e. the energy deposited in matter by ionising radiation per unit mass [3].

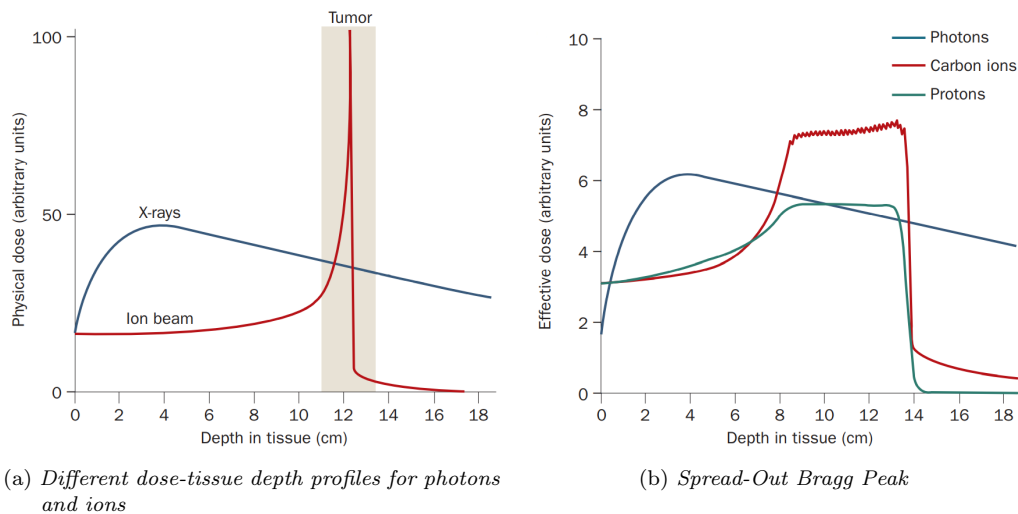


Figure 1.1. Schematic representation of the dose-tissue depth profile for photons, protons, charged ions (adapted from reference [4]). Charged particles have an advantageous radiation dose-tissue depth profile compared with photons (Figure 1.1a). In the treatment of large tumors, the Bragg peak must be broadened by the use of overlapping beams with different energies (Figure 1.1b).

In principle, the delivery of a higher dose to the tumour corresponds to a higher probability of success of the treatment, because a considerable quantity of energy can be deposited in abnormal cells and eventually damage the DNA double helix [3]. In reality, the physics of photons limits the applicability of this concept. In fact, photons interact in matter in many ways. In clinical applications, photoelectric effect, Compton effect and pair production are the most relevant ones and represent the major processes responsible for generating secondary charged particles (as electrons and positrons), which ultimately ionise and excite atoms and molecules in tissues [3]. As a result, radiation dose soon reaches a peak and exponentially decreases with increasing tissue depth (Figure 1.1a).

Even if advanced geometries of irradiation may be implemented and photons' energy can be modulated, selective deposition of radiation dose in depth is a difficult task. Therefore, a side effect of radiation therapy is the delivery of a non-negligible fraction of dose to normal tissues. Their tolerance and preventing the occurrence of toxic effects limit the radiation dose that can be used.

Within this scheme, it was not until 1946 that Wilson proposed the clinical use of accelerated protons for localised cancer therapy [4] [2]. The first treatment of humans was performed in the 1950s, while hospital-based proton facilities became feasible in the mid-1980s.

1.1.1 Hadron therapy

The physical limits of conventional radiation therapy can be overcome by hadron therapy. In particle physics, a hadron is a subatomic composite particle made of two or more quarks. Baryons, made of an odd number of quarks (usually three), and mesons, made of an even number of quarks (usually a quark and an antiquark), are the two families categorised as hadrons [3]. Ordinary matter mostly comes from two

hadrons: proton and neutron, which are baryons. In hadron therapy, dose is delivered to tumours through charged hadrons and ions (which are constituted by protons and neutrons) accelerated in particle accelerators.

Charged particles interact with matter in a very different way with respect to photons. For a striking charged hadron, the energy deposition per unit length inside a target material is well described by the Bethe-Bloch formula, which states that the projectile's energy deposition per unit length ($-dE/dx$) is proportional to its speed v and charge ze , and to the target's number density N and atomic number Z [34]:

$$-\frac{dE}{dx} = \frac{4\pi e^4 z^2}{m_0 v^2} N Z \left[\ln \left(\frac{2m_0 v^2}{I} \right) - \ln \left(1 - \frac{v^2}{c^2} \right) - \frac{v^2}{c^2} \right]$$

where m_0 is the electron rest mass, e the electronic charge, I the target's average excitation and ionisation potential and c the speed of light in vacuum. For hadrons at low energy, continuous electrons' *capture and loss* processes start to play a predominant role and Bethe-Block formula does not hold anymore. Based on this relation, the energy deposition versus tissue depth can be plotted. For high energy of the incoming charged hadron, little energy is deposited in the outermost tissue layers; instead, most of the deposition takes place just before it comes to rest, producing the so-called *Bragg peak*. As schematically drawn in Figure 1.1a, the Bragg peak is very narrow. The contrast with photons is evident: when treating a deep-seated tumour, less dose is given to proximal healthy tissues and almost null dose to distal cells.

One key concept at the base of hadron therapy is the possibility of depositing radiation dose to cover the whole tumour thickness by finely tuning hadrons' energy. In this way, a Spread-Out Bragg Peak (SOBP) is produced (Figure 1.1b). The downside of achieving a uniform deposition of radiation dose over the tumour depth is an increment of the proximal dose. Nevertheless, the fraction of dose delivered to healthy tissues remains favourable to hadron therapy, if compared to conventional radiotherapy. Passive (*shifters* of variable thickness and materials) and active (energy of the particle beam can be varied in the accelerator) systems can guarantee a correct energy modulation [3].

In addition, when charged hadrons propagate inside a medium, their path is not erratic, but straight until the slowing down process is completed. Strictly speaking, hadrons show low energy and spatial *straggling* [34]. This characteristic allows to highlight another physical advantage of ion beams for cancer treatment, that is the intrinsic ballistic precision of hadrons. Clearly, advances in *beam delivery*, i.e. the set of techniques and technologies that orient the beam over the patient's body, are essential to fully exploit this feature.

To reach deep-seated tumours, charged hadrons require to be accelerated to energies in the order of MeV u^{-1} , a fact that necessarily implies the use of modern, complex particle accelerators, resulting in the construction of facilities way more expensive than conventional radiotherapy compact LINACS (linear accelerators).

Moving to hadrons heavier than protons, lateral straggling and proximal dose deposition are further reduced, improving the dose distribution to the target area (Figure 1.1b). On the other hand, particle fragmentation increases the distal dose [3]. For heavy hadrons, biological advantages sum up to physical ones, in the sense that heavy ions show higher Radiobiological Effectiveness (RBE) and Oxygen Enhancement Ratio (OER) [4].

RBE is defined as the ratio of X-ray and particle dose producing the same biological effect (in terms of cell survival) [4]. It depends on the Linear Energy Transfer (LET), i.e. the energy per unit length [$\text{keV } \mu\text{m}^{-1}$] transferred to the medium by ionising radiation crossing it. A high LET guarantees an increased ionization density and, consequently, an increased probability of damaging the DNA double helix (*double strand break*), by which tumour cells are deactivated and killed. Fast moving, light ions have low LET, and RBE is nearly one. In contrast, slow, heavy ions are more effective than X-rays in killing cells in virtue of their high RBE. LET itself is not sufficient to fully characterise the response of cells to ionising radiations. Other dependencies of RBE are the dose, particles considered, target cells and their physiological parameters. Traditionally, RBE is studied with irradiation experiments on cell cultures.

When irradiated with photons or low-LET ions, cells manifest a different survival behaviour, depending on the presence or absence of oxygen. OER is defined as the ratio of radiation that produces the same cell survival under anoxic and oxic conditions, respectively [4]. For instance, for X-rays the OER ranges from 2.5 to 3; this means that a 2.5 to 3 times higher photon dose is required to kill oxygen-deprived cells with respect to irradiating the same cells in aerobic conditions. OER is reduced at high LET, approaching unity for $150 \text{ keV } \mu\text{m}^{-1}$ to $300 \text{ keV } \mu\text{m}^{-1}$. In this favourable situation, oxygen content in the tumour is less critical than in conventional radiotherapy, and hypoxic tumours can be treated without necessarily increasing the dose delivered.

In conclusion, the characteristics of hadronic interactions with matter attest Proton Therapy (PT) to offer high ballistic precision and superior control of undesired dose delivery to healthy tissues. For this reason, PT can represent a technical improvement for conformal therapy [4]. Heavier ions feature an additional set of biological advantages. Most of the clinical experience involves carbon, which has a range of about 20 cm at $300 \text{ MeV } \text{u}^{-1}$ in water, and can be used to treat deep tumours [3]. RBE is almost unitary at the entrance channel, and as high as 3 in the Bragg peak region; therefore, carbon ions guarantee a significantly higher cell death at the tumour location and the same complications in normal tissues than conventional treatment, or, from another viewpoint, the same cell survival fraction with a dose about three times lower. Superior OER, close to one, make re-oxygenation of tumour cells less critical and offer a potential breakthrough for the treatment of radiotherapy-resistant cancers.

On-topic aspects of the continuous research in hadron therapy, to mention a few, are the implementation of beams made of heavier ions, the possibility to address non-solid tumours, the treatment of cancers in non-static organs and tissues (e.g. follow precisely the chest cavity movement during breathing, to attack tumours in the thorax), advances in patient positioning, improvements and fast decision tools to draw up an always more dynamic and personalised treatment plan [3] [4].

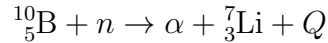
1.1.2 Boron Neutron Capture Therapy

Boron Neutron Capture Therapy (BNCT) is a kind of hadron therapy based on the use of neutron beams to irradiate tumours previously enriched in boron, using specific pharmaceuticals [3]. In its fundamental idea, BNCT consists in the exploitation of the nuclear capture reaction between thermal neutrons and isotope $^{10}_5\text{B}$ (20 % natural abundance) to damage, and eventually kill, tumour cells with the energy deposited in

tissues by the reaction products [3].

Historically, the foundation of this therapy goes back to the 1930s, when in few years the neutron was discovered (by Chadwick, 1932), the neutron capture reaction described (by Taylor and Goldhaber, 1935) and the intuition of exploiting the latter in human tissues for cancer treatment was proposed (by Locher, 1936) [3]. The first BNCT trials, instead, took place in the USA in the early 1960s. Since then, this therapy has undergone alternate acceptance and is far from conventional medicine [7].

The principal feature of BNCT is the ability to deliver the radiation dose selectively at the cellular level, in virtue of the reaction



which is characterised by a considerable cross section (3800 b) at neutron thermal energy (0.025 eV) and a *Q-value*, i.e. the reaction total energy release, of 2.79 MeV. The products of this reaction have a high LET (α particle, $\approx 150 \text{ keV } \mu\text{m}^{-1}$, ${}^7\text{Li}$ ion, $\approx 175 \text{ keV } \mu\text{m}^{-1}$) and can cause irreversible damage to the DNA, inactivating the cell where the reaction takes place. In tissues, the path lengths of these particles are in the range of 4 μm to 10 μm [7], so their energy deposition is limited to the diameter of a single cell. Hence, under the condition in which ${}^{10}\text{B}$ atoms selectively accumulate in the tumour, thermal neutron irradiation to the region can destroy malignant cells with a substantial sparing of the healthy surrounding tissues.

As said, BNCT can create a large dose gradient between normal and tumour cells; therefore, local recurrent tumours can receive dose while sparing pre-irradiated normal cells and tissues. This characteristic constitutes a relevant difference with respect to radiotherapy, for the reason that in conventional treatment re-irradiation is usually contraindicated because of severe adverse events in normal tissues. Recurrent tumours or with a poor response to traditional therapies such as surgery, γ -radiotherapy and chemotherapy are thus the best candidates to undergo BNCT. The first tumour treated was Glioblastoma Multiforme and, since then, head and neck cancers, melanoma, liver tumour were other diseases frequently tackled.

Successful BNCT mainly depends on the selective accumulation of ${}^{10}\text{B}$ in tumour cells. Two agents, boronophenylalanine (BPA) and borocaptate sodium (BSH), are currently used as boron carriers [6]. In general, the interaction of these pharmaceuticals with the human body, in terms of toxicity, pharmacokinetics, persistence in the tumour, selectivity, removal rate from healthy tissues represents an on-topic aspect of research [3] [6] [7].

The second aspect of great relevance is the production of an appropriate neutron radiation field, which is a fairly complex task. Over the past 60 years, about 15 different neutron facilities (all nuclear research reactor) have provided suitable thermal (0.025 eV) or epithermal (from 0.5 eV to 10 keV) neutron fields. More recently, the need of developing multi-institutional, large-scale clinical trials has brought to light hospital-based accelerators as alternative neutron sources (Figure 1.2), together with all the patient care possibilities of a modern hospital [6]. In addition, these machines are usually compact, known to hospitals' radiotherapy departments, rather simple to install and maintain; when the neutron field is not needed, they can be easily turned off; licensing process is easier and less expensive than nuclear reactors' one [7].

In accelerator-based Boron Neutron Capture Therapy (ab-BNCT), neutrons are yielded by a nuclear reaction between accelerated protons and a beryllium or lithium

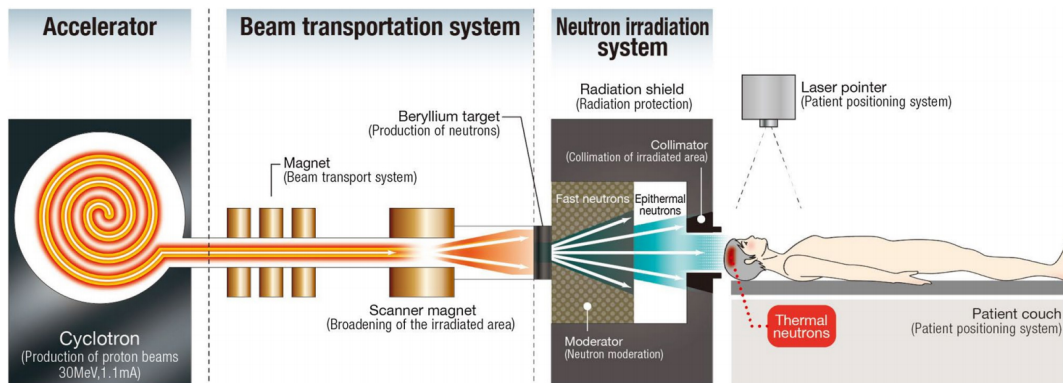


Figure 1.2. Schematic view of the accelerator-based Boron Neutron Capture Therapy (ab-BNCT) system, from reference [6]. In this case, protons are accelerated in a cyclotron and are directed onto a beryllium target.

target [6]. The greater control on the occurring nuclear reactions, together with neutron moderation, should *shape* the neutron beam and *tailor* it in energy in a more effective way than in nuclear reactors. For ab-BNCT, the most advanced programmes are currently found in Japan [7].

The shift from a reactor-based treatment to a hospital-based one should give rise, in the next years, to an improvement in the ability to gather clinical data, to make BNCT accessible to a larger number of eligible patients, and to possibly extend treatments to other types of tumour. In a not so distant future, constant research in boron carriers, radiobiology and accelerators may attest ab-BNCT as a reliable and effective treatment for cancer therapy [6] [7].

1.2 CNAO

Centro Nazionale di Adroterapia Oncologica (CNAO), an Italian acronym that stands for *Italian national Center for Oncological Hadron therapy*, is the only Italian facility that performs hadron therapy with both protons and carbon ions to treat tumours. In the world, only six centres are equipped to offer this feature [5]. CNAO is located in Pavia, conveniently close to hospitals, the city university campus and well linked to highways, to achieve and promote the transfer of knowledge and the creation of synergies and collaborations [8].

At CNAO, radio-resistant and surgically inoperable tumours are treated everyday in both adults and pediatric patients. Treatment sessions depend on various factors, such as the type of particle used, the type of tumour, its dimension and location; on average, they last from 2 to 7 weeks (one session per day, five days a week) [5]. For Italian citizens, hadron therapy is included in the list of treatments covered by the Italian National Health Service since 1 January 2014. The facility constitutes also a Research and Development Centre, with interests and activities from radiobiological to translational clinical research.

The history of this centre started with the publication of the report “For a centre of teletherapy with hadrons” in 1991, signed by Amaldi and Tosi [8]. After years of preparation, preliminary studies, research of qualified personnel, the signature of

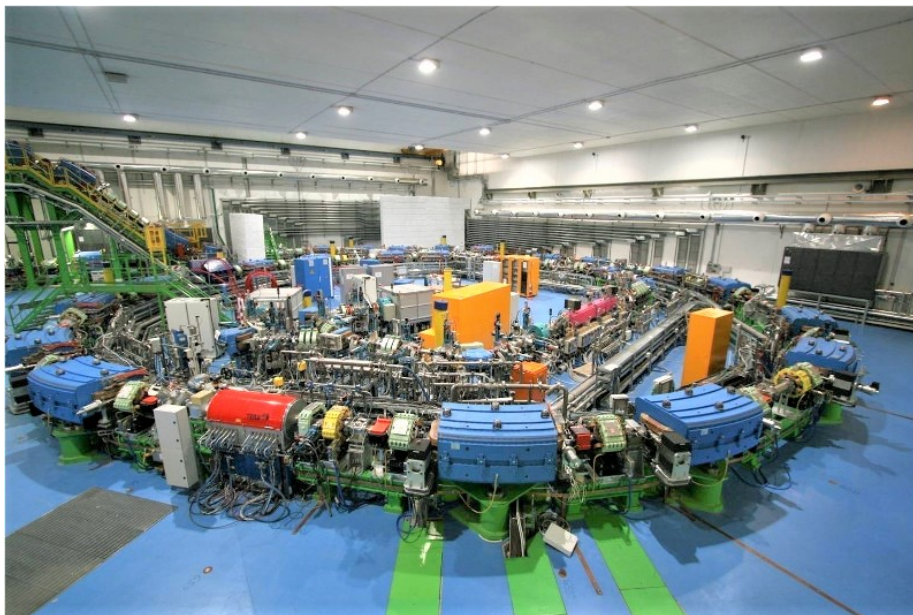


Figure 1.3. View of the CNAO synchrotron bunker. The accelerator is a circular ring with a diameter of 25 m and an 80 m circumference.

eminent collaborations (with universities and institutes) and fundraising, the laying of the first stone took place in 2005. Five years later, CNAO was inaugurated on the 15th of February 2010 and in 2011 the first patient concluded a proton therapy treatment. By the end of 2019, 2500 patients were treated in eight years of operations [5]. This clinical facility is financed by the Italian Ministry of Health.

1.2.1 Particle accelerator and therapy

To address the medical and clinical aspects of the treatment process, from the access through all the preliminary medical tests, a dedicated area of the facility was set to guarantee an organised and effective workflow. From an engineering and physical viewpoint, instead, the core of hadron therapy at CNAO is undoubtedly its synchrotron (Figure 1.3).

This machine can accelerate protons and carbon ions (C^{6+}), but further advances in treatments will allow using also other light ions (He^{2+} , Li^{3+} , Be^{4+} , B^{5+} , O^{8+}). Protons can be accelerated to energies from 60 MeV to 250 MeV, while carbon ions from 120 MeV u^{-1} to 400 MeV u^{-1} , thus allowing particles to cover a range in water up to 27 cm, with steps of 1 mm [8]. Therefore, in patients, deep-seated tumours can be reached without technical difficulties and dose can be deposited with high precision exploiting the SOBP (Section 1.1.1). CNAO's synchrotron was designed specifically for the purpose, starting as an inspiring prototype to become a model to imitate [5]. The particle accelerator is located in a 1600 m^2 bunker, shielded to protect visitors from radiation hazards. It is a circular ring with a diameter of 25 m and an 80 m circumference. Protons and carbon ions are extracted from two different source points, in which helium and carbon dioxide gases are brought to the state of plasma, by means of magnetic fields and radio frequencies. Billions of particles are *spilt* at each extraction and injected in the synchrotron ring after completing a multi-step

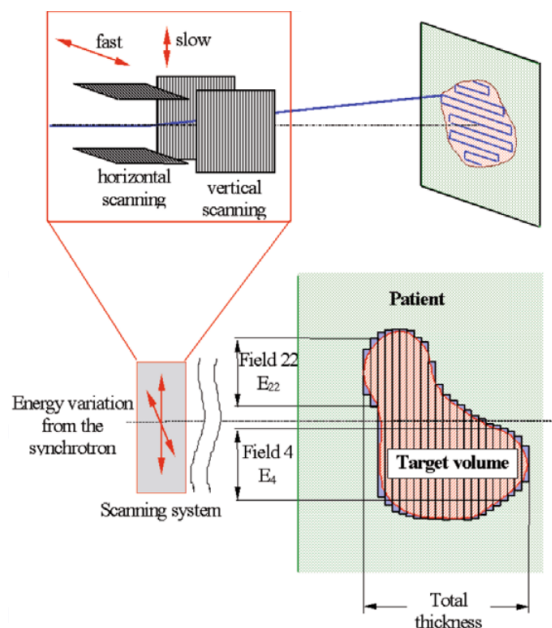


Figure 1.4. Schematic representation of the *active dose distribution system*.

process of acceleration of the beam. Inside the synchrotron, a resonant cavity further accelerates particles and several magnets keep the beam on the designed trajectory [8]. Eventually, when the desired beam energy is reached, particles are extracted from the ring in four different extraction lines of about 50 m and headed to three treatment and one experimental room. In the central treatment hall, both a horizontal and a vertical beam are directed; in the other rooms, only a horizontal beam is driven [8].

At CNAO, the curative beam is made impinging on the patient using the so-called *active dose distribution system*. The tumour is ideally divided into *slices*, i.e. regions that are reached by particles of the same energy, during the treatment plan. During hadron therapy sessions (usually a few minutes of irradiation), slices at increasing depth are reached by increasing the energy of the beam in the synchrotron. A sophisticated system of scanning magnets distributes particles to each tumour slice with an accuracy of $200\ \mu\text{m}$; in practice, the movement of the so-called *pencil-beam* resembles the technique used in cathode ray tube televisions for displaying images on screens (Figure 1.4).

Of course, monitoring and safety systems are spread all over the most critical points of the whole therapy chain [8] to guarantee an effective and safe treatment and to prevent radiation hazards in the facility. In regards to ionising radiations, the *radiation protection office* – the office at which this thesis work was developed – is responsible for supervising and maintaining up-to-date compliance with national regulation, designing facilities from a dosimetric viewpoint at any scale, ensuring the safety of CNAO’s workers and of the external population, adopting the methods of *Radiation Protection*, a discipline in which particle Physics, radioactivity and engineering are deeply interconnected.

1.2.2 Topography

As already mentioned, CNAO is located in Pavia, near hospital buildings and the city university campus. In the development of this work, accurate knowledge of the area was required, in order to critically discuss approximations and results of evaluations. In fact, models and methods implemented starting from Chapter 2 relied, in a certain way, on local topography and meteorological data.

Some information about the area was collected personally and using Google Earth (credits: *Google Earth Pro, version 7.3.3.7786.*) and was summarised in Figure 1.5 and Table 1.1 at the end of this Chapter.

From east to west, for some hundreds of metres, the area to the north of CNAO is mainly flat and wide open, occupied by car parks and fields. To the east, there are hospital Policlinico San Matteo's towers and buildings. Hence, in these directions, workers and visitors are the two categories of people primarily represented. To the south-east, blocks of flats (points B, C, E in Figure 1.5) offer some solutions to host visiting physicians and patients in need of accommodation during long therapies.

For motives explained later in the developing of this work, residential time around a facility that operates with ionising radiation is an important detail from a radiation protection viewpoint because it is related to *submersion dose* and *inhalation dose* quantities (Chapter 2).

1.2.3 Expansion project

On the 29th of October 2020, the City of Pavia approved an expansion project of CNAO [5]. A new, two-floors building of approximately 4000 m², funded and supported by some public institutions, will host a Proton Therapy (PT) and an accelerator-based Boron Neutron Capture Therapy (ab-BNCT), enlarging the number of possible treatments and the number of patients.

PT will feature a synchrotron built by Hitachi, while the ab-BNCT is the product of a collaboration between TAE Life Systems and Neuboron Therapy System, which decided to invest in research at CNAO and will cooperate in various aspects of the expansion plan. Strong synergy is already in place between the three companies, the radiation protection service and other offices, to guarantee the optimal completion of the project.

1.3 Concluding remarks and aim of this work

For the expansion project, as well as for the already operating synchrotron, the discharge of radioactive air is foreseen as a consequence of normal operations. In fact, when particle accelerators are run and treatments are performed in the dedicated rooms, several nuclear reactions are responsible for the production of radioactive isotopes, which must be removed to maintain indoor air safe from a radiologic viewpoint. This activity is classified as a *chronic release* and is part of the regular management of accelerator facilities (Chapter 2).

Generally, the in-air release of radioactive contaminants does not constitute a hazard for the population and workers [10]: safety and monitoring systems are accurately installed and careful designs are rigidly implemented. Moreover, a number

of steps prior to commissioning must be performed. These include radiation protection simulations and estimates, comparison with existing regulation and participation of several authorities, depending on the country. In addition, during operations or following relevant modification of the design project, recurring (on a yearly basis, or more) reports must be provided to the competent authority.

Without going into the details, in Italy all the major issues regarding ionising radiation are regulated by law. The recent Decreto Legislativo (D.Lgs.) 101/2020 [9], issued on the 31st of July 2020, implements the EU *Council Directive 2013/59/Euratom of 5 December 2013* laying down basic safety standards for protection against the dangers arising from exposure to ionising radiation. Part of an Italian *Expert in radiation protection's* job is to constantly guarantee the compliance of the supervised facility with current regulation, and hence, ultimately, with the mentioned D.Lgs.

The present M.Sc. thesis is inserted in the framework of hadron therapy at CNAO and air management at accelerator facilities, which are addressed from a radiation protection point of view. A generic computational method was developed for assessing the dose due to chronic release of radioactive air in the surrounding area of a hadron therapy facility and later applied – with a further refinement – to some realistic data that could fit the CNAO case study. The work is organised as follows.

In Chapter 2, all the theoretical concepts necessary to develop the subsequent evaluations are introduced. These include air activation at accelerator facilities, models for in-air transport of radioactive contaminants and a specific dissertation about the Gaussian Plume Model (GPM), on which all the evaluations are focused, introductory meteorological and radiation protection concepts.

In Chapter 3, two toolbox codes certified by the Department Of Energy of the United States of America (DOE) and available at CNAO's radiation protection office are presented and their algorithm for dose calculation is analysed. The limits of the software are underlined, also with reference to the literature. Lastly, the Monte Carlo transport code FLUKA is introduced as a possible solution for some of the issues mentioned above.

In Chapter 4, a generic simplified scenario is set in the codes. In FLUKA, the GPM is implemented in a user-written source routine and tested. Simulations are run and results are compared to verify the convergence of codes when the same underlying hypotheses are met in all of them. The proposed computational method is discussed in its results and main assumptions.

In Chapter 5, the results of a previous M.Sc. thesis are collected and summarised to give some realistic – yet conservative – data about CNAO operations and in-air releases. Later, real meteorological data about Pavia is gathered and elaborated using MATLAB.

In Chapter 6, the GPM previously developed is applied to CNAO, using data about the in-air release evaluated in Chapter 5. To model the variability that winds inevitably introduce in the dispersion of contaminants in the atmosphere, FLUKA results are exported to MATLAB and merged with the meteorological data analysis. The user-written code is discussed in its main steps, since it constitutes a generic approach to interface the Monte Carlo code findings with another programming language. Lastly, maps of the annual dose in the area surrounding emission stacks are plotted.



Figure 1.5. Aerial map of CNAO (highlighted in red) and the surrounding area. Placeholders are described in Table 1.1. Credits: *Google Earth Pro, version 7.3.3.7786*.

Table 1.1. Localisation and description of the placeholders contained in Figure 1.5. In the fourth column, distances are calculated from point S.

Symbol	Latitude	Longitude	Distance [m]	Description
S	45°12'04"N	9°8'40"E	-	Synchrotron emission stack
1	-	-	-	CNAO main entrance
2	-	-	-	Synchrotron bunker
A	45°12'01"N	9°8'38"E	127	Istituto Zooprofilattico Sperimentale
B	45°11'59"N	9°8'36"E	171	Apartment building
C	45°12'00"N	9°8'35"E	170	Apartment building
D	45°11'58"N	9°8'36"E	200	Avis comunale di Pavia
E	45°11'59"N	9°8'34"E	194	Apartment building
F	45°12'01"N	9°8'31"E	221	University of Pavia building
G	45°12'02"N	9°8'32"E	189	Nursing school
H	45°12'03"N	9°8'36"E	112	CNAO - High voltage control unit
J	45°12'04"N	9°8'47"E	159	Policlinico San Matteo - hospital
K	45°12'02"N	9°8'48"E	189	Policlinico San Matteo - hospital
L	45°12'02"N	9°8'45"E	143	Policlinico San Matteo - hospital
M	45°12'01"N	9°8'42"E	110	Policlinico San Matteo - hospital
N	45°11'58"N	9°8'41"E	182	Policlinico San Matteo - hospital

Chapter 2

Theoretical background

In this Chapter, the theoretical notions necessary to develop this thesis work are introduced. Four main topics are addressed: air activation at accelerator facilities, atmospheric dispersion models for the transport of contaminants, introductory meteorological concepts, fundamentals of radiation protection. In particular, in the last section, the units of measure adopted are briefly presented and discussed in the light of the up-to-date international guidelines.

2.1 Air activation at accelerator facilities

Air activation is an on-topic aspect of radiation protection at accelerator facilities. In this sense, reference [10] by National Council on Radiation Protection and Measurements (NCRP) represents a comprehensive work to address this issue. Regarding Centro Nazionale di Adroterapia Oncologica (CNAO), other documents have been produced in the early stages of its design phase [29] [35]. In the development of the theoretical background, air activation constitutes the first logical step, because it encloses the physical phenomena at the base of the production of radioactive contaminants.

When particle accelerators are operated, two sources of radiation may constitute a potential hazard for the environment: prompt radiation and induced radioactivity [10]. The first one exists only when the accelerator is operating and fades out at its turning off. Its characteristics strongly depend on the type and energy of the particle being accelerated. In an ideal case, accelerated particles follow well-defined trajectories. In reality, parasite radiation is generated by an incomplete deflection of accelerated particles, which lose the designed trajectory and hit accelerator structures and ancillary components (*beam losses*), or by the contact of the beam with air in treatment and experimental rooms. Here, in fact, the beam is extracted (or *spilt*) from the vacuum accelerating line and crosses a finite length (about 1 m) before colliding on patients or experimental targets.

Induced radioactivity, in contrast, is defined as the radiation originated by the decay of unstable isotopes generated in the accelerator structure and its ancillary components by the particle beam, or by prompt radiation itself. Induced radioactivity represents a hazard for several reasons, depending on the physical state of the activated material [10]:

- Solids: accelerator structure and other components may become radioactive and

be a potential source of dose to workers during maintenance and decommissioning; also, components and shielding must be managed carefully for a correct release or disposal of materials.

- Gases and liquids: air and water can become radioactive and, in absence of a proper containment system, might be released into the environment because of their high mobility.

As a further classification of prompt radiation, primary and secondary particles may be distinguished. The first ones represent the nuclear species that is accelerated. The second, instead, is the product of immediate nuclear reactions fed by beam losses, or by the beam crossing air in treatment and experimental rooms [29].

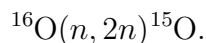
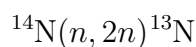
2.1.1 Radionuclides produced in air

Interaction of primary and secondary particles directly with air's constituent nuclei represents the main source of airborne radioactivity. In this sense, this physical phenomenon is described by the general formula of the activation process, in which the produced specific activity (activity per mass unit) is proportional to the target atomic density, the incoming particle flux and the reaction cross section, with an increasing production in time governed by the radionuclide decay constant. A simplified formulation (average cross sections, mono-energetic flux, simplified target geometry) can be given [29] [11] [25], while an exhaustive investigation of the process requires more advanced computational techniques, such as Monte Carlo codes (one is presented in Chapter 3).

To a lesser degree, secondary sources of airborne radioactivity are dust (formed by natural erosion and wear, or by work on radioactive accelerator components) and emission of gaseous radioactivity from liquids irradiated in the accelerator environment. These two contributions are not considered in this work.

Generally speaking, the radionuclides of significance for environmental contamination are ^3H , ^7Be , ^{11}C , ^{13}N , ^{15}O , ^{41}Ar [10] [35]. Except for the first two, all the listed isotopes show a short or medium half-life (seconds to days). These can undergo a significant decay in the time required for their discharge. At CNAO, it was calculated that about 81 % of the airborne activity produced in the synchrotron bunker has a half-life longer than 1.5 min [29] [28]. From a radiation protection point of view, this fraction requires the implementation of countermeasures, while it is clear that the remaining part (19 %, with half-life less than 1.5 min) can be managed imposing a waiting time before access to the accelerator environment is permitted.

At hadron therapy centres, most radionuclides are produced by spallation reactions [10] [35] [36]. Activation may be imputed also to high-energy secondary neutrons, which interact with energies above production thresholds of approximately 20 MeV with air target constituents via other spallation reactions, e.g.:



A particular mention should be given to ^{40}Ar : despite its low abundance in air (0.93 % by volume), this isotope shows a relevant cross section at ambient temperature

(660 mb) for the thermal neutron capture reaction



Thermal neutrons may be generated as secondary radiation (or as thermalization of secondary high-energy neutrons); moreover, they play a crucial role in Boron Neutron Capture Therapy (BNCT), where they emerge as a result of the thermalization of epithermal neutrons, generated for treatment purposes.

2.1.2 Ventilation system

Without a ventilation system, radioactive air confined inside the accelerator bunker is not released to the environment during accelerator operations. On the other hand, a rather high concentration of radioactive gases may accumulate inside the enclosure and would prolong the waiting time before entry is permitted. In reality, an air ventilation system is normally installed, mainly for cooling purposes. The air change rate allows keeping the production of high concentrations of radioactive gases with long half-lives as low as possible [10].

At CNAO, an air ventilation system forces air circulation inside experimental and treatment rooms and synchrotron bunker. Air change allows reducing in-air radioactivity to be compliant, at worst, with the maximum allowed activity concentration inside closed environments, i.e. 1 Bq g^{-1} (CNAO's internal recommendations). Three parallel lines extract air from the experimental room, the synchrotron bunker, and the three treatment rooms together, and lead to absolute filters. In each branch, a safety system - EGAM (Enhanced Gaseous Activity Monitor) manufactured by Technology Nuclear Electronics - is installed [28]. This continuously operates to detect the presence of radionuclides not stopped by filters. A potential passing of the activity concentration clearance level would be detected and would stop all operations. Eventually, the air is discharged through emission stacks.

The equations that describe air activation and discharge in presence of a ventilation system are presented in Chapter 5.

2.2 Atmospheric dispersion models for the transport of contaminants

Atmospheric dispersion models are a mathematical description of the physical and chemical governing processes of transport, dispersion and transformation of pollutants in the atmosphere. Their major goal is the ability to estimate downwind air pollution concentrations, once a contaminant release (in normal operations or accidental scenarios) has occurred, in the most complete way possible. An atmospheric dispersion model relies on the knowledge of, at least, four elements [11] [12]:

- Emission model: individuation of sources, temporal and spatial emission rates, physical characteristics of the emission (e.g. effluent temperature and velocity), influence of structures and buildings in the proximity of stacks.

- Meteorological model: assessment of the local meteorological conditions, their effect on the transport of contaminants (e.g. vertical mixing, dispersion, deposition), relevant topographic information (urbanized or rural terrains, presence of mountainous elevations).
- Chemical (and nuclear) model: knowledge about pollutants, their characterization, possible interactions in air, nuclear data (for radioactive isotopes).
- Receptor model: individuation of the final receptors' position and characteristics, their interaction with pollutants, and modelisation of the health or environmental impact.

As said, the correct use of this information inside a transport model allows estimating the concentration of contaminants measured at receptors. One important aspect of in-air dispersion models is the fact that industrial facilities are required to obtain permits to emit pollutants into the atmosphere. Atmospheric dispersion models are used to demonstrate compliance with local regulations in terms of environmental impact [12]. In radiation protection, this translates primarily in evaluating the dose due to the release of radioactive pollutants in the areas affected by the contamination.

Usually, a more accurate description is achieved by increasing the degree of detail of the model, and the number of parameters and physical processes taken into account. Intuitively, the time required to obtain results is destined to augment, too. This increased complexity was largely made possible by the development of computers and numerical methods. Reference [37] provides a review of the considerable number of dispersion models available in the literature. Contextually, a list of the most representative corresponding software implementations is given. Over the years, in fact, many public institutions, like the Department Of Energy of the United States of America (DOE), Lawrence Livermore National Laboratory (LLNL), Pacific Northwest National Laboratory (PNNL), National Atmospheric Release Advisory Center (NARAC), Environmental Protection Agency (EPA), International Atomic Energy Agency (IAEA) and private developers have provided toolboxes and guidelines for the use of atmospheric dispersion models.

Historically, in the past 50-60 years a transition from analytical to computational codes was observed. Gaussian Plume Models (GPMs) were largely diffused starting from the 1960s and 1970s; in the 1980s - 1990s, Lagrangian-puff models and random walk models were introduced. From the 2000s, the development of Computation Fluid Dynamics (CFD) techniques was received also in risk assessment, emergency response and radiation protection methods. As a hint, the biggest effort in pursuing finer modeling of dispersion has regarded the complexities of turbulence and local meteorological conditions, since they are inevitably correlated to the presence of buildings and urbanization in general, specific microclimates, low or null wind speed, in contrast with macro-scale meteorology and average variables [37]. In analytical models, empirical and semi-empirical corrections and parameterizations were progressively added to address the challenges cited above. Anyway, the transition to CFD should not be taken for granted, since field experiments for code validation are not simple and the necessary computational resources might be large [37].

To sum up, each model involves a set of trade-offs. Average and conservative results of a simpler analytical model may be adequate in an emergency scenario or for

initial *upper-bound* estimates, while high temporal and spatial resolution CFD models for complex topographies may be necessary for detailed *past accidents* or *prognostic* studies.

2.2.1 Gaussian Plume Model

The Gaussian Plume Model (GPM) is one of the most consolidated models for the atmospheric dispersion of contaminants. Historically, it was also one of the first to be extensively exploited for dispersion evaluations: its origin is found in works by Sutton (1932), Pasquill (1961, 1974), and Gifford (1961, 1968) [13]. Nowadays, this model remains at the core of most regulatory models and certified software for risk assessment, emergency scenario and health impact evaluations following chronic and accidental releases of radioactive contaminants (Chapter 3), because of its considerable agreement with experimental data, the ease to perform calculations on its equation, its consistency with the random nature of turbulence [13]. Its widest application is for short-term (hourly, daily) as well as long-term (seasonal, annual) steady release rates, for both radioactive and stable gases and particulate matter.

The GPM is the steady-state solution to the Fickian diffusion equation, assuming constant wind speed, wind direction and mass diffusivity for a point source emission. If an activity release rate is given in input, the model returns the activity concentration χ , in $[\text{Bq m}^{-3}]$, for a point located in space:

$$\chi(x, y, z) = \frac{Q}{2\pi\sigma_y(x)\sigma_z(x)u} \exp\left(-\frac{y^2}{2\sigma_y^2(x)}\right) \exp\left(-\frac{\lambda x}{u}\right) \left[\exp\left(-\frac{(z-H)^2}{2\sigma_z^2(x)}\right) + \exp\left(-\frac{(z+H)^2}{2\sigma_z^2(x)}\right) \right] \quad (2.2)$$

where Q is the source strength in $[\text{Bq s}^{-1}]$, H the effective release height in $[\text{m}]$, u the mean wind speed at release height in $[\text{m s}^{-1}]$, $\sigma_y(x)$ and $\sigma_z(x)$ the lateral and vertical dispersion coefficients, respectively, in $[\text{m}]$. If the pollutant is radioactive, the activity concentration distribution can be modified considering the nuclear decay $\exp(-\lambda x/u)$ term, where λ is the isotope decay constant in $[\text{s}^{-1}]$. Actually, H , u , $\sigma_y(x)$ and $\sigma_z(x)$ are complicated functions of other parameters, such as temperature (external and of the emitted contaminated gas), the velocity of emission, stack diameter and meteorological conditions [11]. The major transport direction due to the wind is usually chosen to lie along the x -axis; there, mass transfer due to bulk motion far out shadows the contribution due to mass diffusion, which in fact is not considered in Equation (2.2). The y -axis is usually named the *cross-wind* axis and is perpendicular to the downwind axis, extending horizontally. The z -axis is the height above ground, which is assumed to be flat and uniform (Figure 2.1a).

The instantaneous concentration of pollutants is irregular since governed by turbulence. The key concept of this model is that the same spatial concentration, if observed for a sufficiently long time, is properly described by two Gaussian distributions in both vertical and cross-wind directions [11] [13]. Other fundamental aspects of the GPM are briefly summarised:

- Dispersion coefficients $\sigma_y(x)$ and $\sigma_z(x)$ represent the standard deviations of the two Gaussian distributions. They are expressed in function of downwind distance

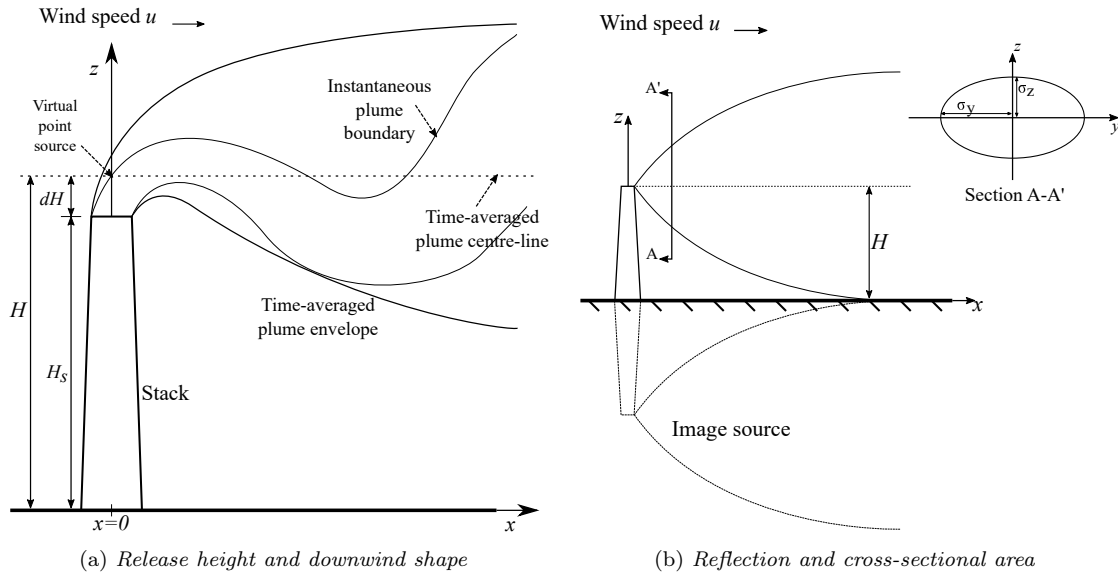


Figure 2.1. Schematic representation of the Gaussian Plume Model (GPM) and main figures of merit (adapted from reference [13]).

x , because their value depends on the progressive spread of contaminants being transported.

- Dispersion coefficients $\sigma_y(x)$ and $\sigma_z(x)$ depend also on meteorological conditions of the atmosphere (Section 2.3.4).
- The plume is totally reflected upon contact with the ground. Figure 2.1b shows this principle schematically: an image source at distance H is placed beneath the ground surface [13].
- Constant meteorological conditions - uniform wind speed, direction and turbulence throughout the entire plume - are assumed. Even though wind speed does vary in the three coordinate directions, the variation is relatively small, making it appropriate to hypothesize a constant u [12].
- In general, *static* scenarios are well represented. In Section 3.2.2, a GPM designed for non-constant wind directions is discussed.

In Equation (2.2), a null wind speed $u = 0$ would make the GPM diverge. Even if it is possible to measure null wind speeds with anemometers near the surface, considerable experience teaches that winds in the planetary boundary layer very seldom stop entirely. For this reason, calm winds are usually defined as a slight drift of $u = 0.5 \text{ m s}^{-1}$ [13].

The last quantity that affects the atmospheric diffusion in the GPM is the effective release height (H), which is reported to be one of the biggest sources of uncertainty [11]. In this parameter, in fact, near-emission turbulence effects, buildings influence on the airflow, characteristics of effluent and release (*source effects*) and *plume rise* (low pressure in the wake of the stack may cause the plume to be drawn downward) are condensed using empirical relations [13]. In general, a plume rise dH (positive or negative) is added to the emission height given by the stack (H_s) to give the effective

release height (H): $H = H_s + dH$. Plume downwash can be significantly limited if the efflux velocity is greater than 1.5 times the wind velocity. References [13] and [11] include a detailed discussion about source effects and plume rise.

In this work, the effective release height was arbitrarily set because the investigated methods regarded first and foremost the radiation protection point of view, and consequently radiation transport and dose evaluations, in a way as generic as possible. In this context, an accurate estimate of the effective release height would have resulted to be site-specific and required design data about the ventilation system (which, for instance, in the CNAO expansion project were not yet defined at the time of this writing). Nevertheless, it must be stated that in a final design phase, also this quantity should be evaluated, accurately considering buildings and topography in the proximity of the emission stack.

2.3 Introductory meteorological concepts

As stated in the previous Section, the GPM spread and shape vary in response to meteorological conditions. For this reason, in the following, some introductory meteorological concepts are given. These conclude the treatise of the GPM, introducing the atmospheric stability classes and Briggs' dispersion coefficients. In Chapter 5, CNAO local meteorological data are analysed from this starting point.

2.3.1 Wind

Wind inevitably affects the dispersion of pollutants. Wind speed and wind direction, as well as temperature, temperature difference, humidity, precipitation, pressure, and solar radiation are considered primary variables, in that they are generally measured directly *in situ* with proper instruments [38].

Wind direction is generally defined as the orientation of the wind vector in the horizontal [38]. For meteorological purposes, wind direction is defined as the direction *from* which the wind is blowing, and is measured in degrees clockwise from true north (N). In Figure 2.2, wind directions and corresponding angles are showed. Furthermore, wind sectors are labelled with a progressive number, starting from the east. This alternative nomenclature was adopted in this work to ease the data manipulation developed in the next Chapters.

Wind speed appears in the denominator of the equation of the steady-state GPM, where it determines the amount of initial dilution experienced by a plume. Moreover, as briefly mentioned in the previous section, wind speed is used in the evaluation of plume rise in point source releases and to quantify aerodynamic effects in downwash calculations. Lastly, anticipating what is discussed in Section 2.3.3, it is used in the determination of atmospheric stability classes.

Calms, periods with little or no air movement, represent one limiting factor for GPM and require special treatment. In fact, being the wind speed in the denominator of Equation (2.2), a null value would lead to an infinite concentration. In literature, some non-steady-state model, such as CALPUFF, were prepared to overcome this issue. EPA recommends that wind speeds less than 1 m s^{-1} be reset to 1 m s^{-1} for use in steady-state dispersion models, to avoid unrealistically high concentration estimates

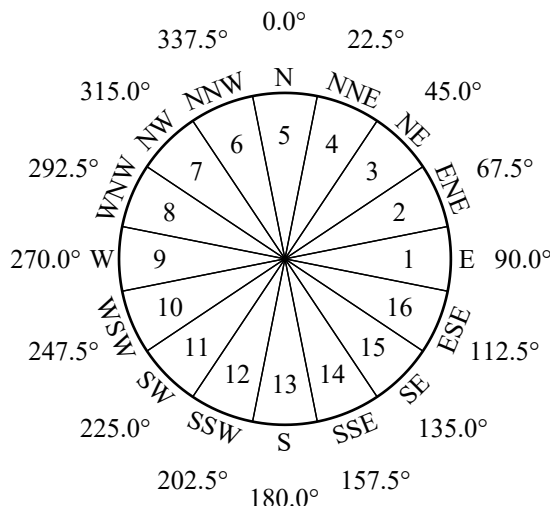


Figure 2.2. Wind directions and corresponding angles and sector numbers. Wind direction is defined as the direction from which the wind is blowing. Correspondence between directions and angles follows the usual convention, while sector numbers were introduced in this work for computational reasons.

at low wind speeds. Wind speed 1 m s^{-1} is often reported to be a conservative value used in the validation of these models [38]. From a technical viewpoint, a calm occurs when the wind speed is below the sensitivity of the measuring instrument, such as an anemometer. In the case of CNAO, this was registered to be 0.4 m s^{-1} (Chapter 5).

2.3.2 Solar radiation

Solar radiation is another primary variable and plays an essential role in the determination of atmospheric stability classes (Section 2.3.3). Solar radiation refers to the electromagnetic energy in the solar spectrum, commonly classified as ultraviolet, visible light, and near-infrared radiation. Usually, data are given in $[\text{W m}^{-2}]$ [38].

2.3.3 Atmospheric stability classes

Atmospheric stability is an example of derived variable, i.e. a quantity whose value depends on primary meteorological variables [38]. Firstly, atmospheric stability is linked to the vertical temperature gradient (also known as *standard lapse rate*) [11]. In the atmosphere, this is equal to $0.0065 \text{ }^\circ\text{C m}^{-1}$ (a decrease of $0.65 \text{ }^\circ\text{C}$ every 100 m), but local meteorological conditions can significantly alter this value and, as a consequence, the shape of a plume, because the movement of masses of air released to the environment is physically related to the atmospheric conditions. Qualitatively, this is the reason for *looping*, *coning*, *fanning*, *lofting* conditions in a plume, which are extensively illustrated in literature [11] [13] [12].

To facilitate estimates in air quality dispersion modeling, atmospheric stability is identified by classes of stability, which represent a qualitative indicator of atmospheric turbulence [11]. In a general way, a letter (or a number) is used to classify the stability of the atmosphere on the basis of some measured meteorological quantities. Class A (or 1) is the most unstable category, in which contaminants are quickly dispersed in the

Table 2.1. Atmospheric stability classes and corresponding qualitative description of atmospheric conditions. In the literature, a further stability class G is occasionally added to classify an extremely stable atmosphere [11].

Stability class	Atmosphere
A	Extremely unstable
B	Moderately unstable
C	Weakly unstable
D	Neutral
E	Weakly stable
F	Moderately stable

air. Class F , in contrast, represents a very stable atmospheric condition, unfavourable for an effective spread of pollutants. Stability classes are listed in Table 2.1. In the literature, a further stability class G is occasionally added to classify an extremely stable atmosphere [11].

Atmospheric stability classes represent a useful and important variable in dispersion modeling, for the reason that lateral and vertical dispersion parameters – i.e. vertical and lateral standard deviations of the Gaussian distributions describing the pollutants concentration inside the plume, $\sigma_y(x)$ and $\sigma_z(x)$ – are frequently estimated with a diagram based on this classification.

The first framework was proposed by Pasquill in 1961. Pasquill’s categorization is based on surface wind speed, daytime insolation and nighttime cloud cover and is traditionally implemented with Turner’s method for routine applications (a detailed focus about this can be found in reference [38]). EPA considers Turner’s method to be the benchmark procedure for determining Pasquill-Gifford (P-G) stability [38].

When representative cloud cover and ceiling data are not available, it is possible to adopt the Solar Radiation Delta-T (SRDT) scheme, as was done in Chapter 5. This method maintains the basic structure and rationale of Turner’s method but uses daily solar irradiation and night vertical temperature gradient in combination with surface layer wind speed (measured at 10 m above the ground) to produce the categorization. Table 2.2 shows the details of this method. Literature about atmospheric stability classes models is wide; again, reference [38] by EPA critically summarises many of them.

2.3.4 Briggs’ coefficients for dispersion modeling

Dispersion coefficients $\sigma_y(x)$ and $\sigma_z(x)$ determine the dispersion of contaminants in the atmosphere. Their value depends on meteorological conditions and downwind distance x at which they are evaluated. For their estimate, turbulence measurements should be preferred [13]. However, in the absence of this data, it is common practice to refer to Pasquill, Gifford and Turner’s work for atmospheric stability categorization and Briggs’ studies for in-air diffusion. In reference [15], the author proposed a parametrization for dispersion coefficients for all Pasquill’s atmospheric stability classes. Briggs produced tables and graphs for downwind distances in the range (1×10^1 m, 1×10^4 m), and emphasized the goodness of this approximation to existing published curves for rural sites in the range (1×10^2 m, 1×10^4 m), which is the usual interval considered for its

Table 2.2. Solar Radiation Delta-T (SRDT) method for estimating Pasquill-Gifford (P-G) atmospheric stability categories. Nighttime refers to the period from one hour before sunset to one hour after sunrise [38].

Daytime				
Wind speed [m s^{-1}]	Solar Radiation [W m^{-2}]			
	≥ 925	925 - 675	675 - 175	< 175
< 2	A	A	B	D
2 - 3	A	B	C	D
3 - 5	B	B	C	D
5 - 6	C	C	D	D
> 6	C	D	D	D
Nighttime				
Wind speed [m s^{-1}]	Vertical Temperature Gradient [$^{\circ}\text{C}$]			
	< 0	≥ 0		
< 2.0	E	F		
2.0 - 2.5	D	E		
≥ 2.5	D	D		

algebraic implementation [16]. This, for both open-country and urban conditions, has the form:

$$\sigma_y(x) = a_y x (1 + c_y x)^{d_y} \quad (2.3)$$

$$\sigma_z(x) = a_z x (1 + c_z x)^{d_z} \quad (2.4)$$

where x is the downwind distance and the other parameters are listed in Table 2.3.

In this M.Sc. thesis, Briggs' parametrization was assumed to be reliable starting from 10 m downwind the release point. This was due to the choice of neglecting source effects (which affects the shape of the plume near the release point) and performing calculations in extremely stable atmospheric conditions (a fact that, in any case, resulted to be credible after the meteorological analysis developed in Chapter 5). For computational necessities, in Equations (2.3) and (2.4) downwind distances lower than 10 m were used. In the discussion of results, this approximation is remarked. The upper-bound limit of applicability (1×10^4 m), instead, was never approached nor questioned.

Briggs' parametrization is one of the most used methods for the calculation of dispersion coefficients because of the satisfactory results it has shown and its simple use. However, care should be given in theoretical extrapolations for applications to problems outside the area of their derivation (e.g., complex terrain, distances greater than 10 km, effective release heights of above 100 m, and other [13]); in this case, direct turbulence measurements or other methodological approaches may result more adequate [37] [13] [16].

To summarise, the main figure of merits of the GPM considered in this work are listed:

- bulk motion of contaminants is given by wind along the downwind axis;
- plume spread results primarily by molecular diffusion;

Table 2.3. Briggs' coefficients for relations (2.3) and (2.4) in open country and urban conditions and various atmospheric stability classes [11].

P-G category	σ_y [m]			σ_z [m]		
	a_y	c_y	d_y	a_z	c_z	d_z
Open-country conditions						
A	0.22	0.0001	-0.5	0.20	0	1.0
B	0.16	0.0001	-0.5	0.12	0	1.0
C	0.11	0.0001	-0.5	0.08	0.0002	-0.5
D	0.08	0.0001	-0.5	0.06	0.0015	-0.5
E	0.06	0.0001	-0.5	0.03	0.0003	-1.0
F	0.04	0.0001	-0.5	0.016	0.0003	-1.0
Urban conditions						
A - B	0.32	0.0004	-0.5	0.24	0.001	0.5
C	0.22	0.0004	-0.5	0.20	0	0
D	0.16	0.0004	-0.5	0.14	0.0003	-0.5
E - F	0.11	0.0004	-0.5	0.08	0.0015	-0.5

- horizontal and vertical pollutant concentrations in the plume are normally distributed;
- source effects and plume rise are neglected;
- plume spread and shape vary in response to meteorological conditions;
- wind speed and direction are assumed to be constant;
- plume spread is described by Briggs' dispersion coefficients.

2.4 Fundamentals of radiation protection

Dose evaluations for in-air releases require taking into account all the possible pathways that radionuclides may follow. Firstly, a population is irradiated by direct exposure to the radioactive cloud (external irradiation) and by inhalation of the contaminated air (internal irradiation). Except for gaseous materials, pollutants eventually reach the ground and vegetation by wet and dry deposition, i.e. the processes of accumulation on soil surface caused by rain, air motion, gravity, chemical and physical interactions. From there, radionuclides still contribute to external irradiation. From vegetation, radioactive materials may enter the food chain and become a further source of internal contamination by ingestion. Lastly, deposited material can be re-suspended in the air again, increasing the inhaled dose contribution [25].

It is clear that the variety of possible pathways (and their combinations) produces a complex interconnection of models. Specific software like GENII V2.10 (Chapter 3) offers a valid set of tools for dose evaluations in chronic and emergency release scenarios.

2.4.1 Dose contributions

All the mentioned pathways are widely addressed in literature. For instance, references [11], [25] and [39] give an overview of the various processes and provide some useful calculations for modeling some external irradiation geometries analytically. References [18] [19] [17] show how pathways are implemented in software for dose evaluation. For the purpose of this work, it is of interest to develop the concepts of external irradiation from submersion in a radioactive cloud and direct inhalation of radioactive contaminants, because pollutants considered in the following all come in gaseous form.

Inhaled dose (*equivalent dose*) at a receptor point, expressed in [Sv] is given by references [11] [25]:

$$D = C R e(50) t \quad (2.5)$$

where C is the in-air activity concentration at the receptor position in [Bq m^{-3}], R the human breathing rate ($R = 1.2 \text{ m}^3 \text{ h}^{-1}$), $e(50)$ the committed equivalent dose conversion coefficient provided by International Commission on Radiological Protection (ICRP) publication 119 (and its updates) in [Sv Bq^{-1}], and t the time of exposure in [s].

External exposure to a radioactive cloud depends on the ability of ionizing radiation to penetrate the human body. In fact, the energy and nature of the radiation determine its range inside tissues and organs. In general, photons manifest the highest penetrating capabilities, while energetic electrons and positrons can be a significant source of dose to the skin.

In the literature, a considerable number of publications suggest analytical models for external dose evaluations for simple geometries of irradiation (for instance, [40] [22]). Other references, instead, starting from an activity concentration χ in [Bq m^{-3}] (obtained, for instance, with a GPM), evaluate the dose using a Dose Conversion Factor (DCF), expressed in [$\text{Sv Bq}^{-1} \text{ m}^3$] [11] [23]:

$$D = \chi DCF \quad (2.6)$$

This methodology is widely spread – it is adopted also in the software used in this work – and is based on the *semi-infinite cloud* approximation. This feature will be addressed in greater detail in the next Chapter.

2.4.2 Radiation protection and dosimetric quantities

In this thesis work, dose evaluations were managed considering the ICRP standards. Anticipating what is explained in detail in Chapter 3, software HotSpot and GENII V2.10 were designed in the US with the guideline provided by EPA in the set of Federal Guidance Reports (FGRs), which summarise ICRP recommendations. In particular, ICRP Publication 60 [41] is the most recent publication implemented in the available software. In FLUKA, both reference [42] and ICRP 60 results were implemented. In this Section, the main quantities used in this work are briefly presented.

Protection quantities

The equivalent dose, H_T , in a tissue or organ, T , is given by:

$$H_T = \sum_R w_R D_{T,R}$$

where $D_{T,R}$ is the average absorbed dose from radiation R , in tissue T [42]. The radiation weighting factor w_R takes into account the nature of radiation R and is tabulated for photons, electrons and muons, neutrons (in energy intervals), protons, alpha particles, fission fragments and heavy nuclei. In fact, each type of ionizing radiation has a different ability to cause biological damage, and equal absorbed doses from two different types of radiation may produce very different effects on organs or tissues of the human body [41].

The effective dose, E , is the sum of the weighted equivalent doses in all the tissues and organs of the body [42]:

$$E = \sum_T w_T H_T$$

where H_T is the equivalent dose previously defined in tissue or organ T and w_T the correspondent tissue weighting factor (tabulated). H_T and E are not directly measurable, but may be calculated if irradiation conditions are known using some conversion coefficients [42]. In Section 4.2.4, this procedure is used to estimate E starting from a fluence of particles, in the framework of a simple model for dose evaluation.

The sum of dose contributions from external (submersion, ground shine, resuspension) and internal material (inhalation) is called Total Effective Dose (TED). This nomenclature is adopted in HotSpot and GENII V2.10 software manuals (Chapter 3).

Operational quantities

Since $D_{T,R}$ cannot be evaluated experimentally, International Commission on Radiation Units and Measurements (ICRU) proposed the use of some operational quantities: ambient dose equivalent, directional dose equivalent, and personal dose equivalent [42] [43]. For strongly penetrating radiation, the ambient dose equivalent should be used. The definition given by ICRU is [43]:

The ambient dose equivalent, $H^*(d)$, at a point in a radiation field, is the dose equivalent that would be produced by the corresponding expanded and aligned field, in the ICRU sphere at a depth, d , on the radius opposing the direction of the aligned field.

Currently, the recommended value for d for penetrating radiation is 10 mm. The unit of measurement is the sievert (Sv). In Chapter 6, evaluations are performed in terms of $H^*(10)$.

Lastly, it should be mentioned that ICRP 60 [41] is not the most recent set released by the Commission: ICRP Publication 103 [44] is newer and presents a further development about the concept of w_T . In ICRP 60, tissue weighting factors were specified for twelve tissues and organs plus the “remainder” in the form of relative values. Their sum is equal to one, with the consequence that a whole body uniform

dose distribution numerically equals the equivalent dose in each organ and tissue of the body. In ICRP 103, the updated methodologies for tissue weighting factors calculation led to changes in w_T for breast (from 0.05 to 0.12), gonads (from 0.20 to 0.08) and remainder tissues (from 0.05 to 0.12). Brain and salivary glands were explicitly quantified with a value of 0.01. Italian legislation Decreto Legislativo (D.Lgs.) 101/20 is currently based on this publication.

Chapter 3

Software

In this Chapter, two computer codes for modeling in-air transport of radioactive contaminants and dose evaluation are presented. The main features and hypotheses of each software are listed, with a special focus on the *semi-infinite cloud approximation*. It is also shown how this critical discussion leads to the necessity of implementing a transport model also for radiation, in order to overcome the limits of the software considered. For this reason, a Monte Carlo transport code is presented in the last part of the Chapter.

3.1 HotSpot

HotSpot is a PC-based atmospheric dispersion software package for rapid assessments of the downwind hazard caused by radiological releases [17]. It is fast-running and field-portable, two characteristics that make it suitable for emergency evaluations. Results are conservative and reliable in near-surface release scenarios and for downwind distances not greater than 10 km.

This software is developed and maintained by National Atmospheric Release Advisory Center (NARAC) at Lawrence Livermore National Laboratory (LLNL). In 2010, HotSpot V2.07.01 was approved by the Department Of Energy of the United States of America (DOE) to be listed in the *Safety Software Quality Assurance - Central Registry*, i.e. a list of toolbox codes that has been tested against DOE *Safety Software Quality Assurance* requirements [20]. Codes of the Central Registry are rigidly analysed and documented, in order to support safety analyses and safety evaluations for DOE nuclear facilities and their operation. HotSpot was available at Centro Nazionale di Adroterapia Oncologica (CNAO) radiation protection service and was previously used in a recent M.Sc. thesis for preliminary evaluations about contaminants in-air dispersion [28]. For these reasons, HotSpot was studied and used as a starting point in this thesis work.

HotSpot implements a Gaussian Plume Model (GPM) and can take into account simple meteorological conditions (atmospheric stability, wind direction and intensity), surface type and roughness, deposition of contaminants and plume rise [14]. In HotSpot, the workflow is straightforward. In the Graphical User Interface (GUI), release source term, radionuclide library, receptors' position and height and other setups are grouped into input panels. For instance, in Figure 3.1 a screen shot of

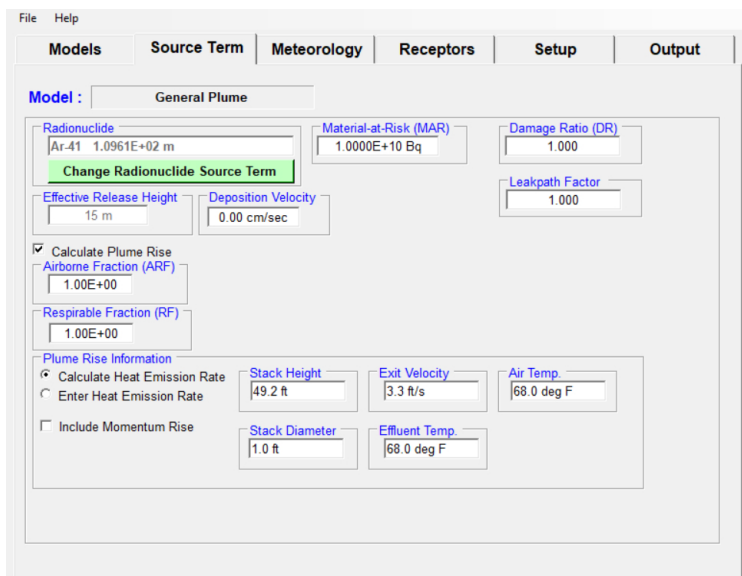


Figure 3.1. Screen shot of *Source Term* panel in HotSpot. Each field is easily accessible for user-defined specifics. In the top bar, other sections are available for input setups. Output panel offers a wide range of options for results visualisation.

the *Source Term* section for a general plume is proposed. Other models are available for fires, explosions, both of general and uranium or plutonium-related scenarios. HotSpot user manual [17] clearly illustrates all the peculiarities of input boxes.

The core of HotSpot for a general plume is the GPM, as expressed in Equation (2.2). For this reason, results for simple open terrain can be considered reliable yet conservative, while urban scenarios can be described less efficiently. Models for resuspension, ground shine and plume rise are available; atmospheric stability classes management is coherent with what is stated in Section 2.3.3; minimum receptor height is 1.5 m above the ground.

Setup input panel allows loading the radionuclide library and radiation dosimetry methodologies. As anticipated in Section 2.4, International Commission on Radiological Protection (ICRP) recommendations (Publications 26/30, Publications 60/66) are adopted. US Environmental Protection Agency (EPA) summarised them in a set of documents called Federal Guidance Reports (FGRs) N. 11, N. 12, N. 13.

Using HotSpot option *FGR N. 13*, the user automatically selects ICRP Publication series 60/70, ICRP 66 lung model, and FGR N. 12 [21] and N. 13. In particular, FGR N. 12 provides the Dose Conversion Factors (DCFs) for external exposure to radionuclides in air, water, or soil in the form of dose per unit time-integrated exposure. Internal exposure, instead, is addressed in FGR N. 13 and the correspondent ICRP 72. DCFs are uploaded in the Source Term panel and multiplied for the pollutant concentration (evaluated with HotSpot's GPM) to give a result in terms of dose. If option *FGR N. 13* is enabled, dose results are given as Total Effective Dose (TED) (Section 2.4). Tables, in which all TED contributions can be distinguished, TED plots (TED vs. downwind distance) and TED contour plots can be requested for data visualisation and storage.

In one of the most recent HotSpot versions, historical meteorological data can be used in the *Percentile Dose* option. In this panel, real local meteorological data can

be uploaded in a specifically formatted file and used to evaluate the 95th percentile TED, i.e. the TED which is exceeded at receptors' location in 5% of the hourly meteorological observations considered. This option allows handling realistic weather conditions, moving the static GPM a step forward in pursuing a more accurate description for dose evaluations.

3.2 GENII V2.10

GENII V2.10 [18] [19] was developed for the US EPA at Pacific Northwest National Laboratory (PNNL). Like HotSpot, also GENII V2.10 is listed in the DOE Safety Software Quality Assurance - Central Registry [20], having successfully demonstrated its compliance with DOE Software Quality Assurance requirements.

GENII V2.10 is a set of codes that can function within the Framework for Risk Analysis in Multimedia Environmental Systems (FRAMES), a framework that allows interconnections between some specific programs to achieve a detailed and wide description of radioactive contaminants transport in different pathways. The GENII system was developed to provide a state-of-the-art, technically peer-reviewed, documented set of programs and transport models for calculating radiation dose and risk from radionuclides released to the environment [18]. Main references include ICRP Publications from 56 to 72 and FGR N. 12 and N. 13.

CNAO requested and obtained a license of this program for internal use. In the framework of this thesis work, GENII V2.10 was studied to give general feedback of the software to the radiation protection office. Once its more detailed design and models were ascertained, it was chosen to be used as a further step in facing the issues of in-air transport of contaminants and dose evaluation.

3.2.1 Basics of the software

Available release scenarios include chronic and acute releases to water or air and initial contamination of soil or surfaces. Groundwater transport is not directly available in GENII V2.10, but a dedicated code, compatible with FRAMES, may be added and used. GENII V2.10 allows modeling a variety of exposure pathways in water (swimming, boating, and fishing), soil (surface and buried sources), air, inhalation, and ingestion (of soil and food). Particular modules are dedicated to tritium release and intake. Such a wide availability of options makes this software flexible yet not immediate to be set up.

A case study is implemented by drawing the so-called *conceptual site model*. This is prepared by loading in the workspace all the available icons that represent the various major environmental media or activities to be modeled. Connecting lines represent the real or potential flow of contamination. An example of a conceptual site model is available in Figure 4.1. In this image, a source term is released in the air; contaminants follow some exposure pathways (chosen in the homonym module) and reach receptors. Health impacts to individuals (or population, depending on the settings) are evaluated in a dedicated module. Lastly, a report of the entire simulation is generated. Item *Constituent* allows loading the radionuclides library, which contains all the physical and chemical properties of isotopes and some chemical substances.

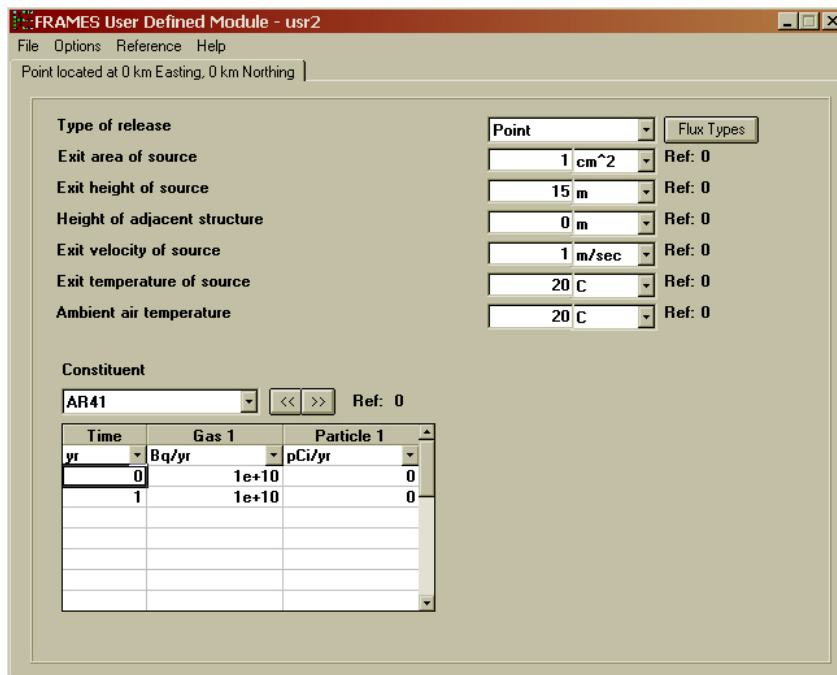


Figure 3.2. Screen shot of *User Defined Module* in GENII V2.10. Each field is easily accessible for user-defined specifics. In the top bar, a menu is available for additional input. In the panel upper part, the characteristics of the source are required. In the bottom part, the quantities of the radionuclides released are expected in input.

The Constituent module must be linked to all the others, in order to pass the data necessary for calculations.

All modules are provided with a GUI that eases the input of all the required parameters. In Figure 3.2, a page of the *User Defined Module*, (i.e. the source term panel) is represented. In the upper part of the input card, the characteristics of the source are required. For instance, this data is used for calculating the plume rise. In the bottom part, the quantity of pollutant released is requested. The list of isotopes loaded in the simulation is passed by the Constituent item, to which the User Defined Module is linked with a connecting line.

Generally speaking, meteorological data are loaded in *GENII Atmospheric Transport Modules*, which can model chronic and acute releases. In Chapter 4, a brief description of the format required is given. For further information and foremost for a detailed report of all the modules available in GENII V2.10, the reader should address references [18] and [19].

3.2.2 GENII Chronic Plume Model

GENII *Chronic Plume Model* is based on the Gaussian solution (here called *straight-line* GPM) to the diffusion equation in a formulation similar to Equation (2.2):

$$\frac{\chi(x, y, z, H, h_{eff})}{Q'(x)} = \frac{1}{2\pi u \sigma_y \sigma_z} \exp\left(-\frac{y^2}{2\sigma_y^2}\right) G(z) \quad (3.1)$$

where $Q'(x)$ is the release rate in Bqs^{-1} , $G(z)$ is the vertical dispersion factor, h_{eff} is the effective release height and all the other symbols are analogous to what was

already written for Equation (2.2). The vertical dispersion factor $G(z)$ is a Gaussian term that includes plume reflection off the ground and the mixing layer (the height of inversion of the vertical temperature gradient) [19].

This module is useful for situations of moderate complexity over open, flat terrain and uses a spatial radial grid (cylindrical coordinates with the release point in the origin). Physical processes of diffusion, deposition, depletion, cloud shine and decay of radionuclides are included in the code; receptor height is fixed to be 1 m. For releases below 12 m, the 10-meter wind speed is always used.

While the straight-line GPM is appropriate for short duration releases (typically, hourly-average concentration estimates), for prolonged or chronic releases the movement of the plume in the compass grid should be modeled. In this case, the GPM is refined in the *sector averaged model* (addressed also in reference [13]), which adopts a cylindrical geometry and the sixteen-sector compass used in Section 2.3:

$$\frac{\chi(\theta_i, r, z)}{Q'(r)} = \frac{1}{\sqrt{2\pi}u\sigma_z\theta_w} G(z) \quad (3.2)$$

where $\chi(\theta_i, r, z)$ is the concentration at distance r in sector θ_i and at height z , θ_w is the arc length in a 22.5° wide sector or 4 times σ_y ; all the remaining parameters follow the usual formalism.

The equations presented assume that the release flow is negligible. In the case of releases from short stacks, if the receptor is near the release point, this assumption is not valid [19]. GENII V2.10 applies a *finite source correction*, which in simple cases coincides with the inclusion of the stack flow in the denominator of the GPM, in the units of $[m^3 s^{-1}]$. For instance, the straight-line GPM is modified to become:

$$\frac{\chi(x, y, z, H, h_{eff})}{Q'(x)} = \frac{1}{2\pi u(h_s)\sigma_y\sigma_z + f_0} \exp\left(-\frac{y^2}{2\sigma_y^2}\right) G(z). \quad (3.3)$$

Equation (3.3) constitutes an example of the various refinements provided by GENII V2.10 to the basic GPM. The Software Design manual [19] describes all the other available alternatives.

Also in this module, dose calculation depends directly on in-air concentration. In fact, in the *Health Impacts Module*, an analogous option with respect to HotSpot – *use FGR N. 12/13* – allows selecting the same DCFs discussed above.

3.3 Limits of the software

After a presentation of the main characteristic of HotSpot and GENII V2.10, it is clear that (by design) dose evaluation depends directly on the in-air concentration of contaminants, in the sense of a direct product between two quantities (an activity concentration and a DCF). For this thesis work, it is of interest to analyze the limits of applicability of this algorithm. This is done in the remaining part of this Section, with reference to literature and the concept of semi-infinite cloud approximation.

3.3.1 Gamma-ray dose from an overhead plume

With an explicit reference to HotSpot and the GPM, two papers [23] [24] present a scenario in which the algorithm mentioned is destined to underestimate the dose: a

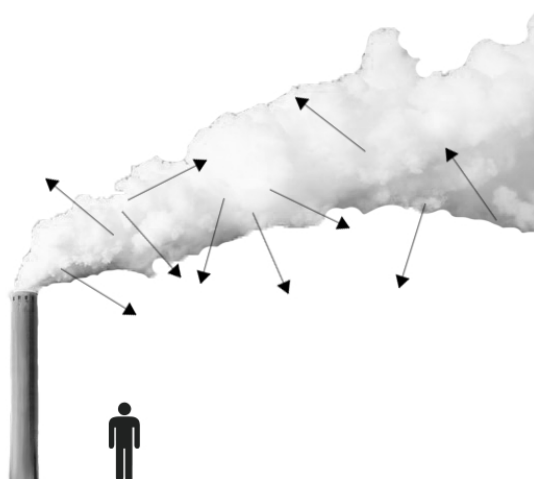


Figure 3.3. Simplified image of an overhead plume of radioactive contaminants. In this case, the receptor is not immersed in the cloud; HotSpot and GENII V2.10 would predict a null dose. Black arrows may represent particles with a significant range in the air – like photons emitted in a nuclear decay process – able to give a significant dose contribution at the ground level.

receptor placed outside a radioactive cloud (where the radionuclide concentration is null) may receive dose from particles with a significant in-air range that can travel towards it. Hence, despite software like HotSpot and GENII V2.10 calculate a null dose, the dose may not be null and even not negligible. A receptor could find itself outside a plume either because it is placed on the ground at short downwind distance from the release point (Figure 3.3), either because if the atmosphere is very stable a radioactive cloud does not reach the ground in hundreds of metres. For instance, for a stability class F GPM in open country with a 15 m-high release point, the activity concentration at the soil level starts to become significant after about 1 km, where σ_z is equal to 12.31 m. In this case, also receptors positioned far away from a stack might see their dose miscalculated by HotSpot and GENII V2.10.

Paper [23] goes back to 1980s experimental evidence noticed at Los Alamos National Laboratory (USA) accelerator facility, where a γ dose contribution was found at the ground owing to the discharge of β^+ emitters ^{11}C , ^{13}N , ^{15}O [45]. In the journal article, both an analytical approach, conceived for fast evaluations in emergency scenarios, and a Monte Carlo approach are proposed. Results demonstrate the inadequacy of a GPM at short downwind distances: the GPM predicts a null dose, while Monte Carlo simulations show the γ dose contribution at the ground. A second study [24] widens what stated in reference [23] in nuclear-plant related scenarios, using the Monte Carlo transport code FLUKA (Section 3.4) to evaluate the DCFs for various downwind distances and atmospheric stability classes A and F. In this case, normal operations releases of ^{41}Ar and ^{135}Xe (their most energetic γ are considered) take place from 100 m-high stacks. Results show that for ground receptors in both classes A and F, DCFs (and so the TED) initially increase with downwind distance, attain a peak (roughly, of the same order of magnitude) in an interval between 300 m and 600 m and then decrease. In stability class F, DCFs remain almost constant with distance. This is caused by the shape of the plume, which shows a small cross-sectional area for downwind distances up to kilometres. Coherently, the standard class F GPM predicts

a null dose along the same length.

As a final addendum, it should be repeated that the inhalation dose is proportional to the activity concentration at receptors' position. Therefore, as stated in reference [23], a product of a concentration with an inhalation DCF is an appropriate estimate of the inhalation dose.

3.3.2 Semi-infinite cloud approximation

The evaluation of the dose given to tissues by an arbitrary distribution of radionuclides is a difficult computational task. For this reason, it is customary to consider simplified geometries and idealized exposures [21]. Among these, the *semi-infinite cloud approximation* represents one example of great relevance. In this model, the radionuclide is thought to be uniformly distributed in air, above the ground, to an infinite extent. Similarly, an infinite cloud extends limitlessly in all directions around a receptor point.

This approximation was used by FGR N. 12 for DCFs evaluation [21]. Using a Monte Carlo method, the authors implemented a multi-step procedure to compute the transport of radiation from an environmental media (one of which is air) to organs and tissues of the human body and the consequent energy deposition. After, DCFs were tabulated for each radionuclide. Results follow ICRP documentation about radiation protection quantities.

In order to better clarify the infinite cloud approximation, let a radioactive contaminant be uniformly distributed in a spherical cloud. Also, let the sphere radius be equal to the range of the particles emitted in the decay process. In such a situation, a receptor placed at the centre of the cloud would consider it as infinite, because any additional external layer of radioactive material would not increment the fluence at the centre. Hence, if the receptor does not perturb the radiation field, for a sufficiently large spherical cloud of contaminants an equilibrium condition between emitted particles and the ones absorbed at the receptor location holds [22]. In conclusion, the particle fluence that gets to the centre of the sphere builds up to reach an asymptotic value, if the radius increases. This last condition coincides with the definition of infinite cloud approximation (if the sphere radius is left unchanged, instead, the fluence is proportional to the concentration of contaminants in the cloud).

This qualitative description can be supported by the calculation of the fluence rate incoming at a receptor placed in the centre of a spherical volume of radius R . Let S be the source strength (or activity concentration) in $[\text{cm}^{-3} \text{s}^{-1}]$ of a homogeneously and infinitely distributed mono-energetic γ -emitting radionuclide in air. Also, let

$$B(E, \mu r) = 1 + C(E)\mu r e^{D(E)\mu r} \quad (3.4)$$

be the expression for photon Kerma¹ build-up (Berger's formula) [25], where μ is the linear attenuation coefficient in air, $C(E) = 1.5$ and $D(E) = 0.035$ for 1 MeV photons in air [25], and r is the distance that photons travel in air in [m]. To evaluate

¹Kerma is a dosimetric quantity. The acronym stands for *Kinetic Energy Released in Matter*. It is defined as the sum of the initial kinetic energies of all the charged particles liberated by uncharged ionizing radiation (i.e., indirectly ionizing radiation such as photons and neutrons) in a sample of matter, divided by the mass of the sample. Its SI unit is the gray [3].

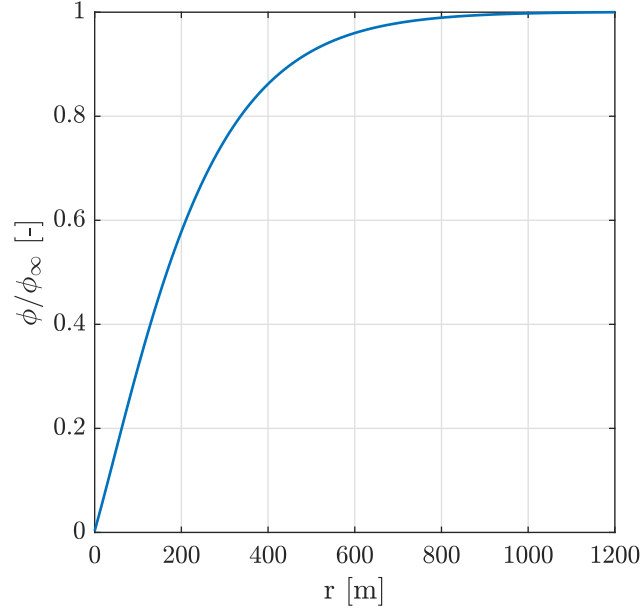


Figure 3.4. Plot of the normalized fluence rate ϕ at the centre of a spherical volume versus the sphere radius, with 1 MeV photons, dry air attenuation coefficient μ from [46], build-up calculated with Equation (3.4).

the photon fluence rate density at the centre of the sphere, the cloud volume can be divided in spherical shells of thickness dr at increasing distance r from the centre. For each of them, the infinitesimal contribution to the total photon fluence rate density is described by the expression [25] [39]:

$$d\phi = S4\pi r^2 B(E, \mu r) f_{K \rightarrow \phi} \frac{e^{-\mu r}}{4\pi r^2} dr \quad 0 \leq r \leq R \quad (3.5)$$

in which $f_{K \rightarrow \phi}$ is the conversion factor that links fluence rate to Kerma².

Equation (3.5) was integrated numerically over the radius r to obtain the total uncollided fluence rate, in $[\text{cm}^{-2} \text{s}^{-1}]$, at the centre of the sphere and plotted in Figure 3.4, where a normalization with respect to the asymptotic value of ϕ , ϕ_∞ (reached at about 800 m), was added. From the graph, it is possible to conclude that the photon fluence rate at the centre of large spheres reaches ϕ_∞ , while for small radii ϕ is a little fraction of ϕ_∞ . For instance, with reference to the same Figure, a sphere of radius 10 m of a 1 MeV γ -emitting radionuclide has at its centre a photon fluence rate equal to 3.30 % of ϕ_∞ , that is to say that the photon fluence rate is 3.30 % of the one present at a point immersed in an infinite cloud.

This degree of detail cannot be modeled by HotSpot: independently from the cloud dimensions, an in-air concentration evaluated with a transport model is multiplied by a DCF. In GENII V2.10 Software Design document [19], instead, the inadequacy of the semi-infinite cloud model near the release point is addressed in a dedicated

²For mono-energetic photons, Kerma is related to fluence (Φ) by the formula [25]:

$$K = \Phi \left(\frac{\mu_{tr}}{\rho} \right) E_{ph}$$

in which μ_{tr}/ρ is the mass energy transfer coefficient and E_{ph} is the photons' energy.

section. In both GPM and puff models, option *Finite Plume Model* enables an adaptive scheme for dose evaluation at short downwind distances that uses various irradiation geometries (point-kernel, line sources, infinite slab, composition of infinite slabs, semi-infinite cloud) depending on the increasing cloud dimensions. However, this approximated method remains analytical; moreover, no indications about the management of annihilation photons for $\beta+$ emitters discharged in the air are given in the manual (three airborne $\beta+$ emitters are considered in Chapter 6).

Since at short downwind distances from an in-air release the radioactive cloud (in this work, modeled with the GPM) is small, the observations presented in this Section support the thesis that the semi-infinite cloud approximation for dose calculation is poor in some circumstances, which depend in the first place on cloud dimensions and energy of the emitted particles, since the latter affects the particles range. In other words, when the dimensions of the radioactive cloud becomes comparable with the range of emitted particles, calculation of the dose at a given point must take into account the complexities of geometry, absorption, and buildup, making the complete solution difficult [22].

3.3.3 Monte Carlo techniques as a possible approach

The two scenarios presented in the previous sections (overhead plume, immersion in a cloud of finite dimensions) are outside the limits of applicability of standard software for radionuclide dispersion in the atmosphere, with which only an approximated solution would be possible. A Monte Carlo transport code is used also in references [23] [24] and appears as a viable approach for computing the dose at short downwind distances, where nor the semi-infinite cloud approximation nor the dose from photons (or other particles with a significant range in the air) from an overhead plume are properly addressed. In this thesis work, the Monte Carlo transport code FLUKA was chosen to be used, since it is extensively used by CNAO radiation protection service. At CNAO, FLUKA is installed on two high-performance multi-core computers which allow parallel computing for faster simulation time (for further information on the computing methods, refer to Section 4.2.3).

3.4 FLUKA

The FLUKA code is a general-purpose Monte Carlo tool for particle transport and interaction with matter [26] [27] [35]. It can manage a considerable number of particles (hadrons, heavy ions, electromagnetic particles from keV to cosmic ray energies, PeV) and materials thanks to the best and up-to-date physical models in terms of completeness and precision. Monte Carlo transport and physics in general are addressed at a microscopic approach [27], in the sense of considering single interaction levels and a full coupling of hadron and electromagnetic parts. FLUKA development and maintenance are performed in the framework of an INFN-CERN agreement. FLUKA has many applications in particle physics, radiation protection, radiation detectors design, medical physics, radiotherapy and hadron therapy.

At CNAO, FLUKA is used with its graphical interface Flair (*FLUKA Advanced Interface*) [47], which ensures a straightforward implementation of the input param-

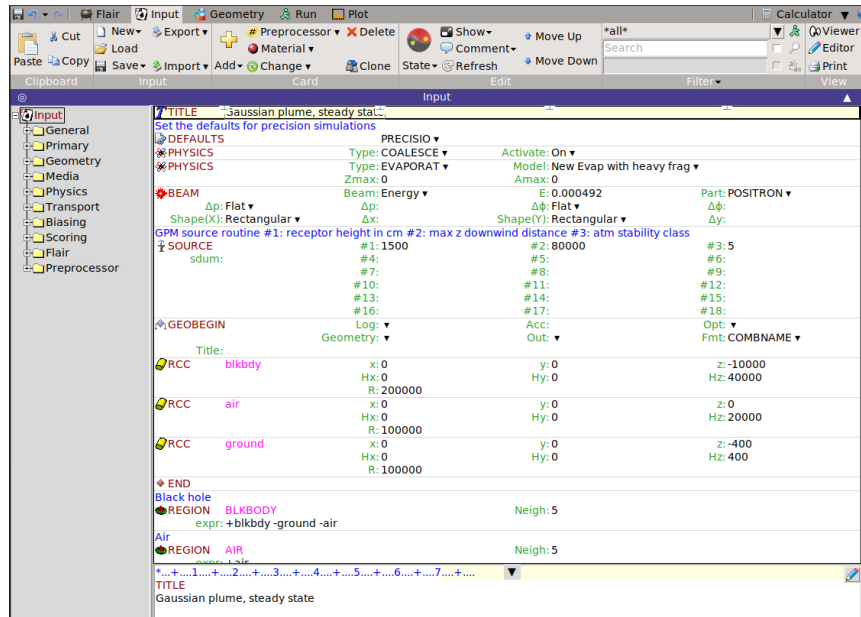


Figure 3.5. Screen shot of Flair Graphical User Interface (GUI) for FLUKA. Each FLUKA card is represented in a box, entitled with the card name and a small icon. The input represented is used in Chapter 6. Card *Source* performs a call to a user implemented routine, as described in Chapter 4.

eters (FLUKA input file) and eases the editing of the simulation geometry in a visual/graphical environment with immediate debugging information. Directives to the software (in terms of geometry description, physical models, requested output) are given using the so-called FLUKA *cards*. In Flair, cards are easily added and modified thanks to accessible input panels and drop-down menus (Figure 3.5).

User programming is reduced at minimum by a large number of available options; in some special cases, however, a number of user interface routines (written in Fortran 77) are available for advanced requirements.

In the following of this thesis work, only specific details about FLUKA will be given. For further information, the reader should refer to the manual [26] and the vast literature that properly and extensively address this code structure, physical models and statistical techniques.

Chapter 4

Software comparison

In this Chapter, a comparison of the performance of the three computer programs presented in Chapter 3 is carried out. A release scenario is introduced in HotSpot and GENII V2.10. The Gaussian Plume Model (GPM) is implemented in FLUKA with a user-written source routine, which is described and tested, also against a simple analytical model. Results are collected for two atmospheric stability classes and discussed.

4.1 Scenario description and rationale of the comparison

With respect to what was stated in the previous Chapter, it should be stressed that the GPM may remain adequate for nuclear reactors-related scenarios, where emission stacks are tens of metres high, sites are scarcely populated, strictly regulated and/or at limited access. The possibility of being immersed in a radioactive plume at short downwind distances, for instance, may not be relevant from the radiation protection point of view, as to say that a properly designed environment can make the issues previously listed less relevant if a GPM is used for dose computation. On the other hand, there is a wide category of industrial and medical facilities in which the production and management of radionuclides is an on-topic task, such as radioisotopes production centres, nuclear medicine hospital departments, proton therapy and hadron therapy centres (reference [1] runs an updated list of particle therapy facilities in clinical operation in the world). It is reasonable to expect that these centres would be at least in the proximity of urbanized areas, with smaller stacks than nuclear power plants, surrounded by buildings of comparable size. In this case, the validity of the core hypothesis of a GPM-based software becomes questionable.

At the time of this writing, it was not possible to find in literature any data that could fit a small-height in-air emission of contaminants on the basis of the issues that come to light in Chapter 3. For this reason, the following general release scenario was considered:

- 10 GBq of ^{41}Ar released to the atmosphere (continuous constant release source term). Argon is a noble gas, activated in the air by the thermal neutron capture reaction on ^{40}Ar . ^{41}Ar is a typical radioactive contaminant managed in hadron

therapy and Boron Neutron Capture Therapy (BNCT) facilities (Chapter 2);

- release point at 15 m above the ground;
- 1 m s^{-1} wind speed, measured at 15 m above the ground (constant in direction and intensity);
- open country Briggs' dispersion coefficients; these coefficients are extensively discussed in the literature and produce more conservative estimates than urban condition coefficients [17];
- atmospheric stability classes A and F, where A is the most unstable category and F the most stable category;

with the goal of testing quantitatively what put in evidence in the previous Chapter. Also, the convergence of the codes was investigated at great downwind distance (up to 1 km), where the plume was expected to approach an infinite cloud.

Centro Nazionale di Adroterapia Oncologica (CNAO) activities and location well represent the context depicted above. As observed in Chapter 1, the Foundation is placed in a semi-urbanized area: to the south, it is surrounded by buildings of comparable size; to the east, Policlinico San Matteo towers stand out well above CNAO stacks; in the other directions, the flat ground surface is occupied by car parks, streets, fields, and CNAO's high voltage control unit. Therefore, depending on the wind direction, a receptor at elevated floors in the vicinity of CNAO may be immersed in the plume that the hadron therapy centre emits during clinical operations.

For this reason, doses were evaluated at the ground and at release height on the plume centre-line, being these two the worst-case points of practical interest due to the symmetry of the GPM.

4.2 Methods

In this Section, the procedures implemented in each software to carry out the comparison are described. For FLUKA, particular emphasis is given to the user-written source routine, which is attached in Appendix A.

4.2.1 HotSpot

In HotSpot, the scenario was easily set using the graphical interface. *General plume* was selected and ^{41}Ar loaded as the source term; *Material-at-risk* was put to 10 GBq and *Damage-ratio* and *Leakpath Factor* to unity. The damage ratio is the fraction of material that is actually damaged by an accident; the leak-path factor is the portion of damaged material that is not contained by safety barriers, and consequently is dispersed in the air [17]. Hence, these two fractions were set to unit to model a total in-air release of ^{41}Ar .

In panel *Setup*, *Wind Input Height* was set to 15 m (instead of 10 m); otherwise, HotSpot would have used a *wind power law* (a simple mathematical relationship that describes how wind speed increases with height in the atmosphere [11] [17]), resulting in a slightly greater wind speed at the release point (15 m above the ground).

In total, four simulations were made to combine two atmospheric stability classes (modified in *Meteorology* input panel) and two receptor heights (set in *Receptors* input panel). Results of each *Table Output*, with option *Display all TED Components* enabled, were saved and data exported to a spreadsheet.

4.2.2 GENII V2.10

GENII V2.10 was installed on a Windows XP virtual machine because after some attempts the software resulted to not be fully compatible with newer Windows distributions. In Figure 4.1 the conceptual site model prepared for the simulation is shown. All modules were used with default options, as recommended by the software User Guide [18]. Briefly, the main characteristics and settings of each module are listed:

- *Constituent*: this module allows to select one database of radioactive contaminants or common chemical compounds. ^{41}Ar was loaded from *GENII Radionuclide Database Selection* with all its default properties.
- *Source Term Definition*: it is used to define the initial release. In this case, a 10 GBq point release was chosen. Doses at the soil level were calculated placing the source at 14.5 m above the ground, because GENII V2.10 default receptor height is 1 m (Section 3.2.2). For the same reason, doses inside the plume were calculated with a source elevation of 1 m. In this way, in all the cases the position of receptors was set to maintain a vertical distance from the release point coherent with HotSpot and the scenario described above. Output data is coupled to an Atmospheric Transport module.
- *Atmospheric Transport*: the sector averaged GPM (Section 3.2.2) of GENII V2.10's Chronic Plume Module was used. Briggs' open country dispersion coefficients were selected. Meteorological data is added in this module.
- *Exposure Pathways*: it provides the available pathways for contamination. In this case, only inhalation and external exposure were selected. Depending on the type of release and scenario, many other pathways are available (food ingestion, swimming, re-suspension of surface soil, irrigation, agriculture, domestic water use).
- *Receptor Intakes*: this module reads exposure media concentration values from Exposure Pathways and evaluates the total activity intake and external exposure. One age group (from 0 to 70 years) was selected.
- *Health Impacts module*: in this module, health impacts are evaluated with risk factors from literature. Option *ICRP 60 – FGR N. 12 and N. 13* was used in this simulation. This choice is coherent with HotSpot settings.
- *Report Generator*: this last module prints results and a complete summary of the run.

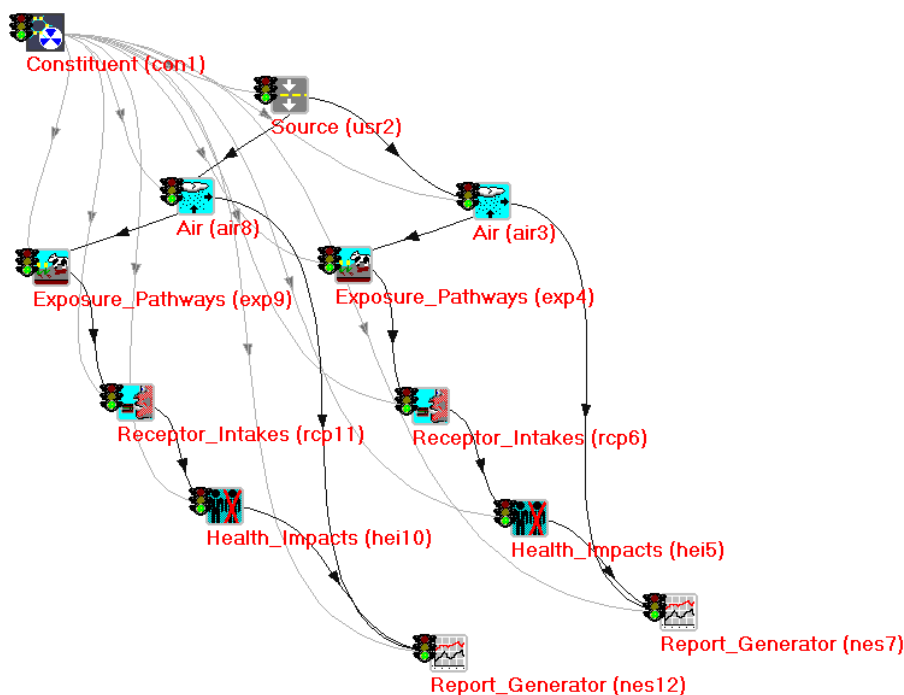


Figure 4.1. GENII V2.10 conceptual site model. Due to a software constraint, two equivalent branches were implemented to evaluate the dose at all the downwind receptors in a single run.

In Figure 4.1, it is possible to observe two analogous branches starting from the Source module. This implementation was due to a software constraint in Atmospheric Transport modules, for which only ten downwind receptors can be managed in a single run. In this way, results for more downwind distances were requested all at once.

As HotSpot, GENII V2.10 was executed for the four cases, i.e. the combination of two receptors' heights and two different atmospheric conditions, and dose results were exported to an external spreadsheet. Meteorological data was uploaded in the Chronic Plume Module after preparing two formatted files.

Formatting meteorological data for GENII V2.10

GENII V2.10 Chronic Plume Module required in input meteorological data in a specific format. A simple MATLAB script was written to prepare it following the structure specified by GENII V2.10 User Manual [18]. In short, one year of hourly meteorological data was arbitrarily set to a 1 m s^{-1} , constant direction (90°) wind speed. Temperature was set to 293.15 K and mixing height (the altitude at which the vertical temperature gradient changes sign) to 2000 m. This last number was chosen to be sufficiently high to not affect the distribution of contaminants in the lower stratum of the atmosphere. Lastly, rain was excluded inserting a null rain rate (0.0 mm h^{-1}) and the GENII V2.10 precipitation type "0". In the first line, surface roughness was set to 0.03 m (which is the default value used in HotSpot), and wind input height was set equal to the release point height (14.5 m) for the same reason described in HotSpot settings for wind speed.

Two files were prepared, one for atmospheric stability class A (labelled as “1”) and one for class F (labelled as “6”), and saved with `.met` file format. All these settings accurately reproduce the scenario described at the beginning of this Chapter and are coherent with HotSpot input options.

The first lines of a GENII V2.10 meteorological data formatted file for atmospheric stability class A were reported in Listing 4.1. From the second row, data records are written in the order: year, month, day, hour, atmospheric stability class, wind direction (in degrees, the direction the wind is blowing *towards*) [19], wind speed (m s^{-1}), dry-bulb temperature (K), mixing height (m), precipitation type, precipitation rate (mm h^{-1}), and a weighting factor (equal to 1 for hourly input data).

Listing 4.1. First lines of a GENII V2.10 meteorological data file for atmospheric stability class A and 1 m s^{-1} wind towards east direction. Details about the file structure are given in the text.

```
0.03, 14.5
 19  1  1  1  1  90.0  1.0 293.15  2000.00  0.00  1.
 19  1  1  2  1  90.0  1.0 293.15  2000.00  0.00  1.
 19  1  1  3  1  90.0  1.0 293.15  2000.00  0.00  1.
 19  1  1  4  1  90.0  1.0 293.15  2000.00  0.00  1.
 19  1  1  5  1  90.0  1.0 293.15  2000.00  0.00  1.
 19  1  1  6  1  90.0  1.0 293.15  2000.00  0.00  1.
 19  1  1  7  1  90.0  1.0 293.15  2000.00  0.00  1.
```

4.2.3 FLUKA

Since FLUKA default geometry options did not allow setting up the shape of a static plume, the Monte Carlo implementation of the GPM required the development of a *user-written source routine*. In FLUKA, this can be done by editing the SOURCE user routine.

SOURCE user routine

Subroutine SOURCE can be called when the implementation of complex source geometries or sampling of primary particle properties are needed [26]. It is activated by card SOURCE in FLUKA input file. The template was written by Alfredo Ferrari and Paola Sala and is provided with FLUKA distributions in the directory `$FLUPRO/usermvax`. In Appendix A, the user-written instructions are attached and briefly commented from the code viewpoint.

In a physical sense, SOURCE routine was designed to distribute in space the initial position of primaries (i.e., the particles emitted in the decay of contaminants released in the air), according to the GPM. In other words, for every Monte Carlo history, SOURCE routine sampled the coordinates (x, y, z) in which a radioactive nucleus contained in the plume was simulated to decay. Then, in the program, primary particles were transported autonomously by FLUKA.

From a coding and mathematical viewpoint, the correct sampling of decay positions in space was implemented starting from an observation regarding the GPM.

Its Equation is here rewritten for simplicity:

$$\chi(x, y, z) = \frac{Q}{2\pi\sigma_y(x)\sigma_z(x)u} \exp\left(-\frac{y^2}{2\sigma_y^2(x)}\right) \exp\left(-\frac{\lambda x}{u}\right) \left[\exp\left(-\frac{(z-H)^2}{2\sigma_z^2(x)}\right) + \exp\left(-\frac{(z+H)^2}{2\sigma_z^2(x)}\right) \right]$$

where $\chi(x, y, z)$ is the activity concentration in space in [Bq m^{-3}], Q the release source term in [Bq s^{-1}], λ the radionuclide decay constant in [s^{-1}], u the wind speed in [m s^{-1}], H the effective release height in [m], σ_y and σ_z Briggs' open country dispersion coefficients in [m]. The GPM Equation includes the plume depletion due to radioactive decay. As a result, activity exponentially decreases along the cloud length, according to the radionuclide decay constant. However, for long-lived radioactive isotopes, neglecting this feature is a valid approximation up to kilometres from the release point. Paper [24] followed this approach for ^{41}Ar and ^{135}Xe releases. For example, ^{41}Ar has a half-life of 109.61 min [48]. At 1 km from the release point, the ratio of an exponentially decreasing activity per unit length over a constant activity per unit length A_0 is:

$$\frac{A_0 \exp(-\lambda x/u)}{A_0} = 0.945. \quad (4.1)$$

This simple evaluation confirms that a uniform downwind distribution of activity for long-lived radionuclides constitutes a pertinent approximation in the first hundreds of metres.

On the contrary, the same approximation would be rough in the case of short-lived radioactive isotopes, like the $\beta+$ emitters to which the same user-written source routine was applied in Chapter 6. For instance, ^{15}O half-life is 122.24 s [48]. If a weak wind is blowing, most of the decays take place in the proximity of the release point and an evaluation analogous to Equation (4.1) returns 0.003 for $x = 1$ km. For this reason, it was decided to model the exponential decrease of activity in the GPM by carrying out a two-step sampling.

Firstly, decay time was extracted with the *inverse transform method*, which states that if t is a continuous random variable with cumulative distribution function $F(t)$, then the random variable $R = F^{-1}(t)$ has a uniform distribution on $[0, 1)$ [49]. Therefore, with this method, random numbers from any probability distribution can be generated by using its inverse cumulative distribution. Radioactivity, which is a stochastic process, can be described by the cumulative distribution function $F(t) = 1 - e^{-\lambda t}$, that represents the probability that a radioactive isotope (with decay constant λ) has of being decayed at time $t \in [0, +\infty)$. In FLUKA, it was possible to sample a random number R from a uniform distribution $\mathcal{U} \sim [0, 1)$, and then get the instant of decay in seconds by inverting $F(t)$:

$$t = -\frac{1}{\lambda} \log(1 - R). \quad (4.2)$$

where λ is the radionuclide decay constant in [s^{-1}] and R a random number in $[0, 1)$ sampled from a uniform distribution. Secondly, the downwind position x , in [m], was

deduced by linking the decay time (t) to wind speed (u) with a simple equation of motion:

$$x = ut. \quad (4.3)$$

In the code, the plume was set to have a maximum length (variable XMAX). Therefore, every x sampled was then compared to this variable and rejected if greater. The reason for this is primarily computational, because sampled points needed to be concentrated in a finite space downwind the release point. The value of XMAX, instead, depended on the range of photons in the air, as explained in the following.

Equation (2.2) states that lateral and vertical shapes of the plume are described by dispersion coefficients $\sigma_y(x)$ and $\sigma_z(x)$; at each downwind positions, these are the standard deviations of two Gaussian distributions that describe the concentration of contaminants along the cross-wind and vertical axes, and are expressed as a function of x through Equations (2.3) and (2.4). Hence, for every downwind position sampled with the inverse transform method, coordinates y and z were computed to be normally distributed. In FLUKA, some auxiliary routines allow sampling real numbers from standard Gaussian distributions. These were exploited with the following rationale:

- Lateral dispersion at each downwind position \bar{x} is described by a Gaussian distribution centred in zero and with standard deviation $\sigma_y(\bar{x})$. Cross-wind coordinates were computed according to:

$$y(\bar{x}) = \sigma_y(\bar{x}) n_1 \quad (4.4)$$

where $\sigma_y(\bar{x})$ is Briggs' cross-wind dispersion coefficient evaluated at downwind distance \bar{x} , and n_1 is a real number sampled from a standard normal distribution $N_1 \sim \mathcal{N}(0, 1)$ provided by FLUKA.

- Vertical dispersion at each downwind position \bar{x} is described by a Gaussian distribution with mean H (the release height) and standard deviation $\sigma_z(\bar{x})$. Vertical coordinates were computed according to:

$$z(\bar{x}) = H + \sigma_z(\bar{x}) n_2 \quad (4.5)$$

where $\sigma_z(\bar{x})$ is Briggs' vertical dispersion coefficient evaluated at downwind distance \bar{x} , and n_2 is a real number sampled from a standard normal distribution $N_2 \sim \mathcal{N}(0, 1)$ provided by FLUKA. In the code, the height of release was saved in the variable RELH (Appendix A).

In this way, sampling from two standard normal distributions and using transformations (4.4) and (4.5), coordinates y and z were computed for each x sampled (and not rejected).

In the code, a totally reflecting ground was assumed: points sampled below the ground level were reflected with respect to it. As a result, at the ground surface, the GPM was folded as shown in Figure 4.2 from reference [50]. Lastly, primary particles were attributed an initial random direction of motion with a FLUKA auxiliary routine. Schematically, the code of the SOURCE routine (Appendix A) can be summarised in the following steps:

1. receive plume length (XMAX), release height (RELH) and atmospheric stability class (STC) from FLUKA input file;

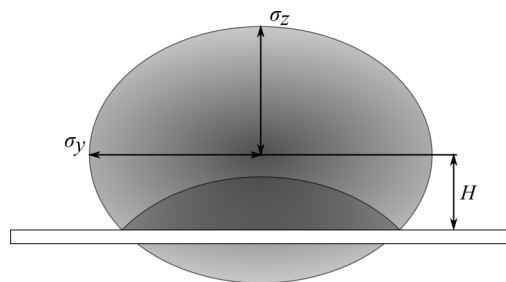


Figure 4.2. Cross-sectional area of a Gaussian Plume Model (GPM) with the assumption of a totally reflective ground.

2. select correct Briggs' open country dispersion parameters (Table 2.3), depending on the atmospheric stability class;
3. sample downwind distance x with Equations (4.2) and (4.3), rejecting values greater than XMAX;
4. for every x , calculate vertical $\sigma_y(x)$ and $\sigma_z(x)$ using Briggs' relations (2.3) and (2.4);
5. sample vertical and lateral coordinates (y and z) using Equations (4.4) and (4.5), reflecting points with a negative z with respect to the ground level;
6. sample a random direction of motion of the primary particle.
7. pass (x, y, z) and primary particle's direction to FLUKA.

In FLUKA, it is essential to use built-in random number generators to preserve history reproducibility. For this reason, in the code random numbers were extracted with calls to auxiliary routines FLRNDM and FLNRR2 (Appendix A).

In the typical workflow of a simulation, SOURCE routine is called every time a Monte Carlo history is started, meaning that in this case steps 1 to 7 were potentially executed millions of times to achieve an acceptable statistical uncertainty of results.

SOURCE routine implementation was tested in two ways: visually, using USBIN scoring card in Flair geometry environment, and quantitatively, in MATLAB. For the latter, spatial coordinates sampled in FLUKA were exported to an external text file by inserting the following code in the user-written source routine:

Listing 4.2. Code for exporting the primaries' sampled positions to an external text file.

```
* Export positions to external file
  OPEN(UNIT = 77,
    &   FILE=' /home/fluka2020/Documents/source_points.txt' ,
    &   ACCESS=' APPEND' , STATUS=' UNKNOWN' )
  WRITE(77,*) X, Y, Z
  CLOSE(77)
```

where X, Y, Z are the primary's Cartesian coordinates sampled in one SOURCE call.

In Figure 4.3, primaries' initial position for an atmospheric stability class F, ^{41}Ar GPM was plotted in space using MATLAB. In Figure 4.4, downwind locations x of

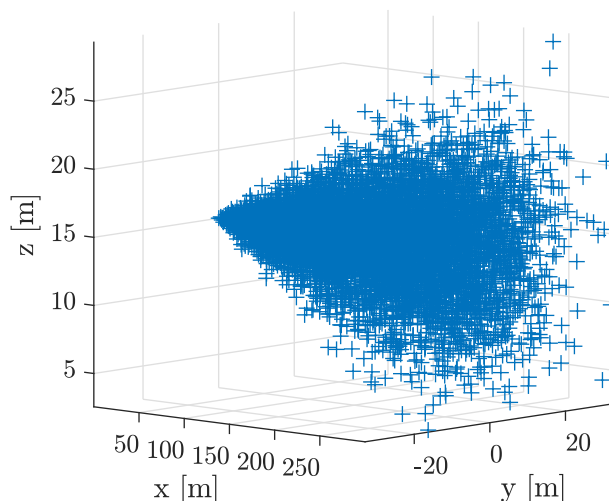


Figure 4.3. 3D spatial representation of an F class, 300 m long GPM of 1×10^4 ^{41}Ar source points. Axes not in scale.

sampled points were plotted in a histogram; in red, the analytical exponential decreasing activity $\exp(-\lambda x/u)$ trend was added for comparison after proper normalisation. In the graph, the agreement between the two items demonstrated that sampled points were correctly distributed along the x -axis to reproduce the transport and decay of contaminants. In Figures 4.5, the same thing was done for cross-wind and vertical distributions of 100 source points; in red, the sampling Gaussian functions were added to verify the correct arrangement of pollutants. Here, the limited number of sampled points made the agreement between histograms and overlying lines less accurate than in the downwind direction.

Simulation

In BEAM input card, 1.293 MeV photons were loaded. This is the most energetic γ -ray present in ^{41}Ar decay scheme (Figure 4.6), caused by an internal conversion following the β - decay [48]. In BEAM card, this was the only parameter needed since the others were evaluated by the user-written source routine.

A simple geometry was chosen, also considering the developments of this work (Chapter 6): it consisted of a cylinder of soil with a cylinder of air onto it; black-body was put all around. Soil and air compositions were found in Federal Guidance Report (FGR) N. 12 and summarised in Tables 4.1. In particular, air was set to be in Normal Temperature Pressure (NTP), i.e. 40% relative humidity, 1 atm, 20 °C, and 1.204 kg m^{-3} density [21]. Custom materials were produced using COMPOUND card.

SOURCE card was activated to call the user-written source routine described above. Doses were evaluated at downwind locations up to 1 km with USRBIN detectors. Maximum plume length (variable XMAX) was calculated to include the contribution of photons emitted up to about three mean free paths beyond the farthest downwind receptor. In fact, since γ -rays are emitted isotropically, dose contributions might come for photons generated far away and directed backwards with respect to the x -axis. For this reason, 1.293 MeV photons massic attenuation coefficient in NTP air was

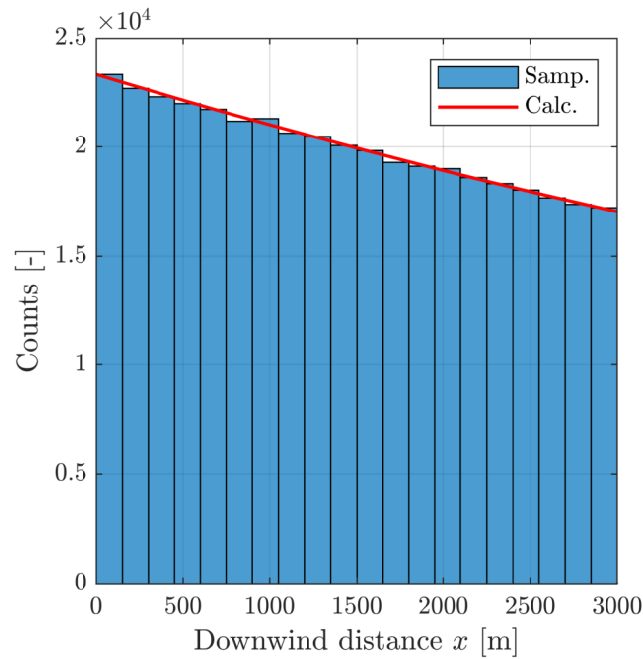


Figure 4.4. Downwind distribution of 4×10^5 ^{41}Ar source points sampled from an F class, 3000 m long Gaussian Plume Model (GPM) (Samp.). In red, the corresponding exponentially decreasing analytical function describing the activity distribution is calculated and overlapped (Calc.).

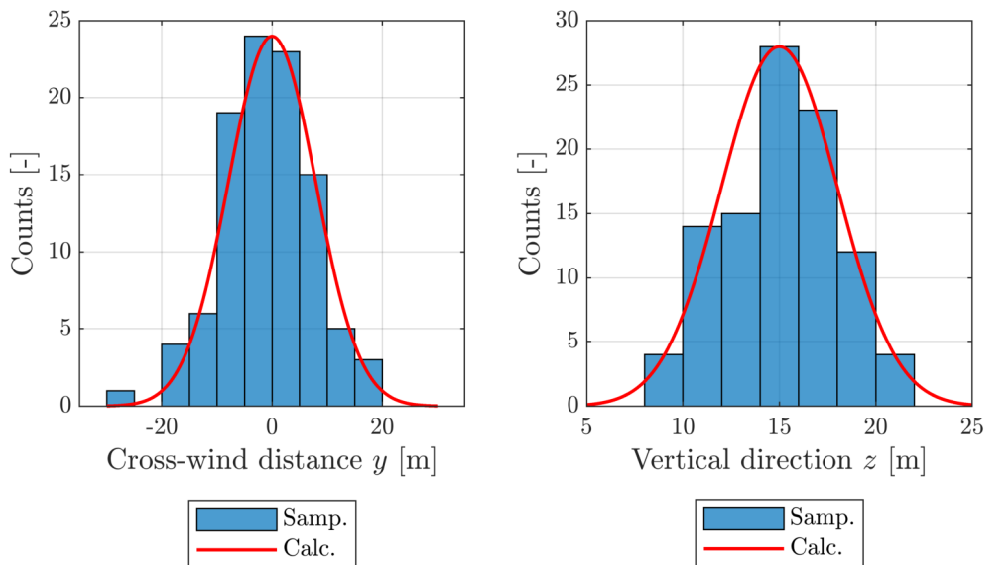


Figure 4.5. Cross-wind and vertical distributions of 1×10^2 ^{41}Ar source points sampled from an F class Gaussian Plume Model (GPM) at 200 m downwind from the release point (Samp.). Release height is 15 m. In red, the corresponding analytical Gaussian distributions are calculated and overlapped (Calc.).

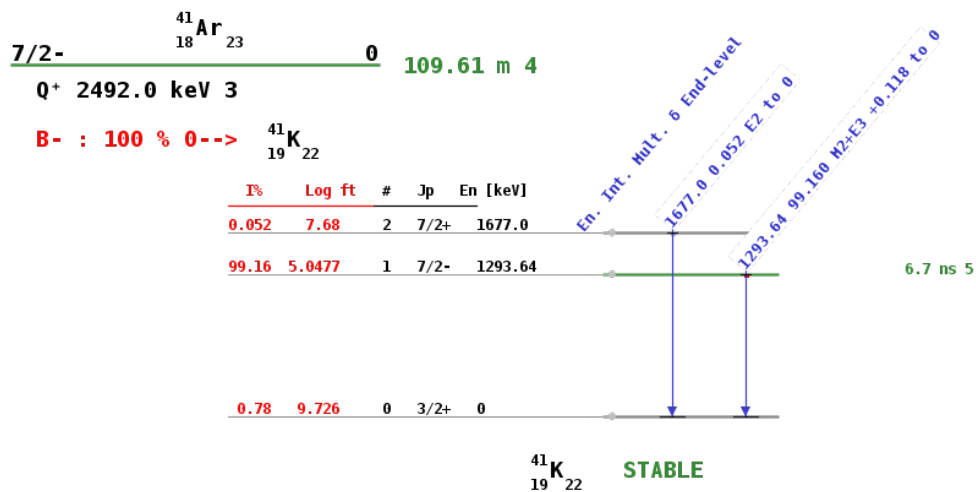


Figure 4.6. ^{41}Ar decay scheme in the elaboration published in reference [48].

computed using the formula [25]:

$$\frac{\mu}{\rho} = \sum_i w_i \left(\frac{\mu}{\rho} \right)_i \quad (4.6)$$

where w_i is the fraction by weight of the i th atomic constituent (Table 4.1a) and $(\mu/\rho)_i$ its massic attenuation coefficient [46]. The mean free path of photons resulted to be equal to 145 m. Therefore, XMAX was set to 1400 m. Accordingly, the radius of the cylindrical geometry was set to 1900 m, in order to completely contain the GPM.

Release height was set to 15 m, atmospheric stability class to A (labelled as “1” in SOURCE card) and F (labelled as “6”) in two different runs. Dose values were computed for thirteen downwind distances, ranging from 25 m to 1 km, using USBIN cards (option DOSE-EQ) at ground level (1.5 m above the soil) and at release height (15 m above the soil). AUXSCORE card was loaded to use FLUKA built-in conversion factors and return results in terms of effective dose (option ewt74, worst possible geometry for the irradiation) [26] [42].

Table 4.1. Elemental composition of soil and air in mass fraction, according to Federal Guidance Report (FGR) N. 12.

Element	Mass fraction	Element	Mass Fraction
H	0.000 64	H	0.021
C	0.000 14	C	0.016
N	0.750 86	O	0.577
O	0.235 55	Al	0.050
Ar	0.012 82	Si	0.271
		K	0.013
		Ca	0.041
		Fe	0.011

(a) Air composition

(b) Soil composition

Simulations were run on a multi-core workstation in use at CNAO radiation protection office. The extensive exploitation of FLUKA parallelization capabilities allowed achieving results in the reasonable time of few hours and statistical uncertainty below 10%.

USRBIN normalisation

USRBIN card scores distribution of several quantities in a regular spatial structure (binning detector) independent from the geometry [26]. In this work, USRBIN detectors were set to score DOSE-EQ (dose equivalent). For this type of scoring, results are expressed in picosievert per unit primary weight [pSv prim⁻¹]. Therefore, a normalization factor (f_{norm}) was applied to compute the dose equivalent in sievert per year:

$$D \left[\frac{\text{Sv}}{\text{y}} \right] = D \left[\frac{\text{pSv}}{\text{prim}} \right] \cdot f_{norm} \left[\frac{\text{prim Sv}}{\text{y pSv}} \right]. \quad (4.7)$$

In f_{norm} , the total number of primaries released in one year was computed considering the plume length, L , and the wind speed, u . In fact, it is reminded that the SOURCE routine was built to receive a plume length L (variable XMAX) and the wind speed u was set to 1 m s⁻¹. In this way, the total number of primaries released in the plume in one year resulted to be:

$$A_{tot} \left[\frac{\text{prim}}{\text{y}} \right] = A_{tot} \left[\frac{\text{Bq}}{\text{y}} \right] = i \left[\frac{\text{Bq}}{\text{y}} \right] \cdot \frac{L [\text{m}]}{u [\text{m s}^{-1}]} \quad (4.8)$$

where i is the contaminant annual release in [Bq y⁻¹]. Equation (4.8) is true if one primary particle corresponds to one isotope disintegration, i.e. if the branching ratio for the decay process is unitary. In conclusion, f_{norm} was computed as the product of Equation (4.8) and the conversion factor from picosievert to sievert:

$$f_{norm} = A_{tot} \left[\frac{\text{prim}}{\text{y}} \right] \cdot 10^{-12} \left[\frac{\text{Sv}}{\text{pSv}} \right] \quad (4.9)$$

4.2.4 Simplified model for dose evaluations

A simplified transport model (hereafter referenced as *sphere model*) was implemented to approach dose computation at the height of release in an analytical way and to obtain a cross-check with FLUKA simulations. In the sphere model, it was assumed that the released activity was entirely contained in a spherical cloud, moved downwind by a constant $u = 1 \text{ m s}^{-1}$ wind.

Considering the meaning of dispersion coefficients, it was reasonable to approximate the shape of the GPM's cross-sectional area at downwind distance x with an ellipse of semi-axes $\sigma_y(x)$ and $\sigma_z(x)$; the sphere model was built to have the same cross-sectional area and, hence, an *equivalent radius* $\sigma(x)$ equal to:

$$\sigma(x) = \sqrt{\sigma_y(x)\sigma_z(x)} \quad [\text{m}].$$

Therefore, the radius of the spherical cloud increased according to Briggs' dispersion coefficients.

In Equation (3.5), a formulation for the uncollided fluence rate at the centre of a sphere of radius R was proposed with reference to the semi-infinite cloud approximation. The same expression was here integrated from $r = 0$ to $r = \sigma(x)$ to obtain the fluence rate at the centre of the spherical cloud (the build-up effect was neglected for simplicity):

$$\phi = \frac{S}{\mu} (1 - e^{-\mu\sigma(x)}) \left[\frac{1}{\text{cm}^2 \text{ s}} \right] \quad (4.10)$$

in which S was the source activity concentration in [$1/\text{cm}^3 \text{ s}$] and $1/\mu$ was the linear attenuation coefficient for photons in air in [m^{-1}]. If a photon is emitted for each disintegration, the activity A_0 [Bq] in the cloud coincides with the number of photons emitted per second. Under this hypothesis, source term S was computed dividing A_0 by the cloud volume and dimensions coincided with an activity concentration [Bq m^{-3}].

The spherical cloud was thought to be moved by a $u = 1 \text{ m s}^{-1}$ wind. In this circumstance, a receptor was immersed in the moving cloud for a time equal to $\Delta t = 2\sigma(x)/u$ seconds. This assumption is conservative: for a receptor standing in a moving cloud sphere, the fluence rate is maximum only in the instant in which the receptor itself is at the sphere centre. Fluence was evaluated integrating Equation (4.10) over the time of submersion and transformed into an effective dose data using fluence-to-effective dose coefficients $f_{E(\epsilon)}$, tabulated in reference [42]:

$$E(\epsilon) = \phi(\epsilon)\Delta t f_{E(\epsilon)} \quad [\text{Sv}] \quad (4.11)$$

where $E(\epsilon)$ is the effective dose is [Sv], $\phi(\epsilon)$ the fluence rate at the centre of the spherical cloud in [$\text{cm}^{-2} \text{ s}^{-1}$] and Δt the time of submersion in [s]. It is reminded that this evaluation was performed under the hypothesis of mono-energetic photons. Also, cloud depletion due to radioactive decay and photon build-up were not modeled.

The sphere model was used to compute the effective dose in spheres at the height of release and the same downwind distances used in the other software, in the two atmospheric stability classes chosen for the analysis. In Section 4.3 results were added to the software performance comparison.

4.3 Results and discussion

HotSpot, GENII V2.10 and FLUKA were run to compute the dose on the basis of what observed in this Chapter. For stability classes A and F and constant 1 m s^{-1} wind, results were collected for receptors at 1.5 m above the ground in Figure 4.7. The same was done for receptors at 15 m (the height of release) in Figure 4.8. In this second case, the sphere model was added. In Tables 4.2 and 4.3 results were summarised and expressed in nanosievert (in the first column, receptors downwind positions can be read).

In FLUKA, statistical uncertainty was kept at minimum with sufficient computational resources; the maximum percentage uncertainty detected in the two simulations was 8.53 %, corresponding to few nanosievert. For HotSpot and GENII V2.10, error analysis was not possible because uncertainties were not provided by the codes.

It is reminded that HotSpot and GENII V2.10 provided results as Total Effective Dose (TED), considering only dose contributions from inhalation and cloud submersion;

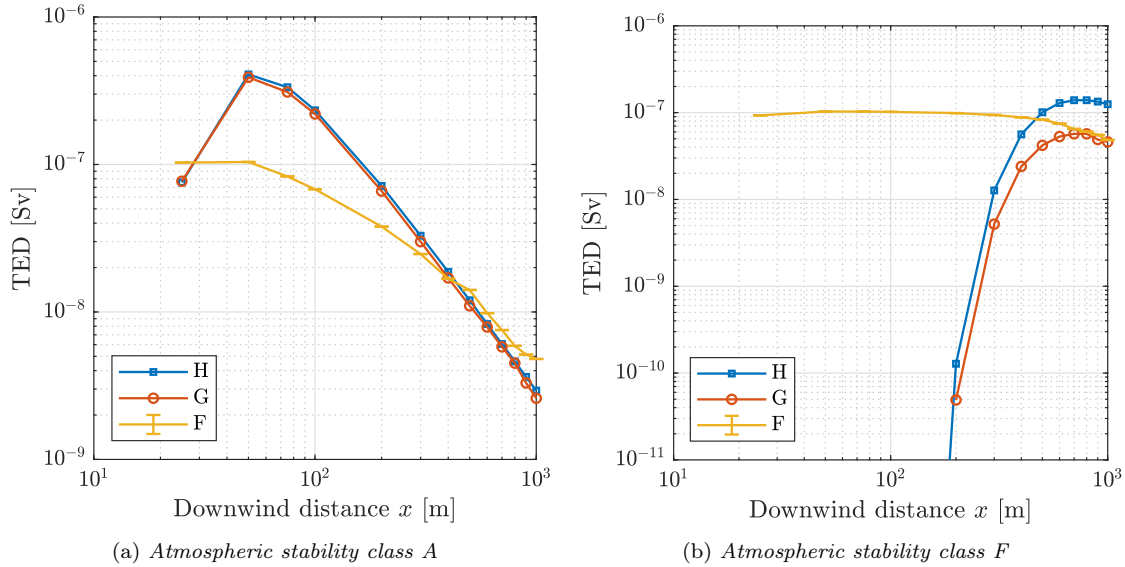


Figure 4.7. Software comparison: Total Effective Dose (TED) results for receptors at 1.5 m above the ground following a 10 GBq release of ^{41}Ar from a 15 m high stack. Doses are calculated on the plume centre-line. H: HotSpot; G: GENII V2.10; F: FLUKA.

for FLUKA USRBIN, instead, data was requested in terms of effective dose. In the case of ^{41}Ar , HotSpot and GENII V2.10 calculated a null dose contribution due to inhalation, being Argon a noble gas. In virtue of this, HotSpot, GENII V2.10 and FLUKA were directly comparable, because they were treating the same protection quantity.

In Figure 4.7a, the maximum TED was found at 50 m from the release point; here, HotSpot and GENII V2.10 predicted a dose over 3.5 times greater than FLUKA. The overestimation was due to the use of Dose Conversion Factors (DCFs) (Section 3.3) where the cloud dimensions are not compatible with the semi-infinite cloud approximation. In Figure 4.7b, the maximum TED in FLUKA was found again at 50 m (103 nSv); in the first 400 m, submersion dose was evaluated to be ranging from 88 nSv to 103 nSv. The other codes predicted a dose different from zero starting from 300 m, and a maximum at 700 m downwind (HotSpot: 139 nSv, GENII V2.10: 57 nSv). The difference in the two values was attributed to the use of the sector averaged GPM by GENII V2.10. Hence, in class F it was possible to find again what theorised in Section 3.3: a very stable plume does not reach the ground in hundreds of metres, producing a null concentration at the terrain level. Despite standard codes evaluate a null dose, Monte Carlo transport codes can show the contribution of photons coming from an overhead plume.

From HotSpot and GENII V2.10 data, it was possible to observe that the peak of maximum concentration at the ground was shifted to greater downwind distance from class A to class F. This is coherent with what predicted by the GPM: greater atmosphere stability means less pollutant dispersion. In both cases, the convergence of results was observed for all the software. In class A, this was detected starting from approximately 400 m, meaning that the plume approached the approximation of semi-infinite cloud at this distance. In class F, an analogous conclusion might be done at 800 m; however, the small vertical spread of the plume represented the limiting

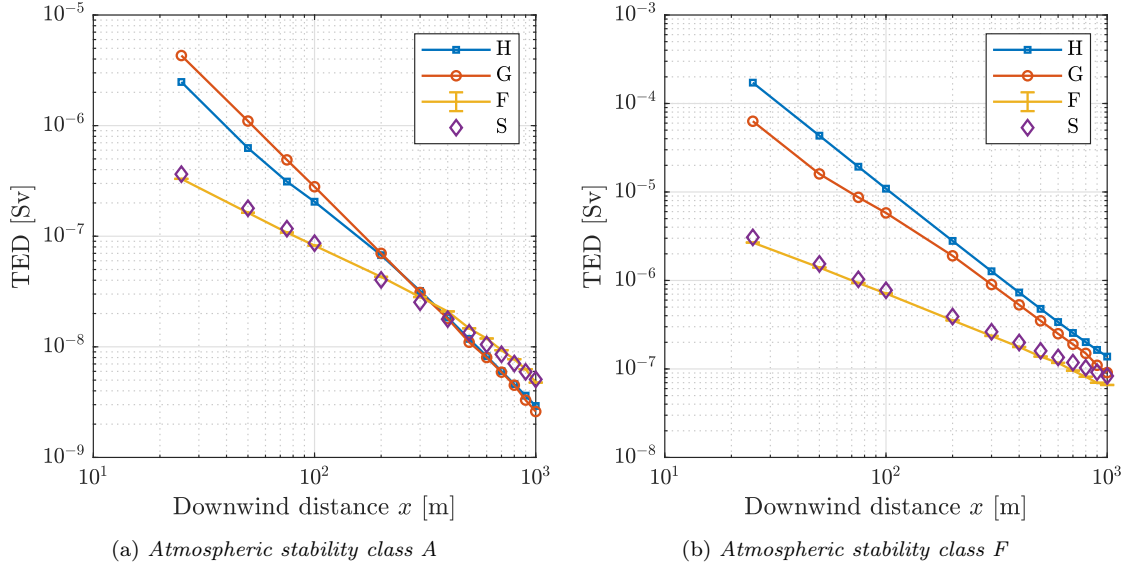


Figure 4.8. Software comparison: Total Effective Dose (TED) results for receptors at 15 m above the ground following a 10 GBq release of ^{41}Ar from a 15 m high stack. H: HotSpot; G: GENII V2.10; F: FLUKA; S: sphere model.

factor for the semi-infinite cloud approximation to occur at the ground in the first hundreds of metres. This would have been reached at kilometres downwind, making the simulation too demanding from a computational point of view.

Regarding the evaluations performed at the height of release, in both Figures 4.8a and 4.8b agreement between HotSpot and GENII V2.10 results was observed. The maximum TED was found at the first receptor point (25 m), where the concentration is maximum inside the cloud. Of course, higher data would have been obtained moving closer to the emission stack.

In stability class A, consistency in results was observed starting from 300 m downwind, where semi-infinite cloud approximation began to hold. In stability class F codes showed a converging trend, but again the low dispersion of contaminants in this class made the full agreement of results impossible in the first kilometre. A remarkable overestimation in HotSpot and GENII V2.10 was detected at short downwind distances, where the cloud is small and far from the semi-infinite cloud approximation.

Lastly, the agreement between FLUKA simulations and the sphere model proved to be solid. Spheres dimensions increased with distance from the release point, coherently with the increasing dimensions of the GPM. The isotropic fluence-to-effective dose coefficient [42] was linearly interpolated at 1.293 MeV, giving $f_{E(e)} = 4.07 \times 10^{-12} \text{ Sv cm}^2$ and used in computations. In class F, the sphere model showed an increasing overestimation with respect to FLUKA, starting from a 9% up to a 32% at 1 km. This is coherent with the absence of a radioactive decay depletion factor in the sphere model with respect to the other software. In class A, despite the same assumption was valid, the overestimation was not always appreciable, and in some points lead to a maximum underestimation of 15%. Table 4.3 and Figure 4.8 showed the adequacy of the sphere model as a simple and fast approximated estimation for critically discussing FLUKA results.

With respect to what was proposed in this Chapter, the Monte Carlo GPM – needed to overcome the issues that came to light in Chapter 3 – can be considered successfully implemented. In the development of this thesis work, the SOURCE routine is further employed in combination with real meteorological data to produce realistic dose predictions for clinical operations at a hadron therapy facility.

Table 4.2. Results of the software comparison, expressed in nanosievert, for two atmospheric stability classes and thirteen downwind distances at 1.5 m above the ground level. Doses are calculated on the plume centre-line. H: HotSpot; G: GENII V2.10; F: FLUKA.

Distance [m]	TED [nSv]					
	<i>Atmospheric stability class A</i>			<i>Atmospheric stability class F</i>		
	H	G	F	H	G	F
25	76	77	103 ± 2	0	0	93 ± 2
50	408	390	104 ± 2	0	0	103 ± 1
75	334	310	83 ± 2	0	0	103 ± 2
100	233	220	68 ± 2	0	0	102 ± 1
200	72	66	38 ± 1	0	0	99 ± 2
300	33	30	25 ± 1	13	5	94 ± 2
400	19	17	17 ± 1	56	24	88 ± 2
500	12	11	14 ± 1	101	42	83 ± 1
600	8	8	10 ± 1	129	53	75 ± 2
700	6	6	8 ± 1	139	57	65 ± 1
800	5	5	6 ± 1	139	57	60 ± 1
900	4	3	5 ± 1	134	49	55 ± 1
1000	3	3	5 ± 1	125	46	48 ± 1

Table 4.3. Results of the software comparison, expressed in nanosievert, for two atmospheric stability classes and thirteen downwind distances at 15 m above the ground level. Doses are calculated on the plume centre-line. H: HotSpot; G: GENII V2.10; F: FLUKA; S: sphere model.

Distance [m]	TED [nSv]							
	<i>Atmospheric stability class A</i>				<i>Atmospheric stability class F</i>			
	H	G	F	S	H	G	F	S
25	2480	4300	330 ± 3	364	172 000	63 000	2681 ± 10	3065
50	627	1100	163 ± 3	179	43 300	16 000	1403 ± 7	1543
75	312	490	108 ± 2	117	19 300	8700	936 ± 6	1032
100	205	280	82 ± 1	86	10 900	5800	712 ± 4	775
200	67	70	43 ± 1	40	2800	1900	354 ± 3	391
300	32	31	28 ± 1	25	1270	900	236 ± 3	263
400	18	18	21 ± 1	18	731	530	177 ± 2	199
500	12	12	15 ± 1	13	478	350	138 ± 2	160
600	8	8	12 ± 1	11	339	250	117 ± 2	135
700	6	6	9 ± 1	9	255	190	96 ± 2	118
800	5	5	8 ± 1	7	201	150	82 ± 1	103
900	4	3	6 ± 1	6	164	110	70 ± 2	92
1000	3	3	5 ± 1	5	138	91	66 ± 1	83

Chapter 5

The CNAO case: radioactive releases and meteorological data

In this Chapter, the equations that describe air activation and management at accelerator facilities are presented. Afterwards, Centro Nazionale di Adroterapia Oncologica (CNAO)'s chronic gaseous annual releases are quantified with reference to a previous M.Sc. thesis and calculations made available by the radiation protection service. Next, local meteorological data are imported from two different weather stations and analysed. In this way, all the necessary data for calculating the dose to individuals in the proximity of CNAO are set up.

5.1 Quantitative formulation of air management

Air activation and management were addressed in Section 2.1. For the purpose of this Chapter, it is sufficient to recall briefly that the in-air activity present in a room can generally vary owing to three factors:

1. source term: in-air radioisotope production is caused by beam losses in the accelerator bunker, or by experiments and medical treatments in dedicated areas;
2. natural decay: a population of radionuclides exponentially decreases with time, as described by the law of radioactive decay;
3. ventilation system: air is continuously extracted from the synchrotron bunker and rooms to reduce the activity concentration. Before reaching stacks, air flows in ducts equipped with monitoring and filtration systems.

Hence, let $A_{IN}(t)$ be the in-air activity inside a room in [Bq]. Its evolution in function of time becomes:

$$\frac{dA_{IN}(t)}{dt} = -\lambda_{eff}A_{IN}(t) + U \quad (5.1)$$

where U is a source term in [Bq s⁻¹] and λ_{eff} an effective “removal” constant in [s⁻¹]. If air ventilation is continuously on during irradiation, the radioactivity level is reduced

by two factors, i.e. nuclear decays (λ_{nucl}) and the rate of air extraction (λ_{air} , expressed in air changes per second):

$$\lambda_{eff} = \lambda_{nucl} + \lambda_{air}. \quad (5.2)$$

Equation (5.1) can be solved by imposing the initial condition $A_{IN}(0) = 0$:

$$A_{IN}(t) = \frac{U}{\lambda_{eff}} (1 - e^{-\lambda_{eff}t}). \quad (5.3)$$

The total quantity of radioactivity extracted (A_{OUT}) by the ventilation system over a time period t can be calculated [29]:

$$A_{OUT}(t) = \lambda_{air} A_{IN}(t). \quad (5.4)$$

At steady-state (for $t \rightarrow +\infty$), and recalling the definition (5.2), the previous gives:

$$A_{OUT,\infty} = \frac{\lambda_{air}}{\lambda_{nucl} + \lambda_{air}} U. \quad (5.5)$$

5.2 Releases at CNAO

In a recent M.Sc. thesis work [28], air activation in the synchrotron bunker, experimental and treatment rooms was studied in FLUKA using simplified and complete geometries and various ion beams and energies. Proton Therapy (PT) and accelerator-based Boron Neutron Capture Therapy (ab-BNCT) facilities have been considered in a CNAO's extensive simulation campaign and another M.Sc. thesis (not yet published), respectively.

5.2.1 Synchrotron, experimental and treatment rooms

This Section recalls the already cited reference [28]. In that work, air activation was addressed taking into account the two different contributions separately:

1. Air activation due to the contact of the primary beam with the air: in experimental and treatment rooms, the beam crosses about 1 m of air when delivered towards patients or target materials;
2. Activation due to secondary radiation: as already mentioned, collisions of particles against accelerator structures, patients and experimental targets is another source of air activation.

A list of the most relevant radionuclides activated in air and a set of tables of their activity contributions in function of a varying beam energy were produced as a result of the analysis. Simulations for air crossed by a particle beam were completed with the following specifics:

- Irradiation target: cylinder filled with air and a volume equal to 1 m^3 ; hadrons were directed to cross the volume along its axis;
- Irradiation time (t_{irr}): 1 s;

- Cooling time (i.e. waiting time before calculating in-air activity): 0 s;
- Proton beam: 1.375×10^{10} p s⁻¹ at various beam energies (50 MeV, 100 MeV, 150 MeV, 200 MeV and 250 MeV);
- Carbon ion beam: 5.56×10^8 ion s⁻¹ at various beam energies (120 MeV u⁻¹, 200 MeV u⁻¹, 300 MeV u⁻¹ and 400 MeV u⁻¹);
- Oxygen (¹⁶O), Lithium (⁷Li), Helium (⁴He) beams at various beam currents and energies. These ion beams constitute a possible upgrade of the existing treatment lines. Calculations were completed and communicated to the radiation protection office without appearing in the following of this work.
- The synchrotron bunker was modeled in a simplified way as a parallelepiped of base 40 m × 40 m and 10 m high;
- Experimental and treatment rooms were modeled in a simplified way as cubes 6 m in side;
- Radionuclides with a half-life lower than 1.5 min were discarded from the analysis. As a result, the most relevant radionuclides resulted to be ¹¹C, ¹³N, ¹⁵O. The production of ⁴¹Ar emerged to be negligible.
- Since direct contact of the beam with the air in the synchrotron bunker was not expected, this data was not produced.

In the second part, ion beams were directed against two targets, in order to quantify air activation due to the secondary field.

- A copper target was used to simulate the production of secondary radiation in the case of particle collisions with accelerator structures or experimental setups placed in the experimental room.
- Polyethylene was chosen to simulate the beam interaction with organic and plastic materials in treatment rooms.
- ⁴¹Ar production from radiative capture reaction (2.1) was considered in virtue of the considerable number of secondary neutrons generated in primary collisions.

FLUKA simulations were run adopting the features listed above and were completed to obtain in-air activity in CNAO rooms. Statistical uncertainty was always below 10 %, with rare exceptions in the case of the carbon ion beam, for which it approached 15 %.

In the present work, activation data was linearly adjusted to up-to-date available information regarding the nominal number of particles that can be used in each beam line (Table 5.1). The total in-air activity generated in rooms in one year of normal operations at CNAO was obtained using the formula:

$$U = \frac{I_{real}}{I_{norm}} (Y_{air} + Y_{target}) \quad (5.6)$$

Table 5.1. Particles per year in each beam line installed at CNAO: treatment rooms (ISO), experimental room (XPR), synchrotron bunker (SYN).

Line	Protons [p y^{-1}]	Carbon ions [ion y^{-1}]
ISO	2.0×10^{16}	8.0×10^{14}
XPR	9.0×10^{16}	3.6×10^{15}
SYN	1.5×10^{17}	6.0×10^{15}

where I_{real} is the actual number of particles used at CNAO in [ion y^{-1}] from Table 5.1, I_{norm} the normalised number of particles used in reference [28] in [ion], Y_{air} the activity generated in air by the particle beam in [Bq], and Y_{target} the activity generated in air by secondary radiation in [Bq].

Y_{air} and Y_{target} represent one fundamental result of reference [28] and, as said, were calculated for various beam energies and a normalised number of particles. In this work, Y_{air} and Y_{target} were always chosen for a beam at maximum energy (protons at 250 MeV, carbon ions at 400 MeV u^{-1}). Generally, this assumption led to upper-bound estimations, with a small exception for air activation with protons. In that simulations, the production of ^{15}O slightly decreased for increasing beam energy, while the same decreasing trend was hardly appreciable for ^{11}C and ^{13}N .

As indicated in reference [28], CNAO records annual beam spectra (number of particles in function of energy per nucleon); a further analysis of this data would lead to a reduction of the estimated quantities of the activity produced and, consequently, released to the air.

The total in-air activity generated in rooms in one year of normal operations at CNAO, U [Bq y^{-1}], was calculated with data of reference [28] and Equation (5.6); U was then used as a source term in Equation (5.5) to calculate the steady-state annual extracted activity. The same quantity was assumed to be eventually released into the atmosphere; in other words, the time spent in ducts was assumed to be null.

Table 5.2 shows an example of data collected for the proton beam. As said, Y_{air} and Y_{target} were taken from reference [28] with $I_{norm} = 1 \times 10^{10} \text{ p y}^{-1}$. Radionuclides decay constants were taken from Table 5.3. At CNAO, the ventilation system guarantees a total air replacement 0.28 times per hour in the synchrotron bunker ($\lambda_{air} = 7.78 \times 10^{-5} \text{ s}^{-1}$) and 15 times per hour in experimental and treatment rooms ($\lambda_{air} = 4.17 \times 10^{-3} \text{ s}^{-1}$). In every room, the activity extracted (A_{out} , the last column in Table 5.2) was assessed separately for each radionuclide, using Equation (5.5). Lastly, contributions pertaining to each radioactive isotope were summed together. The final result for the proton beam was reported in Table 5.4a. Analogous evaluations were performed also for the other ions. Considering all the cases, the proton beam resulted to be the major source of air activation in synchrotron, experimental and treatment rooms.

The same reference compared this emission rate with the maximum in-air concentration allowed in closed spaces according to CNAO's internal recommendations, i.e. 1 Bq g^{-1} . In fact, assuming an air discharge of $1.74 \times 10^4 \text{ m}^3 \text{ h}^{-1}$ by the ventilation system (considering the simplified room volumes and the given air change rates) and an air density of 1.22 kg m^{-3} , the hypothetical maximum activity discharged in one

Table 5.2. Example of calculation of the activity discharged in one year using available data from reference [28] and the procedure described in Section 5.2. In reference [28] the activity was normalised to 1×10^{10} p; λ_{air} was set to $4.17 \times 10^{-3} \text{ s}^{-1}$ in experimental (XPR) and treatment rooms (ISO) and to $7.78 \times 10^{-5} \text{ s}^{-1}$ in synchrotron bunker (SYN). Equations (5.6) and (5.5) were used to compute source term U and extracted activity A_{out} , respectively. As said, in ISO and XPR ^{41}Ar was not considered. Y_{air} was not calculated for SYN.

Room	Isotope	$\lambda_{eff} [\text{s}^{-1}]$	$Y_{air} [\text{Bq}]$	$Y_{target} [\text{Bq}]$	$U [\text{Bq y}^{-1}]$	$A_{out} [\text{Bq y}^{-1}]$
ISO	^{11}C	4.73×10^{-3}	3.01×10^2	4.21×10^1	6.86×10^8	6.04×10^8
	^{13}N	5.34×10^{-3}	1.39×10^3	2.47×10^2	3.27×10^9	2.56×10^9
	^{15}O	9.85×10^{-3}	3.45×10^3	5.16×10^2	7.93×10^9	3.36×10^9
	^{41}Ar	4.27×10^{-3}	-	5.75×10^0	1.15×10^7	1.12×10^7
XPR	^{11}C	4.73×10^{-3}	3.01×10^2	5.66×10^1	3.22×10^9	2.83×10^9
	^{13}N	5.34×10^{-3}	1.39×10^3	3.51×10^2	1.57×10^{10}	1.22×10^{10}
	^{15}O	9.85×10^{-3}	3.45×10^3	7.32×10^2	3.76×10^{10}	1.59×10^{10}
	^{41}Ar	4.27×10^{-3}	-	2.37×10^1	2.13×10^8	2.08×10^8
SYN	^{11}C	6.45×10^{-4}	-	2.54×10^2	3.81×10^9	4.60×10^8
	^{13}N	1.25×10^{-3}	-	1.57×10^3	2.36×10^{10}	1.47×10^9
	^{15}O	5.76×10^{-3}	-	3.38×10^3	5.07×10^{10}	6.85×10^8
	^{41}Ar	1.83×10^{-4}	-	7.43×10^1	1.11×10^9	4.74×10^8

year of operations – 7355 h y^{-1} [28] [29] – was calculated:

$$1 \frac{\text{Bq}}{\text{g}} \cdot 1000 \frac{\text{g}}{\text{kg}} \cdot 1.22 \frac{\text{kg}}{\text{m}^3} \cdot 1.74 \times 10^4 \frac{\text{m}^3}{\text{h}} \cdot 7355 \frac{\text{h}}{\text{y}} = 1.56 \times 10^{11} \frac{\text{Bq}}{\text{y}}$$

In Table 5.4b the maximum activity release allowed by CNAO’s internal recommendations was distributed assuming that radionuclides contributed in the same proportions as Table 5.4a.

5.2.2 Expansion project

The new PT facility is currently under study at the radiation protection office. Using the same approach described in the previous section, internal calculations predicted a total annual gaseous release of approximately 3 GBq, in a mixture of ^{11}C , ^{13}N , ^{15}O , ^{41}Ar (Table 5.4c).

By the time of this writing, the ab-BNCT facility is undergoing a careful design study, too. Using FLUKA, a parallel M.Sc. thesis (not yet published) is confirming the significant activation of ^{41}Ar in the air of treatment rooms. This radionuclide is produced by the radiative capture reaction (2.1) induced by ab-BNCT thermal neutrons. In Table 5.4d, an annual release of 37 GBq was conservatively assumed.

Relevant nuclear data about all the radionuclides previously mentioned and used in computations was listed in Table 5.3.

Table 5.3. Relevant radionuclides produced at CNAO and released in the air during normal operations. Nuclear data from reference [48].

Radionuclide	$T_{1/2}$ [s]	λ [s^{-1}]	Decay mode	Energy [keV]
^{11}C	1.22×10^3	5.67×10^{-4}	$\beta+$	3.84×10^2 ^a
^{13}N	5.92×10^2	1.17×10^{-3}	$\beta+$	4.90×10^2 ^a
^{15}O	1.22×10^2	5.68×10^{-3}	$\beta+$	7.35×10^2 ^a
^{41}Ar	6.60×10^3	1.05×10^{-4}	$\beta-$	1.29×10^3 ^b

^a Average positron energy.

^b Most energetic photon, internal conversion following $\beta-$ decay (see Section 4.2.3).

 Table 5.4. Estimated annual activity released by CNAO during normal operations, expressed in [Bq y^{-1}] and corresponding USRBIN normalization factors (f_{norm}) for the Monte Carlo Gaussian Plume Model (GPM) (Chapters 4 and 6).

(a) Maximum proton beam energies and number of particles from Table 5.1

Radionuclide	Annual release [Bq y^{-1}]	f_{norm} [$\text{prim Sv y}^{-1} \text{pSv}^{-1}$]
^{11}C	5.10×10^9	4.08×10^9
^{13}N	2.14×10^{10}	1.71×10^{10}
^{15}O	2.67×10^{10}	2.13×10^{10}
^{41}Ar	7.16×10^8	5.73×10^8
Total	5.39×10^{10}	-

(b) CNAO's internal recommendation about maximum indoor activity concentration

Radionuclide	Annual release [Bq y^{-1}]	f_{norm} [$\text{prim Sv y}^{-1} \text{pSv}^{-1}$]
^{11}C	1.64×10^{10}	1.29×10^{10}
^{13}N	6.26×10^{10}	5.01×10^{10}
^{15}O	7.53×10^{10}	6.03×10^{10}
^{41}Ar	2.06×10^9	1.64×10^9
Total	8.97×10^{10}	-

(c) Estimates for the Proton Therapy

Radionuclide	Annual release [Bq y^{-1}]	f_{norm} [$\text{prim Sv y}^{-1} \text{pSv}^{-1}$]
^{11}C	2.99×10^8	2.39×10^8
^{13}N	1.06×10^9	8.48×10^8
^{15}O	1.25×10^9	1.00×10^9
^{41}Ar	4.17×10^7	3.34×10^7
Total	2.65×10^9	-

(d) Estimates for the ab-BNCT

Radionuclide	Annual release [Bq y^{-1}]	f_{norm} [$\text{prim Sv y}^{-1} \text{pSv}^{-1}$]
^{41}Ar	3.70×10^{10}	2.96×10^{10}
Total	3.70×10^{10}	-

5.3 Meteorological data analysis

Local meteorological data was collected from two different detection points:

1. Cascina Pelizza, in the suburbs of Pavia, at 700 m to the west of CNAO, with a Vantage Pro2 weather station [31] managed by Centro Meteorologico Lombardo (CML). This detection station was put in operation on January 1st 2005. CML is an association whose goal is to study and spread knowledge about Lombardy regional climate [30]. The anemometer is placed at 12 m above the ground. Data is recorded every 5 min.
2. CNAO, where the same weather station model was installed on a wide terrace in June 2018 by the radiation protection service. During this thesis work, it turned out that its collocation is not final, but there is the intent to move it above the synchrotron bunker. The anemometer is currently positioned at 10 m above the ground. Data is recorded every 5 min.

Meteorological data analysis was completed to study wind preferential directions and the most frequent atmospheric stability classes over the year. It was reputed useful to compare the two sets of data, in order to have feedback on the functioning of CNAO's weather station against the CML standard. This study is presented in Appendix B.

Meteorological data was downloaded from weather stations and imported in MATLAB. From the over thirty variables measured by Vantage Pro2 weather stations, the following were selected:

- date and time of measurement
- external temperature, measured in [°C]
- wind speed, measured in [km h⁻¹]
- wind direction (i.e. the direction the wind is coming from), using the rule presented in Figure 2.2
- atmospheric pressure, measured in [hPa]
- rain, measured in [mm]
- rain rate, measured in [mm h⁻¹]
- solar radiation, measured in [W m⁻²].

The analysis was conducted for the years 2018 and 2019 using meteorological data recorded by CML. After a first screening of missing or corrupted items, unusable for the statistical processing, the total number of entries over the time considered was 210 228. Corrupted data was concentrated in some days of the years, probably owing to momentary malfunctions of the weather station.

Some user-written scripts were implemented to handle raw information and to extrapolate useful specifics. MATLAB *column-wise* approach for tall arrays of data was followed to reduce at minimum computational time. The analysis of available

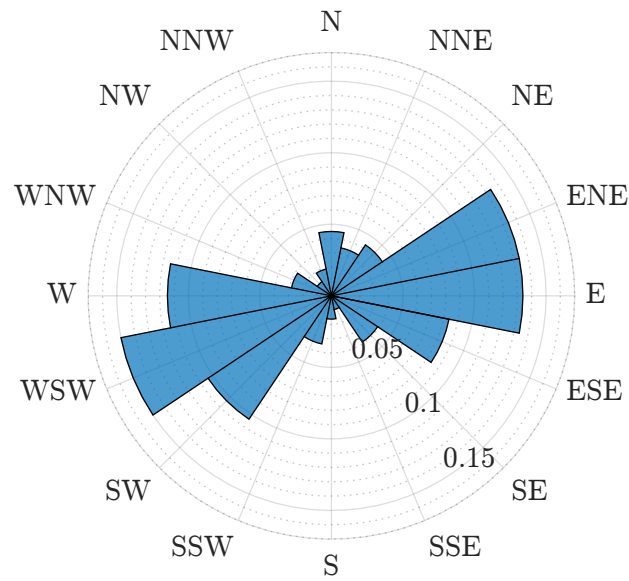


Figure 5.1. Frequency distribution of wind directions in the years 2018 and 2019, recorded by Centro Meteorologico Lombardo (CML). Sixteen 22.5° sectors were considered and calm wind data was discarded. Wind direction is the orientation the wind is coming *from*.

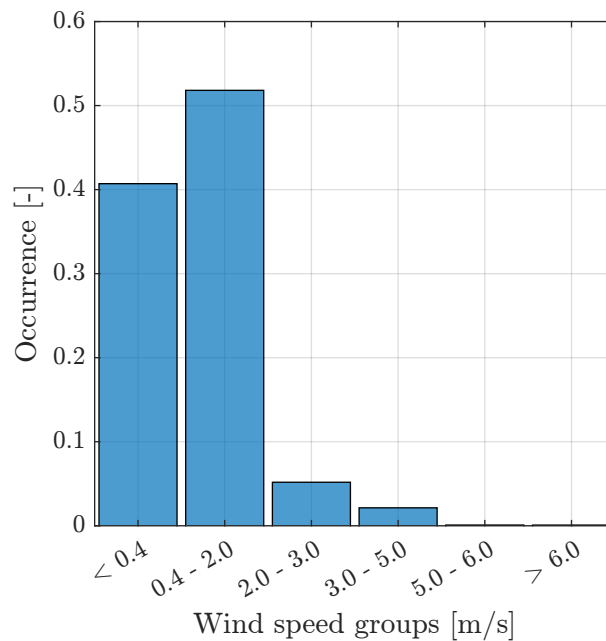


Figure 5.2. Histogram of wind speed data in $[m\ s^{-1}]$ in the years 2018 and 2019, recorded by Centro Meteorologico Lombardo (CML). Groups were inherited from the Solar Radiation Delta-T (SRDT) method, except for the first group, which was split in low-intensity wind and calm wind, i.e. wind below the anemometer’s sensitivity.

records for the years 2018 and 2019 took 20 s to be completed on a personal computer (Intel® Core™ i7-7500U CPU @ 2.70 GHz, quad-core, 8 GB RAM).

Wind directions were grouped in 16 sectors plus calm wind and a polar plot of their frequency distribution was produced (a mention to calm winds appears in Section 2.3). Calm wind data was detected in 29.54% of the observations. In Figure 5.1, wind frequency distribution was normalized over the existing data, excluding calm winds. Predominant direction was west-south-west (WSW).

Wind speed is an essential piece of information for atmospheric stability class evaluation (Table 2.2). After proper conversion from $[\text{km h}^{-1}]$ to $[\text{m s}^{-1}]$, winds were grouped with the same scheme adopted by the SRDT method, except for the first group, which was split into low-intensity wind and calm wind. Wind below 2 m s^{-1} resulted to be the most frequent over the period of observation (Figure 5.2).

Lastly, the atmospheric stability class was computed for each valid meteorological record implementing the SRDT method. From Table 2.2, it should be noted that atmospheric stability class computation is different from daytime to nighttime. To address this issue, `sunrise.m` MATLAB function [51] was used. Its header is here reported:

Listing 5.1. `sunrise.m` MATLAB function header.

```
function varargout = sunrise(varargin)
%SUNRISE Computes sunset and sunrise time.
% SUNRISE(LAT,LON,ALT,TZ) displays time of sunrise and
% sunset at location latitude LAT (decimal degrees,
% positive towards North), longitude LON (decimal degrees,
% positive towards East), altitude ALT (in m above sea
% level) for today. Time zone TZ (in hour) is recommended
% but optional (default is the computer system time zone).
%
% SUNRISE(LAT,LON,ALT,TZ,DATE) computes sunrise and sunset
% time for date DATE (in any datenum compatible format).
% DATE can be scalar, vector or matrix of dates (strings
% or datenum).
```

The function required latitude, longitude and height of the location of interest and returned local sunrise and sunset time. The synchrotron emission stack (point S of Table 1.1) was given in input and the altitude above the sea level was set to 81 m. The implementation of the SRDT method was then developed with the following key concepts:

1. all meteorological data were stored in a MATLAB table variable named `meteo`.
2. For each row of `meteo` (i.e. for each available record), sunrise and sunset were calculated with function `sunrise.m` and stored in columns `meteo.SRISE` and `meteo.SSET`, respectively.
3. Beginning of the day (`meteo.STARTD`) and its end (`meteo.ENDD`) were computed as one hour after sunrise and one hour before sunset, respectively, as indicated by the SRDT method [38].

4. Flag variable `ISDAYT` allowed to distinguish between daytime and nighttime with a simple comparison of times, in which `meteo.DATETIME` contained date and time of each record.
5. The correct rules for the assignment of the atmospheric stability class were consequently chosen and results were saved in column `meteo.STC`.

In this regard, Listing 5.2 is included to show the user-written code prepared to find and assign stability class A in meteorological data:

Listing 5.2. Code for atmospheric stability class A selection.

```
[meteo.SRISE,meteo.SSET,~] = ...
    sunrise(lat,lon,height,tz,meteo.DATETIME);
meteo.STARTD = datetime(datestr(meteo.SRISE))+ hours(1);
meteo.ENDD   = datetime(datestr(meteo.SSET)) - hours(1);

meteo.ISDAYT(meteo.DATETIME >= meteo.STARTD & ...
    meteo.DATETIME <= meteo.ENDD) = true;
meteo.ISDAYT(meteo.DATETIME < meteo.STARTD | ...
    meteo.DATETIME > meteo.ENDD) = false;

% atm stability class A
meteo.STC(meteo.ISDAYT == true & ...
    meteo.WSPEED <= 2 & ...
    meteo.SOLARRAD >= 925) = 'A';
```

In the last instruction, it is possible to note that the stability class A was assigned for all the records featuring a wind speed (`meteo.WSPEED`) lower than 2 m s^{-1} and solar radiation (`meteo.SOLARRAD`) higher than 925 W m^{-2} . All the remaining cases described in Table 2.2 followed an analogous structure. In the code, two approximations were made:

- daylight savings time was not addressed by `sunrise.m`;
- at nighttime, the correct classification of the atmospheric stability class required the knowledge of the vertical temperature gradient. Neither of the two weather stations could calculate this data (according to reference [38], temperatures at 2 m and at 10 m above the ground are needed). For this reason, for each night wind speed group in Table 2.2, the positive vertical temperature gradient case was considered. A positive vertical temperature gradient coincides with the phenomenon known as *temperature inversion*, and represents the worst case for the dispersion of contaminants [11]. In fact, under a positive vertical temperature gradient air convection is stopped. For instance, for night wind speed between 2.0 m s^{-1} and 2.5 m s^{-1} , the code was forced to select class E.

Solar irradiation was plotted in Figure 5.3 for daytime records only. Groups were defined by the SRDT method.

Atmospheric stability class data was plotted in Figure 5.4. A consistent recurrence of high stability classes (D and F) was observed; this data was determined by the stability of nighttime, low wind speeds, and moderate or little solar radiation.

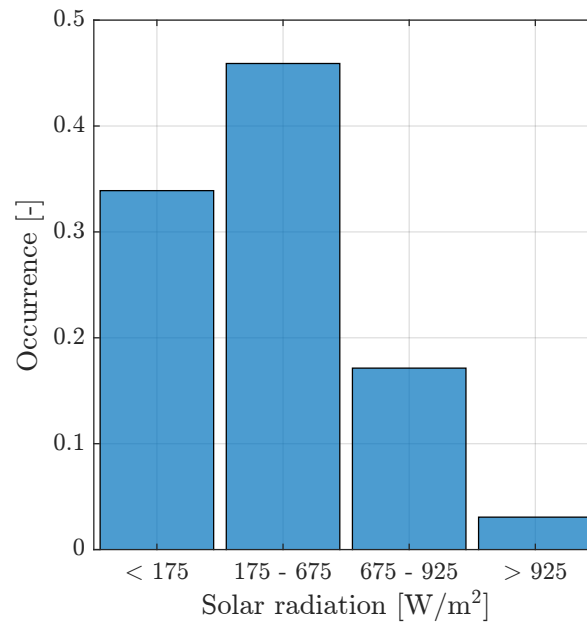


Figure 5.3. Histogram of solar irradiation data in [W m^{-2}] in the years 2018 and 2019, recorded by Centro Meteorologico Lombardo (CML). Groups were inherited from the Solar Radiation Delta-T (SRDT) method.

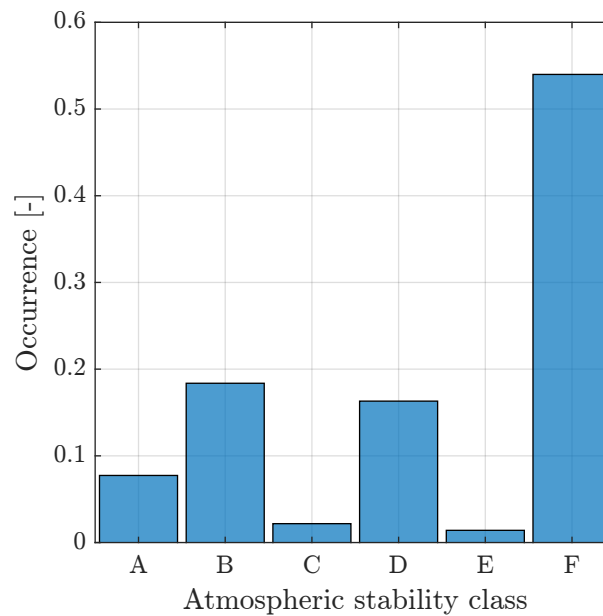


Figure 5.4. Histogram of atmospheric stability classes data in the years 2018 and 2019, calculated with the Solar Radiation Delta-T (SRDT) method.

Chapter 6

The CNAO case: dose evaluations

In this Chapter, inhalation and submersion dose due to the in-air release of contaminants during Centro Nazionale di Adroterapia Oncologica (CNAO)'s normal operations are evaluated. More specifically, the inhalation dose is calculated with GENII V2.10. Submersion dose data is produced completing several simulations with the Gaussian Plume Model (GPM) implemented in FLUKA. Afterwards, an algorithm prepared in MATLAB to merge submersion dose estimates of the static Monte Carlo GPM and real local meteorological data is presented. As a final result, submersion dose maps of the area surrounding CNAO are presented.

6.1 Inhalation dose

Inhalation dose was evaluated by performing a complete simulation in GENII V2.10. In this sense, no particular element of novelty was introduced, but rather a complete application of GENII V2.10 User Manual [18] indications. As already considered in Chapter 2 and Chapter 3, the evaluation of the inhaled dose using in-air activity concentrations and inhalation Dose Conversion Factors (DCFs) represents a valid methodology, widely employed in the literature.

6.1.1 GENII V2.10 simulation

The same conceptual model prepared in Chapter 4 was used. In the Constituent module, ^{11}C , ^{13}N , ^{15}O and ^{41}Ar were selected (Table 5.4a). In the User-defined module, quantities released by synchrotron, experimental and treatment rooms were considered. For ^{41}Ar , also accelerator-based Boron Neutron Capture Therapy (ab-BNCT) contribution was added because significant ($3.7 \times 10^{10} \text{ Bq y}^{-1}$).

The sector averaged chronic plume model was activated in the Atmospheric Transport module. After an extended analysis (Chapter 5), real local meteorological data of Centro Meteorologico Lombardo (CML) weather station for the year 2019 was available to be saved into a GENII V2.10 .met file, in the required format. The same approach was used in Chapter 4, but there a static artificial atmospheric condition was implemented. Records were written to the meteorological data file using some user-written MATLAB scripts, mainly adapted from the meteorological data analysis. These are not further commented for brevity and lack of relevant notes, but remain

available at CNAO radiation protection office for their simplicity and effectiveness in formatting data for its use in GENII V2.10. The atmospheric stability class was calculated with the Solar Radiation Delta-T (SRDT) method.

Observing Figure 1.5, the hospital building closest to the emission stack is at about 100 m. In simulations, GENII V2.10 provides the inhaled dose estimation for the worst point on the space grid. Being the inhaled dose proportional to the activity concentration, which in turn depends on the distance from the source point, it was thus necessary to set GENII V2.10's first receptor point to 100 m to obtain the required data. Of course, higher dose values would have been obtained moving closer to the emission stack. Receptors' height was put to the height of release, i.e. 15 m. The adult male reference was considered and GENII V2.10 automatically uploaded DCFs from its internal database.

Contextually, the skin equivalent dose due to positrons was evaluated. From reference [25], for 700 keV positrons – about the maximum average positron energy considered in this work (Table 5.3) – the mean range in air is $3.135 \times 10^{-1} \text{ g cm}^{-2}$, equal to 260 cm for a 1.204 kg m^{-3} air density. At 100 m from the release point, in unstable and moderately stable atmosphere conditions, the plume is sufficiently spread to feature dimensions comparable or even higher than the positrons' range. Hence, the assumption of semi-infinite cloud dimensions is applicable.

6.1.2 Results and discussion

Inhalation dose results were collected from the Report Generator module for the worst point on the space grid. Alternatively – but more laboriously – it is possible to gather concentration activity estimates, provided in the same final report by the Air Transport module, and manually multiply them by the suitable DCF. This procedure is not straightforward but allows to obtain more data in one single run.

The inhalation dose at 100 m from the release point, at release height, resulted to be $9.87 \times 10^{-10} \text{ Sv}$, due to gaseous ^{11}C . This low value was determined by the use of realistic meteorological data, in which daytime unstable atmosphere and variable wind speed and direction ensured an effective dispersion of contaminants. Since dose was calculated on the plume centre-line – where pollutants are mostly concentrated – it was concluded that at the distance under examination this inhalation pathway was not relevant from a radiation protection viewpoint. In addition, the skin equivalent dose resulted to be $1.7 \times 10^{-6} \text{ Sv}$, well below the radiation protection annual limit of 50 mSv for the population [9].

6.2 Submersion dose

The user-defined routine presented in Chapter 4 was used to evaluate the submersion dose caused by CNAO's in-air releases. FLUKA simulations were imported in MATLAB to consider the wind flow and obtain a more realistic description of the dose in the proximity of CNAO buildings. In a certain sense, several elements of this two-step method are inspired by the sector averaged GPM, but the introduction of radiation transport and the interface to MATLAB offer a practical solution to the issues listed in Chapter 3 regarding the static GPM and the use of DCFs.

6.2.1 FLUKA: radiation transport simulation

Dose evaluations were carried out exploiting FLUKA radiation transport capabilities, in an area of radius 300 m around the emission stack. For this purpose, the same FLUKA input used in Chapter 4 was used. In particular, the cylindrical geometry and materials were not modified. Release height was set to 15 m and plume length to 800 m to consider the contribution of primaries originated at greater distance and directed backward (Section 4.2.3). Also in this set of simulations source effects (Section 2.2.1) were neglected. Further data on the emission would allow computing the plume rise and/or downwash; practically, for the way SOURCE routine is implemented, this information would lead to a change in the release height contained in variable RELH (Appendix A).

Simulations were run in atmospheric stability class F. This was the most frequent atmospheric stability class found in the meteorological data analysis (and the worst condition for contaminants' dispersion). Briggs' dispersion coefficients for open country conditions were used. This choice was somewhat arbitrary, because in some directions tall buildings may affect air transport (a map of the region was presented in Chapter 1). As already pointed out, CNAO is located in a semi-urbanized area, in the outskirts of Pavia. The variability of the area was not introduced in the user-written source routine but, since open country dispersion coefficients produce more conservative estimations [17], it was decided to adopt this approach in the evaluation.

To calculate the dose in a circular region, two cylindrical-geometry USRBINS were set at two different height (1.5 m, ground level, and 15 m, release height) and with the following characteristics:

- R- Φ -Z type
- Radius R: 30 bins, from 0 m to 300 m
- Angle Φ : 80 bins, from 0 rad to 2π rad;
- Height Z: 1 bin from 0.5 m to 1.5 m, and 1 bin from 14.5 m to 15.5 m above the ground level.

The requested angular binning allowed to score the dose in 4.5° circular sectors, thus producing a rather dense mapping of the dose itself. In addition, the number of bins was thought to be organised in sixteen main sectors, each one with five *sub-bins*. This choice goes in the direction of merging USRBIN data with the frequency distribution of wind directions; in fact, it is reminded that wind sectors are sixteen, too. It is important to underline that this organisation does not have a practical correspondence in FLUKA commands, but represents a conceptual detail for the continuation of the work.

A second issue arose trying to ideally align wind sectors and angular binning: the R- Φ -Z type USRBIN adopts polar coordinates; hence, angles are computed starting from the x -axis of a Cartesian plane and increase counterclockwise. This implementation produces a shift of 11.25° with respect to wind directions and correspondent wind sectors (the displacement is illustrated in Figure 6.1). In order to precisely merge meteorological and dose data, cards ROTPRBIN and ROT-DEFIni [26] were activated to rotate cylindrical USRBINS and make them match the orientation of wind sectors.

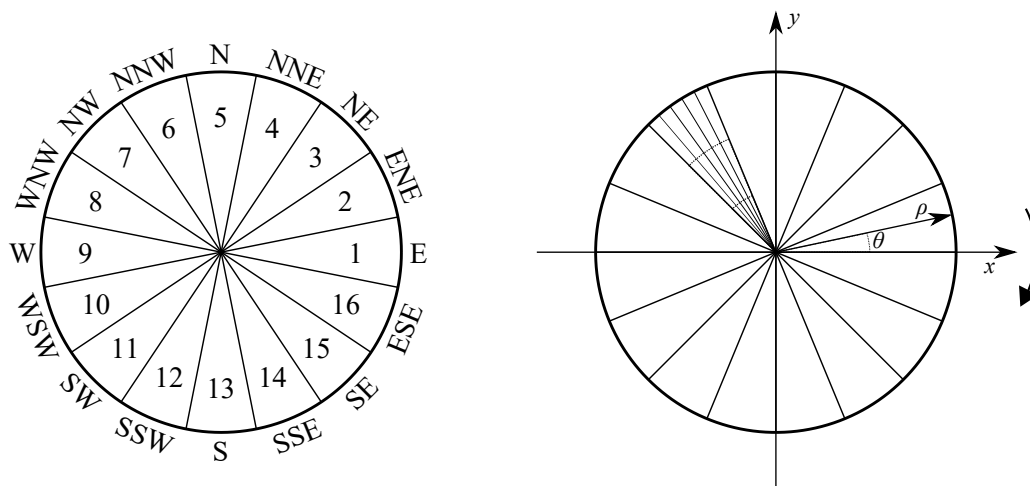


Figure 6.1. Comparison between wind sectors and a simplified representation of the R- Φ -Z type USBIN used in FLUKA simulations. In the latter, five *sub-bins* and three radial bins are represented. FLUKA USBIN and wind directions are shifted by 11.25° . In order to precisely merge meteorological and dose data, cards ROTPRBIN and ROT-DEFINI were activated to rotate cylindrical USBINs and make them match wind sectors.

As a concluding note about the simulation geometry, it is reminded that, for the way SOURCE routine was implemented, the GPM centre-line lies along the x -axis in FLUKA's three-dimensional space; for this reason, the plume can be thought to be transported to the east. This aspect is remarked in the Section dedicated to the results of this first part of simulations.

For each radionuclide listed in Table 5.3, a simulation was performed. In BEAM card, primaries were loaded according to the same Table. Hence, for ^{41}Ar , 1.29×10^3 keV photons were given in input. For β^+ emitters, the average positron emission energy was loaded. It is reminded that the direction of primaries was autonomously handled by the user-written source routine. AUXSCORE was loaded to use FLUKA built-in conversion factors and return results in terms of ambient dose equivalent $H^*(10)$ (option amb74) [42], selectively scoring only photons.

Partial results

Four different simulations, for ^{11}C , ^{13}N , ^{15}O and ^{41}Ar , were carried out. A graph analogous to Figure 4.4 was plotted in Figure 6.2 for ^{15}O , a β^+ emitter with short half-life [48]. As discussed in Chapter 4, in this case the importance of achieving a non-uniform downwind distribution is noticeable: in the case of a low-intensity constant wind, a short-lived radionuclide produces a negligible activity concentration at some hundreds of metres from the release point.

FLUKA R- Φ -Z type USBIN results for ^{41}Ar were plotted in Figure 6.3a and 6.3b, for receptor at 15 m and 1.5 m, respectively. As anticipated, the plume is transported to increasing positive values of the x -axis (the areas of higher dose confirmed this remark). With respect to the correspondence between wind and R- Φ -Z type USBIN sectors, FLUKA simulations were performed under a constant wind from west to east.

It is recalled that USBIN detectors were set to score DOSE-EQ (dose equivalent), but required a normalisation factor (f_{norm}) to convert results from picosievert per

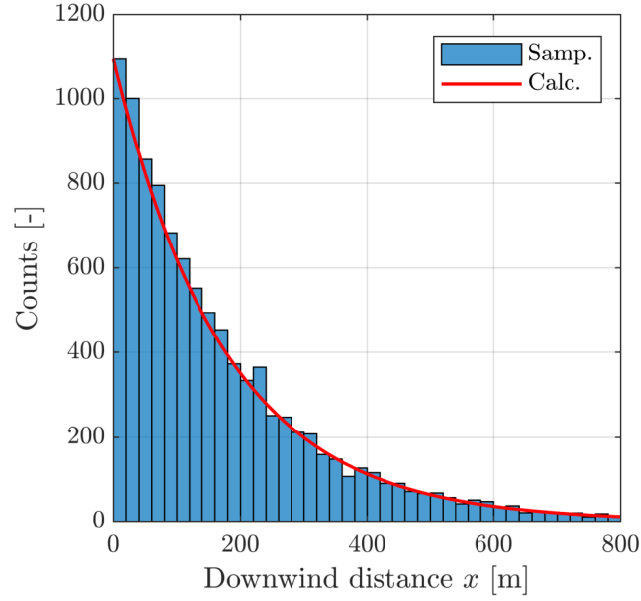


Figure 6.2. Downwind distribution of ^{15}O source points sampled from an F class, 800 m long Gaussian Plume Model (GPM) (Samp.). In red, the corresponding analytical exponential decreasing activity function was calculated and overlapped (Calc.).

unit primary weight [pSv prim^{-1}] to the desired unit of measurement, in this case nanosievert per year. The normalisation factor depends on the contaminant annual in-air release (i), the plume length in the GPM source routine (L), and wind speed (u) through the formula (Section 4.2.3):

$$D \left[\frac{\text{nSv}}{\text{y}} \right] = D \left[\frac{\text{pSv}}{\text{prim}} \right] \cdot f_{norm} \left[\frac{\text{prim nSv}}{\text{y pSv}} \right]$$

where

$$f_{norm} \left[\frac{\text{prim nSv}}{\text{y pSv}} \right] = i \left[\frac{\text{prim}}{\text{y}} \right] \cdot \frac{L [\text{m}]}{u [\text{m s}^{-1}]} \cdot 10^{-3} \left[\frac{\text{nSv}}{\text{pSv}} \right]$$

in which the annual released activity i can be expressed in [Bq y^{-1}] if the branching ratio of the radioactive decay is unitary. In Chapter 5, the total activity discharged in one year was evaluated for the synchrotron bunker (together with three treatment rooms and one experimental room), the Proton Therapy (PT) and the ab-BNCT planned facilities, separately; results were summarised in Table 5.4. Contextually, a normalisation factor was calculated for each radionuclide expelled. For the example given in Figure 6.3, USRBIN data was taken from ab-BNCT emissions (Table 5.4d).

As expected, doses were higher at the release height; an (unrealistic) annual permanence inside the plume would lead to a submersion dose contribution in the order of $1 \mu\text{Sv}$ to $10 \mu\text{Sv}$. At the ground, instead, the static GPM predicted a dose of 500 nSv y^{-1} . The cylindrical USRBIN allowed detecting the presence of a dose contribution in every sector, owing to photons that travel outside the plume in all directions.

R- Φ -Z type USRBIN data was not treated directly in FLUKA. Figures like 6.3a and 6.3b were prepared for illustrative purposes and to verify the correct outcome of simulations. USRBIN data .bnn files were converted to the ASCII format

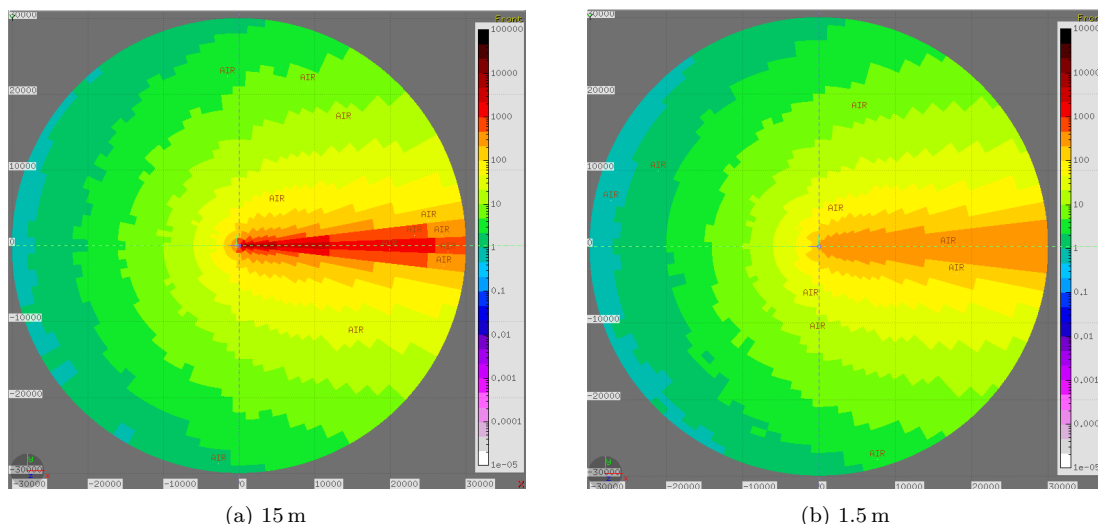


Figure 6.3. FLUKA visualisation of cylindrical USBINs at two receptor heights of the annual dose given by a static Gaussian Plume Model (GPM) of ^{41}Ar in an area of 300 m around the emission stack. Annual release and normalisation factor were given in Table 5.4d.

(.bnn.lis file extension) using a dedicated routine in Flair panel *Run - files*. Two ASCII files for each radionuclide were produced and exported, namely one for the dose at the height of release and one for the ground level. In these files, USBIN data are typically not normalised (normalisation is given in input in Flair *geometry* panel).

6.2.2 MATLAB: merge dose and meteorological data

A set of MATLAB scripts was prepared to merge USBIN dose data with real local meteorological records and produce dose maps in terms of ambient dose equivalent. In the first part of the procedure implemented, USBIN data were imported and underwent initial processing. At a later stage, dose estimates were normalised using Table 5.4, as explained in the previous Section, and maps were generated for the synchrotron bunker (together with three treatment rooms and one experimental room), the PT and the ab-BNCT planned facilities, separately. In the following, the key concepts of the method implemented are highlighted.

Physical explanation

Performing the same steps completed in Section 4.2.3 in the framework of the software comparison, the user-written source routine allowed to implement in FLUKA the GPM and conveniently model the transport of particles.

The routine is static, in the sense that the radioactive cloud extends only in one direction. In the previous pages, it was explained that the plume is directed along the x -axis – or to the east, if the correspondence between wind directions and the R- Φ -Z type USBIN is considered. Dose maps like 6.3a and 6.3b, hence, showed the annual dose given by the continuous release of contaminants transported in one single direction for one year.

The sector averaged GPM was introduced in Chapter 3 with the specific intention of modeling the variability of wind. In fact, over a long period of time, the wind

direction is likely to touch all the points of the compass. Therefore, given an annual wind rose, the distribution of annual average concentrations in a polar grid space around a continuous source can be estimated [13]. In FLUKA, the polar grid space was implemented adopting the R- Φ -Z type USRBIN (organised in sixteen main sectors); plus, a sixteen-sector annual wind rose was obtained by analysing meteorological data (Chapter 5).

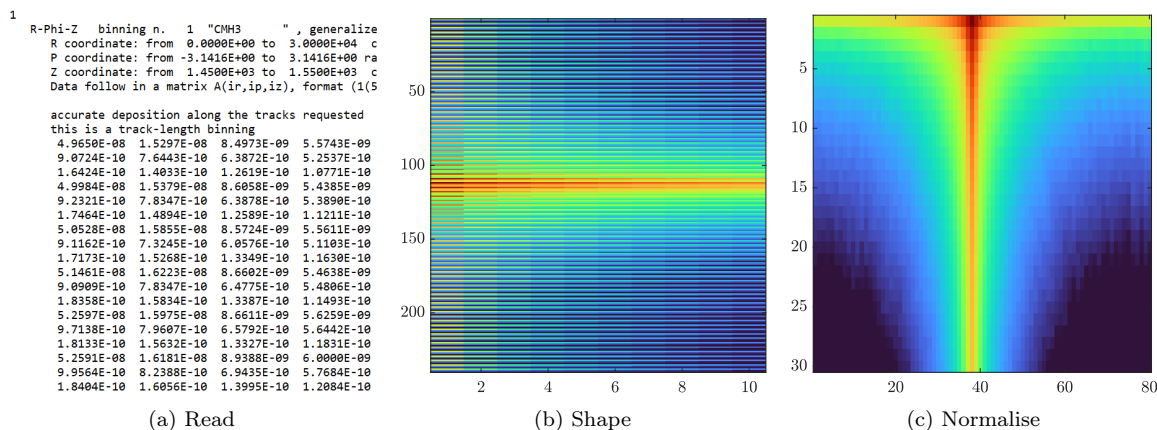
A wind frequency data represents the fraction of the year during which the wind blows towards a certain wind sector, and thus for how much time the plume is directed towards a certain point of the compass. In MATLAB, dose maps like 6.3a and 6.3b were multiplied by the frequency distribution of wind directions: if a wind blew for a fraction f_i of the year towards the sector i , then FLUKA dose maps were oriented to align the plume centre-line towards wind sector i and weighted for f_i . The total annual dose map was calculated summing all the weighted contributions of the sixteen plume (and so dose maps) orientations on the compass grid. Figure 6.5 was prepared to illustrate this concept and is further discussed in the next Sections, together with a more detailed description of the algorithm implemented.

Data pre-processing: **FL_prepData.m**

As a first task, USRBIN dose files in `.bnn.lis` format were imported and prepared for the subsequent analysis. Function `FL_prepData` was implemented to fulfil this purpose performing the following main steps (visually summarised in Figure 6.4):

- (a) *Read* `.bnn.lis` dose file using function `readUSRBIN` (Appendix C). This function scans the whole USRBIN file and imports numeric data in a MATLAB matrix variable, discarding at the same time the descriptive text appended by FLUKA. In the dose file, data is arranged in ten columns, and corresponding statistical uncertainty follows scoring values; `readUSRBIN` function imports dose data in the upper half of the matrix rows and parallel errors in the bottom half. Moreover, maximum statistical uncertainty in results is researched and printed. Being `readUSRBIN` the ideal starting point of any MATLAB code that handles USRBIN data, this MATLAB function represents a valid attempt to extend the post-processing of FLUKA results outside this Monte Carlo software.
- (b) *Shape* `readUSRBIN` matrix to the same dimensions of the FLUKA R- Φ -Z type USRBIN presented in the previous Section (30 radial bins, 80 angular bins). This is done with MATLAB command `reshape`. Figure 6.4b shows a visualisation of the dose matrix through colors, from which it is possible to observe that dose values are not ordered to reproduce the GPM dose maps, as in Figure 6.3 (except for a shift from a circular to a rectangular shape of the map).
- (c) *Normalise* USRBIN data using the procedure described in Section 4.2.3 and recalled in the previous one. In the third image of Figure 6.4, 80 columns correspond to the 80 angular bins, while 30 rows are the correspondent radial distances. At this point, the circular dose map visualised in Figure 6.3 is conveniently and correctly imported in MATLAB.

Recalling the previous Section, FLUKA simulations were performed for four radionuclides, i.e. the main radioactive isotopes emitted from a typical hadron therapy

Figure 6.4. Visualisation of the main steps performed in `prepData` function.

or accelerator facility (Table 5.3: ^{11}C , ^{13}N , ^{15}O and ^{41}Ar). For each of them, USRBIN scoring detectors were placed at ground level and release height. Therefore, for each radionuclide, radiation transport data was produced inside FLUKA.

The usefulness of USRBIN normalisation becomes evident at this point: each facility, i.e. synchrotron (with experimental and treatment rooms, hereafter implicitly considered together), PT, ab-BNCT, showed different mixtures and quantities of isotopes released, but the underlying physics of the diffusion process of contaminants and radiation transport remained unchanged. Hence, modifying the normalisation factor was sufficient to adapt FLUKA simulations to every facility considered, or to future changes in released quantities. Of course, if further studies revealed the presence of other isotopes released to the atmosphere, new evaluations should start from radiation transport inside FLUKA.

From Table 5.4, or from its extract about synchrotron operations and releases reported in Table 6.1, it is possible to observe that every facility emits a mixture of radionuclides. For each radionuclide, function `FL_prepData` was called with the correct normalisation factor and a dose matrix was obtained as output. The submersion photon ambient dose equivalent was eventually calculated combining all the matrices with an entry-wise matrix addition. For instance, concluding the example about synchrotron emissions (Table 6.1), the final dose map was computed performing the operation:

$$D_{tot} = D(^{11}\text{C}) + D(^{13}\text{N}) + D(^{15}\text{O}) + D(^{41}\text{Ar}) \quad (6.1)$$

in which D_{tot} is the final map in terms of $H^*(10)$, and the other addends are ambient dose equivalent maps for each radionuclide, as returned by the pre-processing function `FL_prepData`. For each facility, this procedure was carried out at the ground level and release height.

MATLAB pre-processing final result is a set of six matrices that represent the $H^*(10)$ submersion dose given by the mixture emitted by each facility, calculated at two different heights. These matrices are normalised with respect to USRBIN rules and ready to be merged with the frequency distribution of wind directions.

Table 6.1. Estimated annual activity released by CNAO during normal operations, expressed in $[\text{Bq y}^{-1}]$ and corresponding USBIN normalization factors (f_{norm}) for the Monte Carlo Gaussian Plume Model (see Chapters 4 and 6). Maximum proton beam energies and number of particles from Table 5.1. Extracted from Table 5.4a.

Radionuclide	Annual release $[\text{Bq y}^{-1}]$	f_{norm} $[\text{prim Sv y}^{-1} \text{ pSv}^{-1}]$
^{11}C	5.10×10^9	4.08×10^9
^{13}N	2.14×10^{10}	1.71×10^{10}
^{15}O	2.67×10^{10}	2.13×10^{10}
^{41}Ar	7.16×10^8	5.73×10^8
Total	5.39×10^{10}	-

Data elaboration: `FL_elabData.m`

Meteorological data was analysed in Section 5.3. In Figure 5.1, frequencies of wind directions over a period of two years were plotted in a wind rose, excluding calm winds. Frequencies were saved and imported in MATLAB, where 180° were added to each direction; in this way, frequencies were transformed in the direction *towards* which the wind was blowing, i.e. where the plume was transported. USBIN data like Figure 6.3, or the corresponding “squared” version in MATLAB, contained doses due to annual releases, but one wind direction. In fact, in the user-written routine the plume is static and does not follow any wind variability.

As said, from a physical viewpoint, in function `FL_elabData` the plume was imagined to be rotating around the emission point owing to the wind flow, and the dose was weighted with respect to the plume’s time of permanence in each one of the sixteen wind sectors, i.e. on the annual wind frequency distribution.

From a mathematical viewpoint, this goal was achieved by introducing the concept of circular permutation of matrices. A permutation π of n elements is an ordering of the set $\{1, 2, \dots, n\}$, and can be thought as a bijective function $\pi : \{1, 2, \dots, n\} \mapsto \{1, 2, \dots, n\}$ [52]. The permutation π may be represented in *two-line form* by

$$\begin{pmatrix} 1 & 2 & \dots & n \\ \pi(1) & \pi(2) & \dots & \pi(n) \end{pmatrix}.$$

In general, the $n \times n$ permutation matrix $P_\pi = p_{ij}$ corresponding to permutation π is obtained permuting the columns of the identity matrix I_n :

$$p_{ij} = \begin{cases} 1 & \text{if } \pi(i) = j \\ 0 & \text{otherwise} \end{cases}.$$

For example, let P_π be the permutation matrix corresponding to the permutation:

$$\pi = \begin{pmatrix} 1 & 2 & 3 & 4 \\ 4 & 1 & 2 & 3 \end{pmatrix}. \quad (6.2)$$

If P_π is applied to a 4×4 square matrix M through the product MP_π , the columns

of M are permuted as follows:

$$MP_{\pi} = (\text{col}_1 \quad \text{col}_2 \quad \text{col}_3 \quad \text{col}_4) \begin{pmatrix} 0 & 1 & 0 & 0 \\ 0 & 0 & 1 & 0 \\ 0 & 0 & 0 & 1 \\ 1 & 0 & 0 & 0 \end{pmatrix} = (\text{col}_4 \quad \text{col}_1 \quad \text{col}_2 \quad \text{col}_3).$$

The result of permutation (6.2) is that all columns are shifted by one position to the right. If an analogous permutation is applied to a dose matrix – D_{tot} , Equation (6.1) – the same effect is obtained: its columns are shifted by one position. In the pre-processing step, it was observed how during the reading phase USRBIN angular bins were made matching the columns of MATLAB dose matrices. Therefore, shifting all the columns by one position has the meaning of rotating all dose values by one angular bin.

Considering only the USRBIN 16 main sectors, the final dose estimate was obtained rotating dose maps D_{tot} 16 times, to align it to the sixteen wind directions, and weighting for the wind frequency f_i of each wind sector. The operation set up to calculate the annual ambient dose equivalent may be written as:

$$H^*(10) = \sum_{i=1}^{16} f_i P_{\pi}^i D_{tot} \quad (6.3)$$

where f_i is the annual wind frequency in the i -th sector, P_{π} the permutation matrix that shifts dose maps of one wind sector, and D_{tot} was calculated in Equation (6.1).

Actually, it should be reminded that R- Φ -Z type USRBIN had five sub-bins per wind sector. In each wind sector, the plume centre-line was set to scan uniformly all the five sub-bins; in other words, when the plume centre-line approached a new wind sector, five rotations of one angular bin were made and rotating dose maps were averaged. As a result, smoother dose maps were obtained. This attempt was made to compensate for the low resolution of wind directions data provided by the weather station (Chapter 5): classifying recorded wind directions in 22.5° wind groups, despite being in agreement with the literature, completely cancels the variability of winds inside each wind sector.

Lastly, from a coding viewpoint, the concept of cyclic permutation of a matrix was applied with MATLAB `circshift` command. In Figure 6.5, a schematic visualisation of the algorithm implemented is shown. In the upper part, the plume is oriented in different wind directions and is weighted for the correct direction frequency. In the bottom part, the analogue code implementation of the same process is visualised. This algorithm was prepared to follow changes in wind direction without neglecting dose contributions: lateral diffused and back-scattered radiation is always correctly considered. In a certain way, the approach tried to develop the concept of sector averaged GPM (Section 3.2.2) with the data produced from a Monte Carlo code.

Data elaboration was organised to be a simple and highly autonomous process. Feedback was provided to report the user possible errors; partial and final results were saved in tables. Function `FL_elabData` last task was to plot matrix $H^*(10)$. Dose maps were prepared by modifying `polarhistogram` MATLAB function. A color map and a legend were added. Dose maps were produced for all the six D_{tot} matrices, i.e. for three facilities at two different receptors' height.

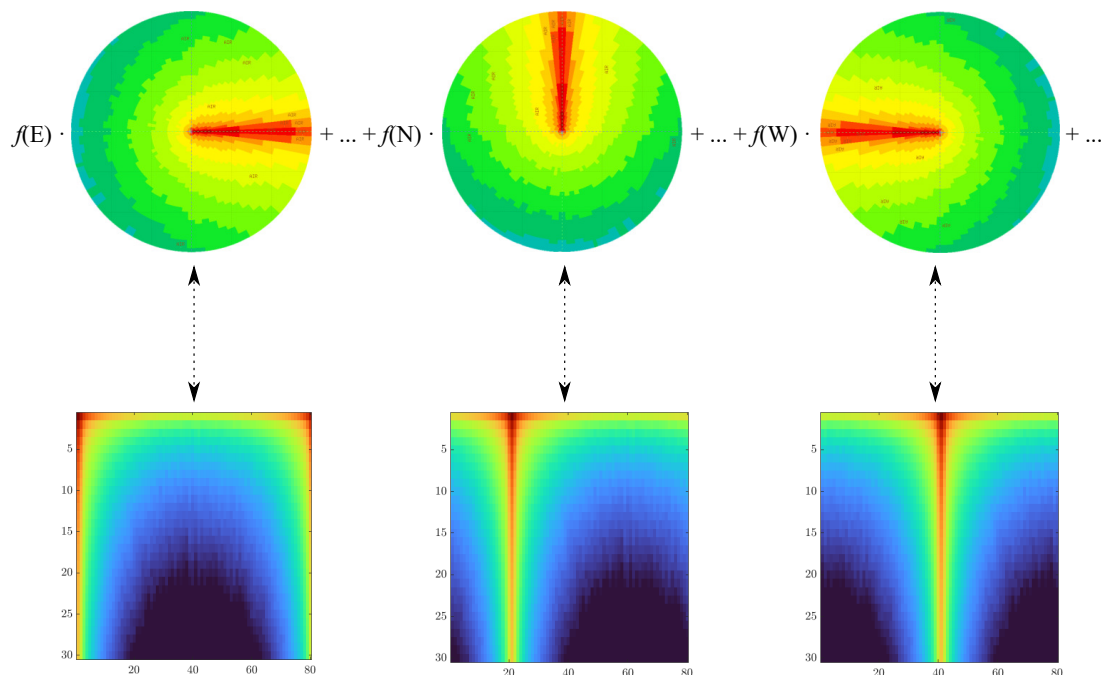


Figure 6.5. Visualisation of the algorithm performed in `elabData` function for three wind directions. In the upper part, the physical change of direction of the plume is illustrated by graphically rotating USRBIN maps; in the bottom part, the corresponding circular permutation of USRBIN matrices is represented.

6.2.3 Results and discussion

FLUKA USRBIN files of the dose given by photons produced in an atmospheric stability class F GPM were analysed inside MATLAB. In all the cases, FLUKA statistical uncertainty was kept below 10% with sufficient computational resources. In general, a larger computation time was needed for simulations involving β^+ emitters. In any case, all the calculations were concluded in the acceptable time of few hours using about ten cores in parallel on CNAO’s workstations. The frequency distribution of winds was manually uploaded in MATLAB from the analysis performed in Chapter 5 (Figure 5.1).

Functions `prepData` and `elabData` were called twice for each facility, to prepare the photon $H^*(10)$ map at release height and ground level. For the synchrotron bunker, experimental and treatment rooms, released quantities and normalisation factors were taken from Table 5.4a for a mixture of ^{11}C , ^{13}N , ^{15}O , ^{41}Ar . It is reminded that results were intended to be conservative in several ways, starting from the in-air activity concentration, which was calculated using synchrotron maximum proton current and proton energy. For the upcoming PT, the same mixture was used, but different released quantities were used (Table 5.4c). Lastly, for ab-BNCT, only ^{41}Ar was considered with an upper-bound estimated emission of 3.7×10^{10} Bq (Table 5.4d). In the following, maps are presented (Figures 6.6, 6.7, 6.8, 6.9, 6.10, 6.11); results were expressed in nanosievert per year and radial distances in metres. It is possible to observe how maps contain dual information about wind directions with respect to the analysis performed in Chapter 5: from a “wind coming *from*”, data was properly transformed to a “wind blowing *towards*” kind of information. In addition, the finer

angular binning requested in FLUKA for the R- Φ -Z type USRBIN is visible; it allowed achieving an accurate mapping of the circular area without exaggerating the detail, a fact that would have led to a smoother visualisation at the cost of a more demanding data management.

Results showed the higher submersion dose contribution given by the operating synchrotron, in virtue of a more relevant in-air discharge of contaminants. As a rough indication for the CNAO case, doses at release height become of interest at around 100 m from the release point. At this radial distance, in fact, in about every direction the area of the facility borders with other buildings. In all the cases, the annual ambient dose equivalent never exceeded few hundreds of nanosievert. At the ground, doses are generally less, even by a factor 10. Also, it should be considered that buildings may shield part of the photons.

Predictably, in all the cases the most exposed areas surrounded emission points. As observed in various parts of this work, it is reminded that results in the first tens of metres rely on an extrapolation of the range of applicability of Briggs' dispersion coefficients, which was considered necessary for the FLUKA source routine implementation. Moreover, in the first metres source effects can play a significant role in an unstable atmosphere (Chapter 2), yet are difficult (or even impossible) to model in an analytical way. For these reasons, results in the first metres are more prone to errors; on the other hand, emission stacks are placed on CNAO's rooftops and are easily accessible (with permission). Hence, the possibility of performing a future set of measurements of in-air activity near stacks – or even continuous monitoring – should compensate for the limits highlighted and clarify the realistic dose data. The same note cannot be given for the more distant receptor points at the ground: predicted dose values are low enough not to be measurable, hidden by the natural environmental background level.

As a last comment, all the major approximations are summarised and briefly commented:

- Range of applicability of Briggs' coefficients (Section 2.3.4): Briggs' results for dispersion coefficients were extrapolated also below 10 m for computational reasons; this decision allowed reproducing reasonably the geometry of the GPM also in the first metres, but remains an arbitrary choice. However, near the emission stacks, direct measurements of in-air activity should be more feasible and, ultimately, rooftops surrounding source points could be classified as restricted areas for precautionary reasons.
- Plume rise and source effects (Section 2.2.1): plume rise and source effects strongly depend on aerodynamic effects and are hardly described by simplified and analytical relationships. Since their major effect on the GPM is a variation of the release height (dH term), it was decided to neglect them and, if needed, rely on future calculations and knowledge about the upcoming ventilation systems for the expansion project, given that the proposed computational method will be modified only by a proper variation of the release height.
- Briggs' open country dispersion coefficients (Section 1.2.2 and 4.1): open country dispersion coefficients are more conservative and therefore considered suitable for a radiation protection evaluation. The use of these coefficients was considered

correct in the area to the north of CNAO, while the southern part is characterised by the presence of buildings of relevant dimensions, which surely introduce several aerodynamic effects on the local wind circulation.

- Average energy of primary particles (Section 4.2.3): in FLUKA BEAM card, the average energy of primary particles was loaded.
- Atmospheric stability class (Section 2.3.3): simulations described in the present Chapter, and used to produce dose maps, were completed for a class F GPM. The use of a high stability class guarantees conservative results. Moreover, this choice proved to be realistic on the basis of the meteorological data analysis performed in Section 5.3.
- 1 m s^{-1} wind (Section 2.2.1 and Section 4.2.3): a low wind speed limits the in-air dispersion of contaminants, resulting in conservative estimates. Also, this is often used as the standard wind speed in the literature concerning radiation protection. In the CNAO case study, the meteorological data analysis showed the persistence of low-intensity winds, making the assumption on wind speed credible.
- Estimates about annual activity releases (Section 5.2): estimates for air activation inside rooms were completed in the framework of a previous M.Sc. thesis and other ongoing studies; the procedure was summarised in Chapter 5. At this level, calculations were performed under conservative assumptions; real air replacement rates were used.

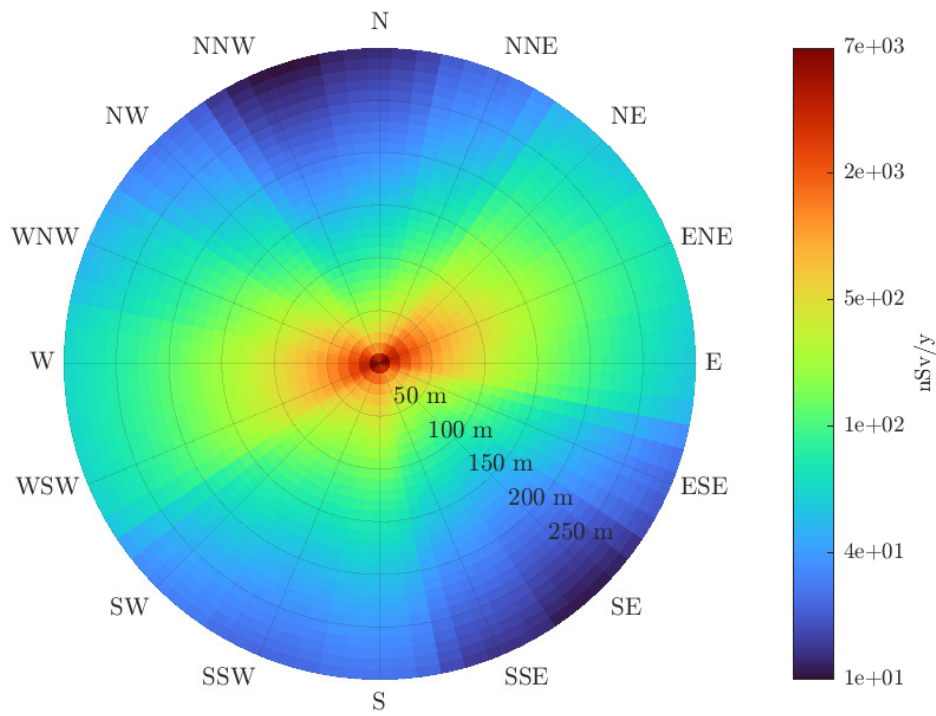


Figure 6.6. Photon submersion dose in terms of $H^*(10)$ [nSv y⁻¹] for synchrotron chronic in-air radioactive releases and 2018 and 2019 meteorological data at release height (15 m).

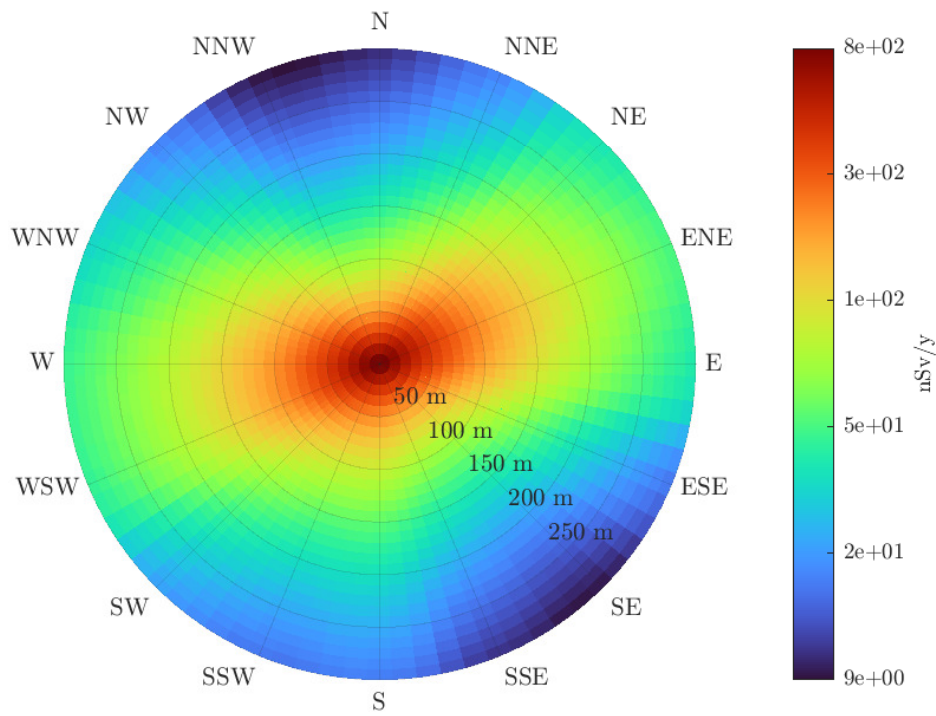


Figure 6.7. Photon submersion dose in terms of $H^*(10)$ [nSv y⁻¹] for synchrotron chronic in-air radioactive releases and 2018 and 2019 meteorological data at ground level (1.5 m).

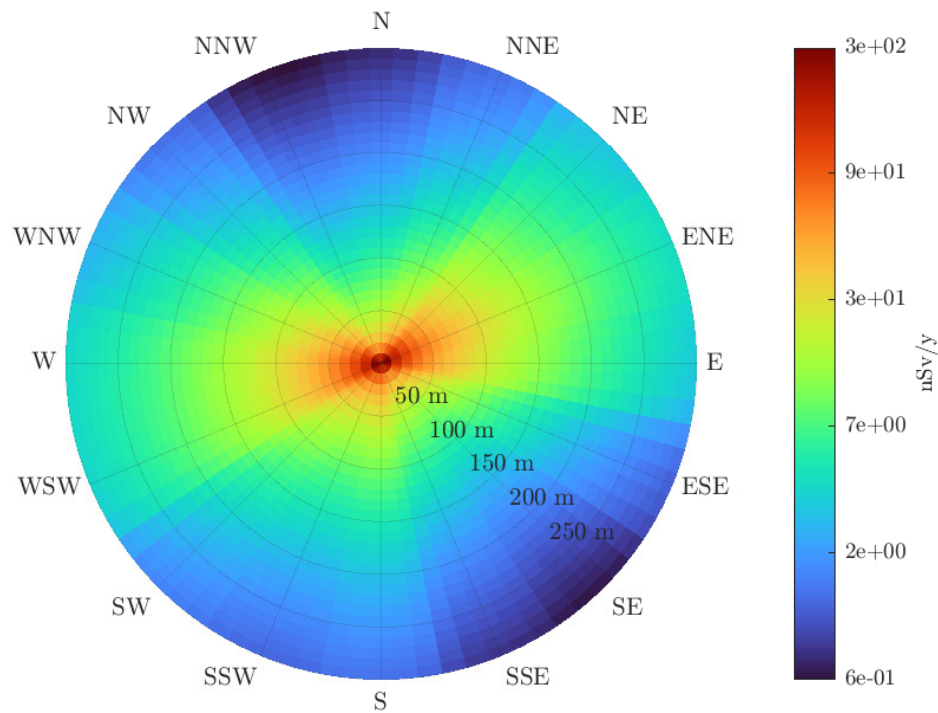


Figure 6.8. Photon submersion dose in terms of $H^*(10)$ [nSv y⁻¹] for PT chronic in-air radioactive releases and 2018 and 2019 meteorological data at release height (15 m).

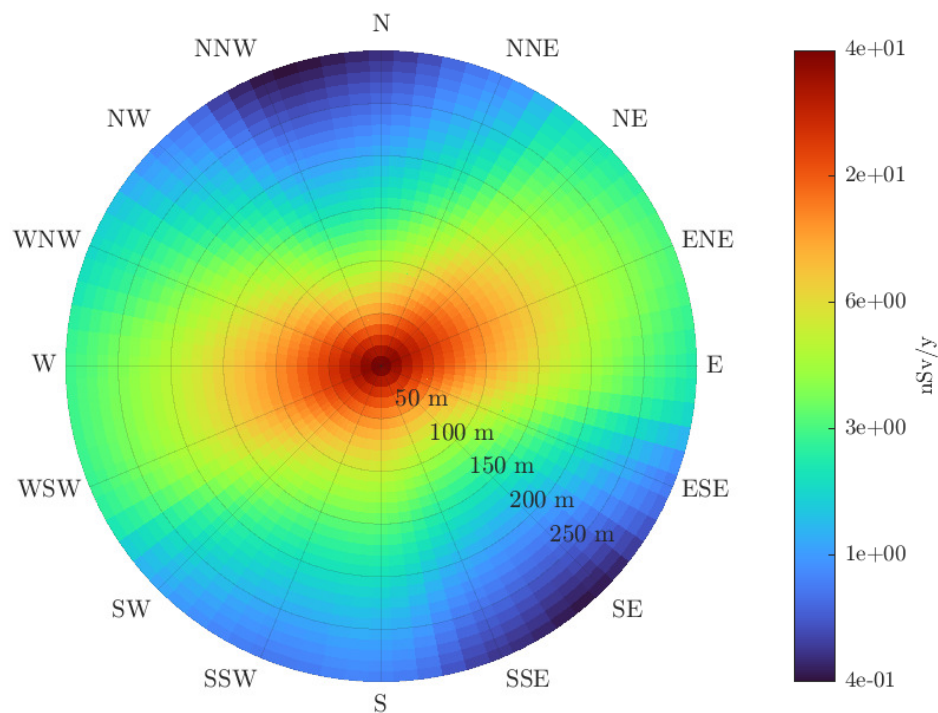


Figure 6.9. Photon submersion dose in terms of $H^*(10)$ [nSv y⁻¹] for PT chronic in-air radioactive releases and 2018 and 2019 meteorological data at ground level (1.5 m).

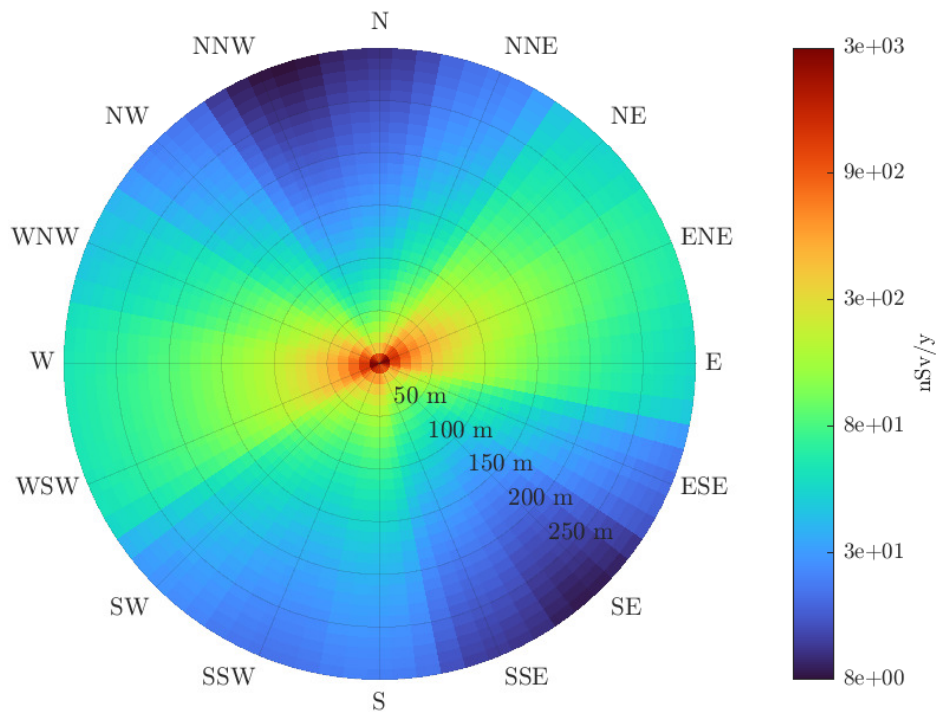


Figure 6.10. Photon submersion dose in terms of $H^*(10)$ [nSv y⁻¹] for ab-BNCT chronic in-air radioactive releases and 2018 and 2019 meteorological data at release height (15 m).

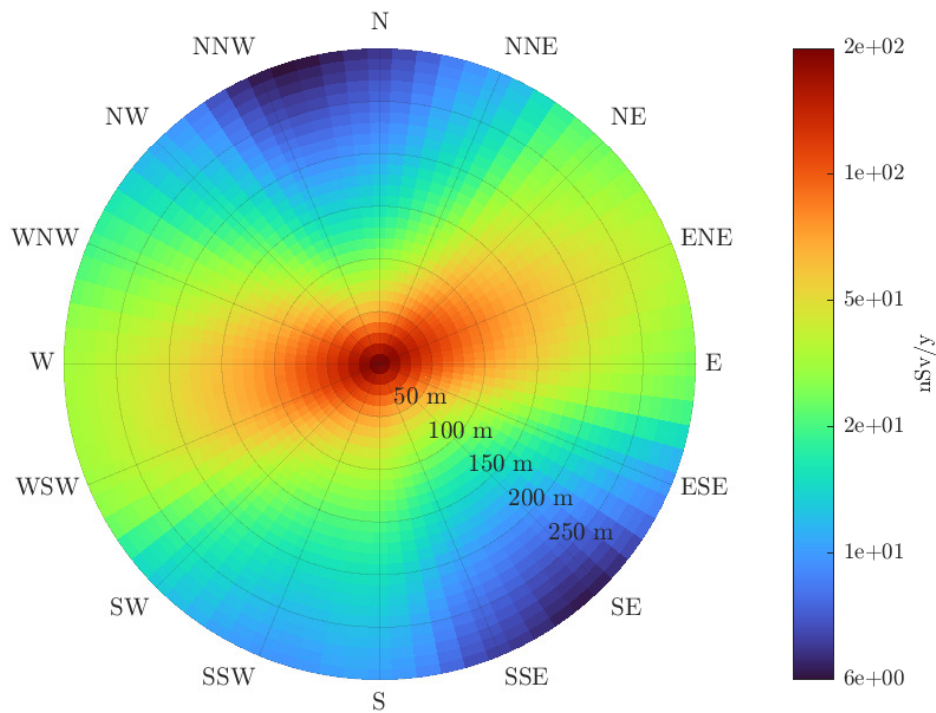


Figure 6.11. Photon submersion dose in terms of $H^*(10)$ [nSv y⁻¹] for ab-BNCT chronic in-air radioactive releases and 2018 and 2019 meteorological data at ground level (1.5 m).

6.3 Concluding remarks and future studies

As a concluding note, the main results achieved in this work are highlighted.

- The physical phenomena of air activation and ventilation at hadron therapy facilities and transport of contaminants in the atmosphere were reviewed from a theoretical viewpoint, analysing several studies and a previous M.Sc. thesis (Chapter 2).
- Department Of Energy of the United States of America (DOE)'s certified software HotSpot and GENII V2.10 were analysed, with reference to literature, to understand the algorithm used for dose evaluations following radioactive releases in air, highlighting its major limits. The use of a Monte Carlo code to address radiation transport was proposed as a viable solution for the issues listed (Chapter 3).
- The FLUKA user-written source routine of a GPM was successfully implemented (Section 4.2.3): the localisation of decay points in FLUKAgeometry was illustrated in some plots, demonstrating the correct Gaussian-like distribution of pollutants along cross-wind and vertical axes; along downwind axis, activity was distributed taking into account radionuclides' half-life and a constant wind speed. At long downwind distance, FLUKA showed a converging trend with respect to HotSpot and GENII V2.10; in the proximity of the release point, the expected submersion dose contribution given by photons (Section 3.3) was detected.
- The user-written source routine of a GPM (Section 4.2.3) was designed to be easily reusable: currently, in the code it is necessary to select only the correct radionuclide decay constant (among ^{11}C , ^{13}N , ^{15}O , ^{41}Ar), while the atmospheric stability class and the release height are given in input to the routine through SOURCE card in Flair input panel. In this way, manual modifications to the source code are limited to the maximum.
- An extensive analysis of local meteorological data was completed (Section 5.3), paying attention to implement an effective computational approach; a comparison between two different weather stations was provided (Appendix B).
- FLUKA USRBIN data and MATLAB were successfully interfaced (Section 6.2.2): this approach was explained to be general and might be useful for other advanced elaborations regarding FLUKA results; the necessary code was attached.
- The computational method proposed for submersion dose calculations is in two steps, but straightforward (Section 6.2): for each radionuclide released in the air, one FLUKA simulation needs to be completed. Then, USRBIN data import to MATLAB is smoothly handled by MATLAB itself. Since results' normalisation occurs in MATLAB, any change in the estimates of in-air released quantities does not affect the Monte Carlo simulations, but the much faster MATLAB part, resulting in considerable time savings.

- Final dose evaluations for CNAO (Section 6.2.3) predicted low doses for individuals. The use of class F GPMs, upper-bound released quantities, Briggs' open country dispersion coefficients, low wind speeds allowed achieving a conservative, but realistic, approach to the case study.

In the future, the user-written source routine may be further developed extending it to other radionuclides. This would be facilitated by loading radionuclide decay constants from FLUKA database (BEAM and HI-PROPE might be useful) and properly modifying the `source.f` file. The improvement would lead to the complete use of the GPM source routine exclusively inside Flair; moreover, the proposed computational method would be applicable with ease for ideally all gaseous radionuclides. A measurement campaign near the emission stacks, and not only inside the ventilation system, could complete the understanding of radioactive emissions at the most critical point, as observed in the series of $H^*(10)$ maps presented.

As commented in Chapter 2, comprehensive knowledge of plume rise and source effects, together with buildings' influence on local aerodynamics, requires the use of finer dispersion modeling instruments. For instance, Computation Fluid Dynamics (CFD) approaches could be merged with radiation transport computations to fully describe the complex set of physical phenomena considered. This ideal strategy appears undoubtedly laborious.

The evaluations presented in this thesis were collocated in the framework of air management and chronic releases at accelerators and hadron therapy facilities. At the end of this work, it should be underlined that also other pathways can eventually be a source of ionising radiation for members of the public and workers. For instance, in a centre like CNAO, a minimal fraction of dose could come from particles not stopped by shielding (dimensioned in the design phase) surrounding particle accelerators, radiopharmaceuticals, nuclear medicine clinical tests, stored radioactive materials. The radiation protection expert, besides the continuous monitoring of radioactivity and dose to workers with ambient and personal detectors, routinely carries out simulations to provide up-to-date estimates and verify the compliance with national regulation, in order to guarantee to hadron therapy facilities the highest degree of safety.

Conclusions

The present work was developed in the framework of air activation and management at particle accelerator and hadron therapy facilities. In particular, a generic computational method for assessing the dose in the surrounding area of a hadron therapy facility due to the chronic release of radioactive air was proposed.

During normal operations, several nuclear reactions that occur in particle accelerator bunkers and treatment rooms are responsible for the production of radioactive isotopes, which must be removed to maintain indoor air safe from a radiologic viewpoint. It was explained that this task is classified as a chronic release and is part of the regular management of accelerator facilities. Once discharged, radionuclides are transported into the atmosphere and may be a source of radiologic hazard. By using the methods of radiation protection, the radiation protection physicist in charge shall quantify the impact of radioactive releases on the population, in order to guarantee a safe and healthy environment, always in compliance with the national regulation. In the first part of this thesis, all the theoretical concepts necessary to develop the subsequent evaluations were introduced, dedicating relevant space also to Centro Nazionale di Adroterapia Oncologica (CNAO) – the facility at which the work was carried out.

The in-air transport of radioactive contaminants was addressed using the Gaussian Plume Model, a physical model which has been extensively discussed and applied in the literature. In this work, HotSpot and GENII V2.10, two toolbox codes certified by the Department Of Energy of the United States of America and available at CNAO's radiation protection office, were used to produce dose estimates exploiting the Gaussian Plume Model. Their algorithm for dose calculation was analysed, and assumptions and limits highlighted, stressing the concept of semi-infinite cloud approximation. The Monte Carlo transport code FLUKA was introduced as a possible solution for exhaustively addressing the phenomenon of radiation transport. Hence, the Gaussian Plume Model was implemented in a user-written source routine and tested in several ways, including a comparison of its performance with HotSpot and GENII V2.10.

Results allowed detecting the overestimation that the use of the semi-infinite cloud approximation causes when radioactive clouds are small, and the so-called dose from an overhead plume. The latter is a submersion dose component given by long-range particles (like energetic photons) generated in a radioactive cloud that extends far above the receptor's position. This situation is appreciable in an extremely stable atmosphere when the dispersion of contaminants is low and their concentration at the ground can be null. In this specific case, Gaussian Plume Model-based software can significantly underestimate the dose – or even erroneously predict a null dose.

In the second part of this work, the results of a previous M.Sc. thesis were

analysed to assess the annual radioactive releases foreseen at CNAO, considering also the planned expansion project (Proton Therapy and accelerator-based Boron Neutron Capture Therapy facilities). Evaluations were performed under conservative assumptions.

Meteorological data was gathered from two local weather stations and an annual wind rose was produced, showing the existence of some preferential wind directions for the years 2018 and 2019 and a recurring stable state of the atmosphere in Pavia.

Realistic data and the user-written source routine implementing the Gaussian Plume Model were used to produce submersion dose estimates for CNAO facility in a two-step method. Firstly, several FLUKA static simulations (one wind direction, annual release) were performed for the most relevant radionuclides discharged by the centre, namely ^{11}C , ^{13}N , ^{15}O , ^{41}Ar . Secondly, to model the variability that winds inevitably introduce in the dispersion of contaminants in the atmosphere, FLUKA dose results were exported to MATLAB and merged with the frequency distribution of wind directions, implementing a dedicated algorithm. In this context, a generic and effective approach to read Monte Carlo findings inside MATLAB was prepared and described.

The annual ambient dose equivalent for the operating synchrotron, the planned Proton Therapy and accelerator-based Boron Neutron Capture Therapy was plotted in dose maps. Results depicted a reassuring situation, in which the submersion dose rarely exceeded some hundreds of nanosievert per year with the only exception of the first metres around the emission point. There, several factors contributed to a higher degree of uncertainty of the evaluations. In this regard, a critical discussion about the approximations made was given. The inhalation dose was calculated with GENII V2.10 and resulted to be negligible.

The user-written source routine describing the Gaussian Plume Model inside the FLUKA code was successfully implemented, tested, and used in a realistic CNAO-related scenario. Its design allows easy reuse for different atmospheric stability classes, release heights and radionuclides. The two-step method for producing dose maps resulted to be straightforward, in which a longer FLUKA simulation was followed by a simple MATLAB code execution.

Future developments of the present work may include further refinement of the routine, in order to completely exclude the need to operate on its source code. Of course, the transport of contaminants may be addressed by exploiting also other models different from the Gaussian Plume Model. As the last frontier, the implementation of a coupling between a Computation Fluid Dynamics approach and a Monte Carlo code for radiation transport may offer the best possible description of the physical phenomena involved in this process. Despite the high degree of detail achievable, this laborious task may even be unnecessary, from an engineering and radiation protection viewpoint, if evaluations are carried out with a sufficiently – but not unduly – conservative approach.

Bibliography

- [1] Particle Therapy Co-Operative Group. Particle therapy facilities in clinical operation. [Online]. Available: <https://www.ptcog.ch/index.php/facilities-in-operation>
- [2] U. Linz, *Ion beam therapy: fundamentals, technology, clinical applications*. Springer Science & Business Media, 2011.
- [3] S. Agosteo, “Lecture notes in medical applications of radiation fields,” December 2019.
- [4] M. Durante and J. S. Loeffler, “Charged particles in radiation oncology,” *Nature reviews Clinical oncology*, vol. 7, no. 1, pp. 37–43, 2010.
- [5] F. CNAO. Fondazione CNAO’s insitutional website. [Online]. Available: <https://fondazionecnao.it/en>
- [6] M. Suzuki, “Boron neutron capture therapy (bnct): A unique role in radiotherapy with a view to entering the accelerator-based BNCT era,” *International journal of clinical oncology*, vol. 25, no. 1, pp. 43–50, 2020.
- [7] R. L. Moss, “Critical review, with an optimistic outlook, on boron neutron capture therapy (BNCT),” *Applied Radiation and Isotopes*, vol. 88, pp. 2–11, 2014.
- [8] S. Rossi, “The status of cnao,” *The European Physical Journal Plus*, vol. 126, no. 8, pp. 1–39, 2011.
- [9] Gazzetta Ufficiale della Repubblica Italiana, *Decreto Legislativo 31 luglio 2020, n. 101*, July 2020.
- [10] NCRP, “NCRP Report No. 144. Radiation protection for Particle Accelerator Facilities,” National Council on Radiation Protection and Measurements, Tech. Rep., 2003.
- [11] M. D’Arienzo, S. Sandri, and A. Consiglio, *Radioprotezione avanzata. Radionuclidi e acceleratori di elettroni fino a 10 MeV*. CISU, 2014.
- [12] R. Bhattacharya, *Atmospheric Dispersion*, International Atomic Energy Agency (IAEA).
- [13] S. R. Hanna, G. A. Briggs, and R. P. Hosker, Jr., “Handbook on atmospheric diffusion,” National Oceanic and Atmospheric Administration, Oak Ridge, TN (USA), Tech. Rep., 1982.

BIBLIOGRAPHY

- [14] M. Pirhalla, “Dispersion Modeling Systems Relevant to Homeland Security Preparedness and Response,” U.S. Environmental Protection Agency (EPA), Tech. Rep. EPA/600/R-20/338, 2020.
- [15] G. A. Briggs, “Diffusion estimation for small emissions,” National Oceanic and Atmospheric Administration, Oak Ridge, TN (USA), Tech. Rep., 1973.
- [16] R. F. Griffiths, “Errors in the use of the Briggs parameterization for atmospheric dispersion coefficients,” *Atmospheric Environment*, vol. 28, no. 17, pp. 2861–2865, 1994.
- [17] S. G. Homann and F. Aluzzi, “HotSpot Health Physics Codes Version 3.1.2 User’s Guide,” National Atmospheric Release Advisory Center, Tech. Rep. LLNL-SM-636474, 2020.
- [18] B. A. Napier, “GENII Version 2 Users’ Guide,” Pacific Northwest National Laboratory (PNNL), Tech. Rep. PNNL-14583. Rev. 4, 2012.
- [19] B. A. Napier, D. L. Streng, J. V. Ramsdell, Jr., P. W. Eslinger, and C. Fomire, “GENII Version 2 Software Design Document,” Pacific Northwest National Laboratory (PNNL), Tech. Rep. PNNL-14584, Rev. 4, 2012.
- [20] Office of Environment, Health, Safety & Security. Safety Software Quality Assurance - Central Registry. [Online]. Available: <https://www.energy.gov/ehss/safety-software-quality-assurance-central-registry>
- [21] K. F. Eckerman and J. C. Ryman, “Federal Guidance Report No. 12: External Exposure to Radionuclides in Air, Water, and Soil,” U.S. Environmental Protection Agency (EPA), Tech. Rep. EPA-402-R-93-081, 1993.
- [22] J. W. Healy and R. E. Baker, *Radioactive Cloud-dose Calculations*. General Electric Co., Schenectady, NY, 1968, ch. 7.
- [23] M. W. McNaughton, J. M. Gillis, E. Ruedig, J. J. Whicker, and D. P. Fuehne, “Gamma-Ray Dose From an Overhead Plume,” *Health physics*, vol. 112, no. 5, pp. 445–450, 2017.
- [24] R. Dey, H. Patni, K. D. Singh, M. Kulkarni, and S. Anand, “Effective dose conversion coefficient for gamma ray exposure from an overhead plume,” *Physics in Medicine & Biology*, vol. 64, no. 15, p. 155001 (10pp), 2019.
- [25] M. Pelliccioni, *Fondamenti fisici della radioprotezione*. Pitagora, 1989.
- [26] A. Fasso, A. Ferrari, J. Ranft, and P. R. Sala, *FLUKA: a multi-particle transport code*, CERN, 2005, Program version 2005.
- [27] G. Battistoni, F. Cerutti, A. Fasso, A. Ferrari, S. Muraro, J. Ranft, S. Roesler, and P. R. Sala, “The FLUKA code: description and benchmarking,” *AIP Conference Proceedings*, vol. 896, no. 1, pp. 31–49, 2007.
- [28] G. Garlaschelli, “Attivazione dell’aria in adroterapia e dispersione dei radionuclidi nell’ambiente,” Master’s thesis, Politecnico di Milano, 2019.

-
- [29] M. Pelliccioni, “Valutazioni preliminari di radioprotezione per il centro CNAO,” (available at CNAO’s radiation protection office).
- [30] Centro Meteorologico Lombardo (CML). Stazione meteo di Pavia Cascina Pelizza (PV). [Online]. Available: <http://www.centrometeolombardo.com/content.asp?contentid=722&ContentType=Stazioni>
- [31] *User Manual. Console for For Vantage Pro2™ and Vantage pro2™ Plus Weather Stations*, 10th ed., Davis Instruments Corp., 3465 Diablo Avenue, Hayward, 2020.
- [32] D. Hanahan and R. A. Weinberg, “The hallmarks of cancer,” *cell*, vol. 100, no. 1, pp. 57–70, 2000.
- [33] World Health Organization (WHO). Cancer. [Online]. Available: <https://www.who.int/news-room/fact-sheets/detail/cancer>
- [34] G. F. Knoll, *Radiation detection and measurement*. John Wiley & Sons, 2010.
- [35] M. Pelliccioni, “Radiation protection at Hadron therapy facilities,” *Radiation Protection Dosimetry*, vol. 146, no. 4, pp. 407–413, 2011.
- [36] R. H. Thomas and G. R. Stevenson, “Radiological Safety Aspects of the Operation of Proton Accelerators,” International Atomic Energy Agency (IAEA), Vienna, Tech. Rep. STI-DOC-010-283, 1988.
- [37] Y. Rentai *et al.*, “Atmospheric dispersion of radioactive material in radiological risk assessment and emergency response,” *Progress in Nuclear Science and Technology*, vol. 1, pp. 7–13, 2011.
- [38] D. T. Bailey, “Meteorological Monitoring Guidance for Regulatory Modeling Applications,” U.S. Environmental Protection Agency (EPA), Tech. Rep. EPA-454/R-99-005, 2000.
- [39] M. G. Stabin, *Radiation protection and dosimetry: an introduction to health physics*. Springer Science & Business Media, 2007.
- [40] A. H. Sullivan, *A Guide to Radiation and Radioactivity Levels Near High Energy Particle Accelerators*. Nuclear Technology Publishing, 1992.
- [41] ICRP, “1990 Recommendations of the International Commission on Radiological Protection. ICRP Publication 60.” International Commission on Radiological Protection, Tech. Rep., 1991.
- [42] M. Pelliccioni, “Overview of fluence-to-effective dose and fluence-to-ambient dose equivalent conversion coefficients for high energy radiation calculated using the FLUKA code,” *Radiation Protection Dosimetry*, vol. 88, no. 4, pp. 279–297, 2000.
- [43] A. Allisy, W. A. Jennings, A. M. Kellerer, and J. W. Müller, “ICRU Report 51. Quantities and Units in Radiation Protection Dosimetry,” International Commission on Radiation Units and Measurements, Tech. Rep., 2016.

- [44] ICRP, “The 2007 Recommendations of the International Commission on Radiological Protection. ICRP Publication 103.” International Commission on Radiological Protection, Tech. Rep., 2007.
- [45] B. M. Bowen, “Long-term tracer study at Los Alamos, New Mexico. Part I: Wind, turbulence, and tracer patterns,” *Journal of Applied Meteorology and Climatology*, vol. 33, no. 11, pp. 1221–1235, 1994.
- [46] J. H. Hubbell and S. M. Seltzer, “Tables of X-ray mass attenuation coefficients and mass energy-absorption coefficients 1 keV to 20 MeV for elements $Z = 1$ to 92 and 48 additional substances of dosimetric interest,” National Institute of Standards and Technology (NIST), MD (USA), Tech. Rep., 2004.
- [47] V. Vlachoudis *et al.*, “Flair: a powerful but user friendly graphical interface for fluka,” in *Proc. Int. Conf. on Mathematics, Computational Methods & Reactor Physics (M&C 2009)*, Saratoga Springs, New York, vol. 176, 2009.
- [48] International Atomic Energy Agency (IAEA). (2021) LiveChart of Nuclides. [Online]. Available: <https://www-nds.iaea.org/relnsd/vcharthtml/VChartHTML.html>
- [49] E. Zio, *The Monte Carlo Simulation Method for System Reliability and Risk Analysis*. Springer-Verlag London, 2013, pp. 22–33.
- [50] S. Thykier-Nielsen, S. Deme, and E. Láng, “Calculation method for gamma dose rates from gaussian puffs,” Risø National Laboratory Denmark, Tech. Rep., 1995.
- [51] F. Beauducel, “SUNRISE: sunrise and sunset times,” 2021. [Online]. Available: <https://github.com/beaudu/sunrise/releases/tag/v1.4.1>
- [52] E. E. M. Schlesinger, *Algebra lineare e geometria*. Zanichelli, 2011.

Appendix A

FLUKA SOURCE user routine

In this Appendix, the code of the user-written source routine described in Section 4.2.3 is attached and briefly commented.

Subroutine SOURCE is activated by card SOURCE in FLUKA input file and offers many advanced possibilities, e.g. sampling primary particle properties from distributions or implementing complex source geometries [26] (the same reference specifies recommendations to achieve a good programming style inside FLUKA).

The template is written by Alfredo Ferrari and Paola Sala and is provided with FLUKA distribution in the directory \$FLUPRO/usermvax. In the SOURCE routine there are some mandatory parts that cannot be modified; they include instructions for particle properties, transport, interactions, and other. All these blocks are omitted from this Appendix for brevity.

In an orderly fashion, the first thing to be noted is at line 196 of SOURCE template. Here a call to subroutine RACO is inserted to return a random 3D direction for the particle generated during the SOURCE call.

```
*  Cosines (tx,ty,tz)  
    CALL RACO (TXX,TYY,TZZ)  
    TXFLK (NPFLKA) = TXX  
    TYFLK (NPFLKA) = TYY  
    TZFLK (NPFLKA) = TZZ
```

where TXFLK, TYFLK, TZFLK are the direction cosines in Cartesian coordinates of particle NPFLKA.

SOURCE can receive in input up to 18 numerical values WHASOU(1-18) from FLUKA input file. For this work, contaminant release height (RELH), plume length (XMAX) and atmospheric stability class (STC) are inserted by the user and passed to the routine. Depending on the atmospheric stability class, Table 2.3 is used to select Briggs' coefficients. Wind speed (WINDSP) is set to 1 m s^{-1} . For each Monte Carlo history started by the input file, SOURCE card activates SOURCE routine and execute the following code:

```
*=====*
```

```
*                                     *
```

```
*           GAUSSIAN PLUME SOURCE           *
```

```
*                                     *
```

```
*=====*
```



```
* WNDSP = wind speed, m/s
```

```
* RELH = release height, cm
```

```
* XMAX = plume length, cm
```

```
* STC = atmospheric stability class, values from 1 to 6
```



```
*-----*
```

```
* Read data from SOURCE card in input file
```

```
  WNDSP = 1.0D+00
```

```
  RELH = WHASOU(1)
```

```
  XMAX = WHASOU(2)
```

```
  STC = WHASOU(3)
```



```
*-----*
```

```
* Atmospheric stability class
```

```
* STABILITY CLASS A
```

```
  IF (STC .EQ. 1) THEN
```

```
    AY = 2.2D-01
```

```
    CY = 1.0D-04
```

```
    DY = -5.0D-01
```

```
    AZ = 2.0D-01
```

```
    CZ = 0.0
```

```
    DZ = 1.0
```

```
* STABILITY CLASS B
```

```
  ELSE IF (STC .EQ. 2) THEN
```

```
    AY = 1.6D-01
```

```
    CY = 1.0D-04
```

```
    DY = -5.0D-01
```

```
    AZ = 1.2D-01
```

```
    CZ = 0.0
```

```
    DZ = 1.0
```

```
* STABILITY CLASS C
```

```
  ELSE IF (STC .EQ. 3) THEN
```

```
    AY = 1.1D-01
```

```
    CY = 1.0D-04
```

```
    DY = -5.0D-01
```

```
    AZ = 8.0D-02
```

```
    CZ = 2.0D-04
```

```
    DZ = -5.0D-01
```

```
* STABILITY CLASS D
```

```
  ELSE IF (STC .EQ. 4) THEN
```



```

        AY = 8.0D-02
        CY = 1.0D-04
        DY = -5.0D-01
        AZ = 6.0D-02
        CZ = 1.5D-03
        DZ = -5.0D-01
* STABILITY CLASS E
        ELSE IF (STC .EQ. 5) THEN
        AY = 6.0D-02
        CY = 1.0D-04
        DY = -5.0D-01
        AZ = 3.0D-02
        CZ = 3.0D-04
        DZ = -1.0
* STABILITY CLASS F
        ELSE IF (STC .EQ. 6) THEN
        AY = 4.0D-02
        CY = 1.0D-04
        DY = -5.0D-01
        AZ = 1.6D-02
        CZ = 3.0D-04
        DZ = -1.0
* ELSE, KEEP STABILITY CLASS D
        ELSE
        AY = 8.0D-02
        CY = 1.0D-04
        DY = -5.0D-01
        AZ = 6.0D-02
        CZ = 1.5D-03
        DZ = -5.0D-01
        END IF

*-----*
* Decay constant, 1/second
* C11
*      XLMBD = 5.67D-04
* N13
*      XLMBD = 1.17D-03
* O15
*      XLMBD = 5.68D-03
* Ar41
*      XLMBD = 1.05D-04

*-----*
* Computation
* Conversion to metres
        RECPH = RECPH * 1.0D-02

```

```

      XMAX = XMAX * 1.0D-02
* Linear extraction of downwind distance
*      X = FLRNDM (XDUMMY) * XMAX
* Instant of decay extraction, seconds
237  RNNN = FLRNDM (TDUMMY)
      TDCY = (-1.0D+00/XLMBD) * LOG (1.0D+00-RNNN)
* Decay position downwind, metre
      X = TDCY * WNDSP
      IF (X .GT. XMAX) THEN
          GOTO 237
      END IF
* Briggs coefficients: open country
      SGMY = AY*X*(1.0D+00+CY*X)**DY
      SGMZ = AZ*X*(1.0D+00+CZ*X)**DZ
* Extraction from gaussian distribution
      CALL FLNRR2 (RGAUS1, RGAUS2)
* Y extraction, metres
      Y = SGMY * RGAUS1
* Z extraction, metres. Z < 0 - do reflection
      Z = SGMZ * RGAUS2 + RECPH
      IF (Z .LT. 1.0D-06) THEN
          Z = -Z
      END IF
* Conversion to centimetres
      XFLK (NPFLKA) = X * 1D+02
      YFLK (NPFLKA) = Y * 1D+02
      ZFLK (NPFLKA) = Z * 1D+02

```

Auxiliary routines FLRNDM and FLNRR2 are called to sample a 64-bit random number in $[0, 1)$ and two uncorrelated normally distributed random numbers (RGAUS1, RGAUS2), respectively. In FLUKA, it is essential not to use any external random generator to preserve history reproducibility. Also, it is reminded that lengths are handled in centimeters.

Besides the physical and mathematical comments provided in Section 4.2.3, it is here remarked that the final goal of the routine is to distribute the contaminants' decay position in space according to the GPM. In fact, in the last lines of the code, FLUKA spatial coordinates for particle NPFLKA, (XFLK, YFLK, ZFLK) are filled with the GPM-sampled variables (X, Y, Z).

Appendix B

Meteorological data analysis

In this Appendix, a comparison of CML and CNAO meteorological data is carried out for the year 2019. Data was analysed with the same approach as Section 5.3. CML provided 105 108 valid records, CNAO 104 901, both sampled every 5 min.

Wind speed was compared in Figure B.1. With reference to the SRDT method, the first wind group (below 2 m s^{-1}) was split in two: calm wind (wind speed below weather station's resolution, i.e. 0.4 m s^{-1} [31]) and wind from 0.4 m s^{-1} to 2.0 m s^{-1} . Both weather stations detected low or null speed during most of the year (97 % of CNAO measurements and 90 % of CML measurements resulted to be below 2.0 m s^{-1}). CNAO weather station recorded less calm winds than CML.

Solar radiation was analysed by dividing available data into the same groups indicated by the SRDT method. Weather stations showed agreement in measurements (Figure B.2).

The generally good agreement between wind speed and solar radiation data led to similar results also for atmospheric stability classes (Figure B.3). Frequent low wind and moderate solar radiation justify unstable class B during daytime. At nighttime, code approximations led to a conservatively high number of class F calculated records.

Wind directions showed considerable differences in results (Figure B.4). In 25 % of CML measurements, wind direction could not be assigned, probably owing to calm wind measurements. In Figure B.1, calm wind corresponds to 35 % of CML observations. Hence, in some circumstances, CML weather station assigned a wind direction even though wind speed was below the anemometer's sensitivity. CNAO weather station measured calm wind 24 % of the time but did not assign a wind direction in 7 % of the records. Also in this case, the CNAO weather station assigned a wind direction even though wind speed was under instruments' sensitivity, but the two operated in different ways. In absence of any other information, it was supposed that meander under light wind conditions, or sudden gusts of wind, may have had a role in wind direction assignment if the sampling time was little. In this way, the average 5 min wind speed can be null, but not necessarily the wind direction. In other words, the randomness of light breezes might explain the two weather stations' different behaviour. Despite the differences in null direction, CML denoted WSW (13 %), W (10 %), E (10 %) as preferential directions. At CNAO, instead, the preponderant data was SW (12 %), N (9 %), SE (9 %). The distance between the two measurement points might explain the differences, but local aerodynamic effects due to buildings should not be excluded.

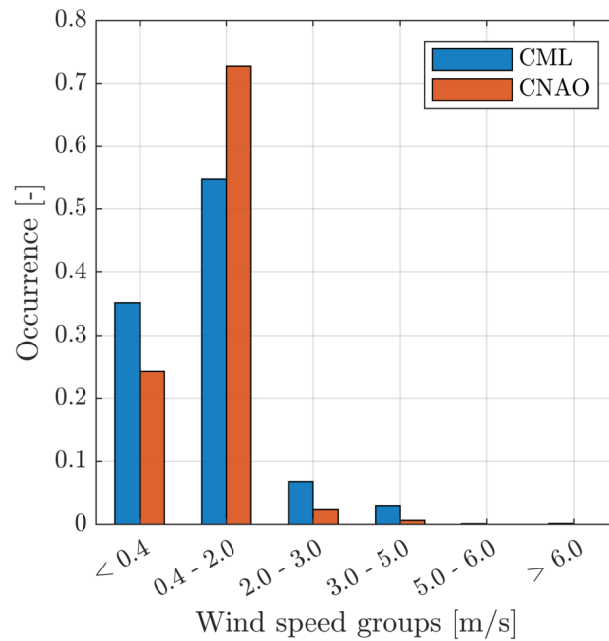


Figure B.1. Histogram of wind speed data in $[\text{m s}^{-1}]$ in the year 2019, recorded by CML and CNAO weather stations. Groups were inherited from the SRDT method, except for the first group, which was split in low-intensity wind and calm wind, i.e. wind below the anemometer's sensitivity.

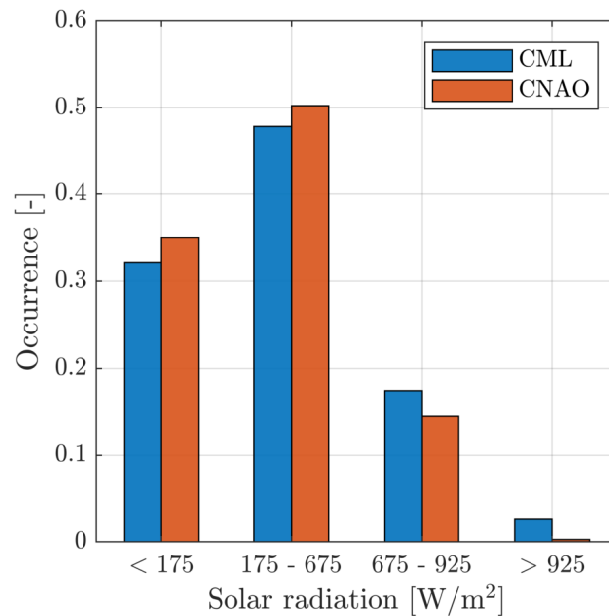


Figure B.2. Histogram of solar radiation data in $[\text{W}^2 \text{m}^{-1}]$ in the year 2019, recorded by CML and CNAO weather stations. Groups were inherited from the SRDT method.

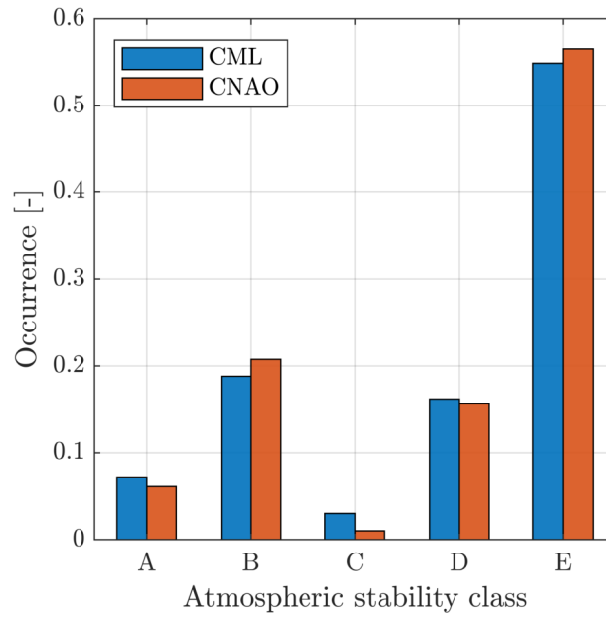


Figure B.3. Histogram of atmospheric stability classes in the year 2019, from data by CML and CNAO weather stations, calculated with the SRDT method.

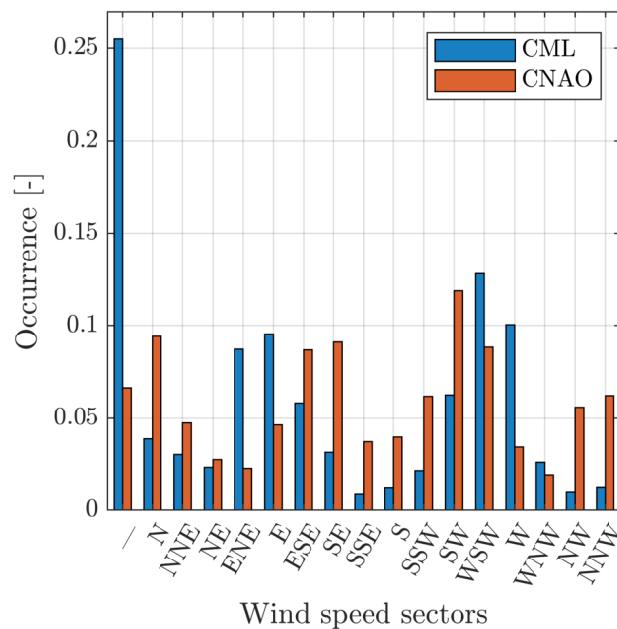


Figure B.4. Histogram of wind direction frequency distribution in the year 2019, recorded by CML and CNAO weather stations. Sixteen 22.5° sectors plus calm wind are considered; wind direction is the orientation wind is coming from.

Appendix C

Importing USRBIN data to MATLAB

In this Appendix, a function for importing FLUKA USRBIN files inside MATLAB is proposed. This function was implemented in the framework of the computations developed in Chapter 6 to achieve an automatic reading of USRBIN data files. In fact, it is not infrequent that the need for further elaboration of FLUKA data requires the use of other software, above all spreadsheets for organised storage. In this sense, being `readUSRBIN` the ideal starting point of any MATLAB code that handles USRBIN data, this MATLAB function represents a first valid attempt to extend the post-processing of FLUKA results outside this Monte Carlo software.

From a coding viewpoint, USRBIN data files need to be converted to ASCII format inside Flair (file extension: `.bnn.lis`). The implemented function scans the whole USRBIN file and imports numeric data in a MATLAB matrix variable (in the code, variable `usrbin_NN`), discarding at the same time the descriptive text appended by FLUKA. Usually, in ASCII files, USRBIN data is arranged in ten columns, and corresponding statistical uncertainty follow scoring values; `readUSRBIN` function imports dose data in the upper half of the matrix rows and parallel errors in the bottom half, keeping the same number of columns and rows of the text file. As explained in Chapter 6, data inside USRBIN files are not normalised; in the development of any analysis this point should be considered. The code is attached below.

Listing C.1. Code of `readUSRBIN` MATLAB function.

```
function usrbin_NN = readUSRBIN(file_name, nCol)
%readUSRBIN read fluka ascii output
% AUTHOR: Tommaso Lorenzon
% INPUT:
%   file_name  string or char array; name of the file to be
%               read, with extension
%   ncol       number of columns in the file, usually 10
% OUTPUT:
%   usrbin_NN  matrix of doubles; usrbin data, not in
%               definitive shape. Not normalised (NN)!

lines = textread(file_name, '%s', 'delimiter', '\r');
```

```
ind = length(lines); % number of lines

usrbin_NN = zeros(ind,nCol); % USBIN matrix, NN
counter = 1;

for iline = 2:length(lines) % for each line
    line_ = lines{iline};
    data = str2num(line_); % line conversion to numbers
    isempty(data); % check if numbers were found
    if ~isempty(data)
        if (length(data) <= nCol) % assign usrbin_NN cells
            usrbin_NN(counter,1:length(data)) = data;
            counter = counter +1;
        end
    end
end
usrbin_NN = usrbin_NN(1:counter-1,:);

end
```


Appendix D

Guide to MATLAB scripts

In this Appendix, the most relevant MATLAB functions and scripts prepared for this M.Sc. thesis are listed and briefly described. Source code is deposited at CNAO radiation protection office.

Function name	Description
<i>Tests for FLUKA user-written source routine</i>	
GPLM	Read in MATLAB the text file containing the GPM source points' spatial coordinates sampled in FLUKA
<i>Meteorological data analysis</i>	
meteo_analysis	Column-wise meteorological data analysis, including atmospheric stability class computation
sunrise	Compute sunrise and sunset time ^a
meteo_plot	Plot results of the meteorological data analysis
meteo_comparison	Plot results of the meteorological data comparison between CNAO and CML weather stations
meteo_GENII	Write GENII V2.10 meteorological formatted file (set of functions)
<i>MATLAB dose maps</i>	
distances	Compute distances from the emission stacks
FL_prepData	Prepare FLUKA data for the subsequent elaboration: read, shape, normalise dose data results
readUSRBIN	Read USRBIN data in ASCII format and save it to a MATLAB matrix
reshapeUSRBIN	Reshape USRBIN matrices to the correct number of rows and columns, corresponding to the radial and angular bins used in FLUKA
FL_elabData	Merge USRBIN matrices with the frequency distribution of wind directions
outputTable	After processing, save data to a text file in table format
polarPlot	Print circular dose maps

^a Author: François Beauducel [51]

Acronyms

ab-BNCT	accelerator-based Boron Neutron Capture Therapy
BNCT	Boron Neutron Capture Therapy
CFD	Computation Fluid Dynamics
CML	Centro Meteorologico Lombardo
CNAO	Centro Nazionale di Adroterapia Oncologica
DCF	Dose Conversion Factor
D.Lgs.	Decreto Legislativo
DOE	Department Of Energy of the United States of America
EPA	Environmental Protection Agency
FGR	Federal Guidance Report
GPM	Gaussian Plume Model
GUI	Graphical User Interface
IAEA	International Atomic Energy Agency
ICRP	International Commission on Radiological Protection
ICRU	International Commission on Radiation Units and Measurements
LET	Linear Energy Transfer
LLNL	Lawrence Livermore National Laboratory
NARAC	National Atmospheric Release Advisory Center
NCRP	National Council on Radiation Protection and Measurements
NTP	Normal Temperature Pressure
OER	Oxygen Enhancement Ratio
P-G	Pasquill-Gifford
PNNL	Pacific Northwest National Laboratory
PT	Proton Therapy
RBE	Radiobiological Effectiveness
SOBP	Spread-Out Bragg Peak
SRDT	Solar Radiation Delta-T
TED	Total Effective Dose